BMP9 and BMP10 act directly on vascular smooth muscle cells for generation and maintenance of the contractile state

INAUGURAL-DISSERTATION

zur Erlangung des Doktorgrades der Naturwissenschaften

- Doctor rerum naturalium -

(Dr. rer. nat.)

vorgelegt dem

Fachbereich 08 - Biologie und Chemie der

Justus-Liebig-Universität Gießen

Durchgeführt am Max-Planck-Institut für Herz- und Lungenforschung,

W.G. Kerckhoff-Institut Bad Nauheim

eingereicht von

Lei Wang, China

Giessen, 2021

Die Untersuchungen zur vorliegenden Arbeit wurden am Max-Planck-Institut für Herz- und Lungenforschung (W. G. Kerckhoff-Institut) in Bad Nauheim unter Leitung von Prof. Dr. Dr. Thomas Braun durchgeführt.

Vom Fachbereich 08 - Biologie und Chemie der Justus-Liebig-Universität Gießen angenommen

Erstgutachter:
Prof. Dr. Dr. Thomas Braun
Abteilung für Entwicklung und Umbau des Herzens
Max-Planck-Institut für Herz- und Lungenforschung
Ludwigstraße 43
D-61231 Bad Nauheim

Zweitgutachter:
Prof. Dr. Norbert Weissmann
Justus Liebig University
Medical Clinic II
ECCPS building
Aulweg 130
D-35392 Giessen

Ehrenwörtliche

Erklärung

Ehrenwörtliche Erklärung:

Ich versichere, dass ich meine Dissertation

BMP9 and BMP10 act directly on vascular smooth muscle cells for generation and maintenance of the contractile state

unter der Leitung von Prof. Dr. Dr. Thomas Braun (Max-Planck-Institut für Herzund Lungenforschung, Bad Nauheim) selbstständig und ohne unerlaubte Hilfe angefertigt und mich dabei keiner anderen als der von mir ausdrücklich angegebener Quellen und Hilfen bedient habe.

Prüfungszwecken gedient.

Giessen,

Lei Wang

I Table of contents

II Summary

Vascular smooth muscle cells (VSMCs) show a remarkable phenotypic plasticity reflecting their ability to acquire contractile or synthetic states. Numerous signaling pathways and conditions are known, which cause loss of contractility and attainment of a synthetic state but knowledge about signaling pathways promoting the contractile state is limited and *in vivo* evidence is critically missing. Here, we investigated the role of BMP9, BMP10, activin receptor-like kinase 1 (ALK1) and Smad7 for controlling formation of contractile VSMCs. Effects of *Bmp9* and *Bmp10* inactivation, conditional deletion of *Alk1* in SMCs, overexpression of *Bmp10* in endothelial cells (ECs) and overexpression of *Smad7* in SMCs were evaluated in respect to coverage of vessels by VSMC, their contractile state and blood pressure. The molecular mechanisms underlying effects of BMP9/BMP10 were studied by treating dedifferentiated SMCs with BMP9/BMP10 *in vitro*.

Concomitant genetic inactivation of BMP9/BMP10 in mice led to a dramatic diminution of VSMC layer, loss of contractile VSMCs and decreased systemic blood pressure. Consistently, overexpression of *Bmp10* in ECs of adult mice dramatically enhanced VSMC contractility and increased formation of contractile VSMCs, indicating that BMP9/BMP10 play fundamental roles for differentiation and contractility of VSMCs. Importantly, treatment of BMP9/BMP10 induced an ALK1-dependent phenotypic switch from synthetic to contractile state in de-differentiated VSMCs. SMC-specific overexpression of inhibitory *Smad7* completely suppressed differentiation and proliferation of VSMCs during embryonic development and reiterated the defects observed in BMP9/BMP10 double mutants in adults. Likewise, deletion of *Alk1* in SMCs recapitulated attenuated VSMCs coverage and loss of contractile VSMCs seen in BMP9/BMP10 mutants but only in pulmonary and not in aortic or coronary arteries. Bulk RNA-seq and single molecule RNA-fluorescent *in situ hybridization* (RNA-FISH) uncovered heterogeneous expression of BMP type I receptors in distinct vessel beds, explaining phenotypic differences between *Alk1* and *Bmp9/Bmp10* inactivation. Furthermore, analysis of BMP9/BMP10 stimulated VSMCs by ATAC-seq combined with RNA-seq revealed that YAP/TEAD and BMP9/BMP10/Smad-signaling converge at promoters of several VSMC genes. Gain-and loss-of-function studies of the YAP-TEAD axis demonstrated that YAP-TEAD axis antagonized BMP9/BMP10 induced VSMCs differentiation and formation of contractile VSMCs.

In conclusion, the study indicated that BMP9 and BMP10 are released into the blood stream by the liver and the right atrium, respectively and bypass the endothelial barrier to directly induce and maintain contractile VSMCs. Importantly, the effects of BMP9/BMP10 in VSMCs are modulated by different combination of BMP type one receptors in a vessel bed specific

manner.

Keywords: BMP9, BMP10, ALK1, Smad7, smooth muscle cells, differentiation, heterogeneity, YAP, TEAD

III Zusammenfassung

Vaskuläre glatte Muskelzellen (VSMCs) verfügen über eine bemerkenswerte phänotypische Plastizität, die eine Umschaltung zwischen einem kontraktilen and einem synthetisch-proliferativen Zustand ermöglicht. Bis dato wurden zahlreiche Signalwege und Bedingungen beschrieben, welche den Übergang von VSMCs aus dem kontraktilen in den synthetischen Zustand fördern. Demgegenüber ist die Erkenntnis über Signalwege, die den kontraktilen Zustand induzieren sehr begrenzt und schlagende *in-vivo* Beweise fehlen. In der vorliegenden Arbeit wurde die Rolle von BMP9, BMP10, Activin-Receptor-like Kinase 1 (ALK1) und Smad7 hinsichtlich der Bildung und Erhaltung kontraktiler VSMCs untersucht. Im Fokus stand dabei die glatte Muskelzellschicht von Blutgefäßen aus konditionalen BMP9/10 Doppel-Knockout (dKO) Mutanten, aus glatten Muskelzell-spezifischen ALK1-KO Mutanten sowie aus endothel-spezifischen BMP10- bzw. VSMC-spezifische SMAD7-Überexpressionsmutanten. Die Abdeckung verschiedener Gefäße mit VSCMs wurde untersucht, ebenso der Blutdruck in den verschiedenen mutanten Mausstämmen, sowie die Kontraktilität der VSMC. Des Weiteren wurden primäre, dedifferenzierte VSMCs *ex-vivo* mit BMP9 / BMP10 stimuliert, um einen Einblick in molekularen Mechanismen zu erlangen, die der Wirkung von BMP9/10 zugrunde liegen.

Eine kombinierte genetische Inaktivierung von BMP9 und BMP10 bei Mäusen führte zu einer dramatischen Verringerung der VSMC-Schicht, einem Verlust kontraktiler VSMCs und einem verringerten systemischen Blutdruck. Im Einklang hiermit führte eine Endothel-spezifische BMP10 Überexpression zu einer verstärkten Bildung von VSMCs, die zudem eine erhöhte Kontraktiliät aufwiesen, was auf eine grundlegende Funktion der beiden Liganden bei der Regulation der VSMC Differenzierung hinweist. Zudem induzierte eine BMP9 / BMP10 Behandlung von de-differenzierten VSMCs einen ALK1-abhängigen phänotypischen Wechsel vom synthetischen in den kontraktilen Zustand. Die VSMC-spezifische Überexpression von inhibitorischem Smad7 blockierte die Differenzierung und Proliferation von VSMCs während der Embryonalentwicklung vollständig und rekapitulierte die bei BMP9 / BMP10-Doppelmutanten beobachteten Defekte im Erwachsenenstadium. Ebenso phänokopierte die Deletion von ALK1 in SMCs die abgeschwächte VSMCs-Abdeckung und den Verlust kontraktiler VSMCs in Lungen-, jedoch nicht in Aorten- oder Koronararterien. Bulk-RNA-seq und Einzelmolekül-RNA-FISH enthüllte eine heterogene Expression von BMP-Typ-I-Rezeptoren in verschiedenen Gefäßbetten, was die phänotypischen Unterschiede der Ausschaltung von BMP9/10 gegenüber einer Inaktivierung von ALK1 erklärt. Die Analyse von BMP9 / BMP10-stimulierten VSMCs durch ATAC-seq in Kombination mit RNA-seq zeigte, dass YAP / TEAD- und BMP9 / BMP10 / Smad-Signale an Promotoren mehrerer VSMC-Gene konvergieren. Funktionsgewinn- und Funktionsverluststudien deuten weiterhin darauf hin,

dass die YAP-TEAD-Achse eine BMP9 / BMP10 induzierte Differenzierung von VSMCs und die Bildung kontraktiler VSMCs antagonisierte.

Zusammenfassend zeigt die Studie, dass im Blutstrom zirkulierendes BMP9 und BMP10 die Endothelbarriere umgehen, um den Eigenschaften kontraktiler VSMCs direkt zu induzieren und aufrechtzuerhalten. Die Wirkungen von BMP9 / BMP10 in VSMCs werden durch unterschiedliche Kombinationen von BMP-Typ-1-Rezeptoren in einer Gefäßbett-spezifischen Weise moduliert.

Schlüsselwörter: BMP9, BMP10, ALK1, Smad7, glatte Muskelzellen, Differenzierung, Heterogenität, YAP, TEAD

1 Introduction

SMCs present remarkable phenotypic plasticity and are capable of reversible switching between a quiescent, contractile state and a synthetic and proliferative phenotype[1]. Differentiated VSMCs highly express functional contractile apparatus proteins. At the other, synthetic end of the spectrum, VSMCs de-differentiated into fibroblast-like SMCs with low expression of contractile proteins and extensive synthesis of extracellular matrix (ECM) [2, 3]. Phenotypic plasticity enables blood vessels with the ability to acquire the flexibility, required to perform efficiently under different long-lasting physiological conditions. Abnormal regulation of VSMC phenotypic switching contributes to numerous vascular diseases including hypertension, atherosclerosis, congenital heart diseases and restenosis[4]. Numerous molecules have been shown to promote the transition of VSMCs from the contractile into the synthetic state. In contrast, the number of signalling factors which promote the contractile phenotype is relative short[2]. Clearly, a better understanding of the mechanisms balancing vascular vasodilatation/vasoconstriction and VSMC phenotype modulation is essential for the development of new therapeutic approaches for vascular diseases[5].

The importance of the TGF-β signaling pathway in VSMC differentiation and phenotypic switching has been demonstrated by a number of studies. One prominent example are activin receptor-like kinase 1 (ALK1) knockout embryos containing virtually no VSMCs[6-8]. However, despite intense research efforts in the past decades, the role of this superfamily and their transmembrane receptors, co-receptors and intermediate Smad proteins in the vasculature and how they work in concert or in opposition to each other is still controversial. BMP9 and BMP10 form a distinct subgroup in the TGF-superfamily and share a high sequence identity at the protein level[9]. They serve as high-affinity ligands for ALK1 and signal via the ALK1/BMPR2 complex[10]. BMP9 and BMP10 have been described as endothelial cell (EC) quiescent factors keeping ECs in a resting state[11, 12]. BMP9 loss-of-function studies as well as studies using dominant-negative *Alk1* mutants suggested that BMP9 might regulate synthesis/release of potent vasoreactive factors in ECs, such as apelin[13-12]. Surprisingly, *Bmp9*$^{-/-}$ mice present a normal vasculature system and are also otherwise phenotypical normal[14]. In contrast, *Bmp10*$^{-/-}$ mice die during embryonic development due to severe angiogenic and cardiac defects[15]. So far, it has been difficult to determine the functional role of BMP10 in adults using genetic tools. Hence, BMP10 was neutralized by antibody injection into *Bmp9*$^{-/-}$ mice, which resulted in symptoms of increased EC intensity in retinas, Hereditary Hemorrhagic Telangiectasia (HHT) and a defective closure of the ductus arteriosus[16, 17]. Although such approaches have been informative, it is necessary to study effects caused by long lasting absence of BMP9/BMP10.

1.1 Cardiovascular structure

In vertebrates, the cardiovascular system is the first functional organ to develop during embryogenesis. The cardiovascular system is a closed system, containing heart, vessel and blood, which delivers oxygen and nutrients to tissues while removing metabolic end products and carbon dioxide. In addition, the cardiovascular system facilitates communication between distinct organs by hormones, cytokines, growth factors or inhibitors. Based on the position in the arterial tree and their structure, arteries can be classified as conducting, conduit or resistance arteries. Conducting arteries include aorta, carotid and pulmonary arteries, and are highly elastic compared to other arteries, allowing them to dampen the pulse wave[18, 19]. The conducting arteries branch into conduit arteries, such as femoral and brachial arteries, delivering blood flow to different regions. The conduit arteries further branch into resistance arteries, which form part of the microvasculature and allow regulation blood flow by dilation or constriction[20].

The cardiovascular system is typically organized in basic three layers: the tunica adventitia, the tunica media and the tunica intima. Each layer is different in its cellular composition, histology, functionality and response to injury. The adventitia is the outer layer of an artery, which provides a connective tissue-rich protective role in vascular maintenance and repair. The adventitia is the most diverse of the three layers, composed of multiple cell types, such as lymphatic vessels, autonomic nerves, adventitial fibroblasts, mast cells, and dendritic cells[21]. The adventitia of the major vessels has been recognized as a stem/progenitor cell compartment, which has been claimed to contain a $Sca1^+$ cell population, capable of giving rise to VSMCs in response to arterial injury[22]. In some large arteries, such as aortae, the adventitia contains *vasa vasorum*, which supply oxygenated blood, allow trafficking immune/inflammatory cells, and regulate communication between the three layers[23].

The tunica media or the middle layer, is the main contractile layer containing VSMCs. In addition to VSMCs, this layer also contain ECM components secreted by both ECs and VSMCs, such as elastin, collagen type I and III and proteoglycans[24,25]. VSMCs are the major type of cells in the media and regulates by dynamic contraction and relaxation vascular tone and blood flow. In the smallest vessels, such as capillaries or postcapillary venules, VSMCs are replaced by a discontinuous coat of pericytes. After recruitment to ECs, VSMCs will assemble into a functional layer and differentiate. In arteries with multiple layers, VSMCs undergo patterning layer by layer from the inside to outward. Several signalling pathways have been found to mediate this radial patterning, such as TGFβ/BMP and Jagged-Notch signalling[26]. VSMCs in the media are arranged circumferentially and are separated by elastic fibers. This highly organized and ordered matrix provides structural integrity and supports VSMCs to carry out contractile function[27].

The tunica intima is the innermost layer of vessels and composed of a single cell layer of ECs at the top of a basal and elastic lamina. ECs coalesce into initial vessel tubes, which give rise to further vessels by a process consisting of EC proliferation, migration, invasion and lumen formation. In the end, newly formed vessels recruit VSMCs and pericytes to stabilize the vessel[28, 29]. Since ECs directly interact with the bloodstream, ECs are poised to regulate the activity of VSMCs and play a crucial role in responding to environmental stimuli[30, 31]. ECs synthesize and secrete a range of molecules responsible for auto-and paracrine regulation on connected tissues[32]. In adults, ECs are quiescent unless activated by several pro-angiogenic signals[33]. Given the crucial role of ECs, it is understandable that perturbed angiogenic balance and dysfunction of ECs are sources of several pathological disorders, such as pulmonary and systemic hypertension, stroke, atherosclerosis, and inflammatory syndromes. Furthermore, ECs play a major role in cancer[34].

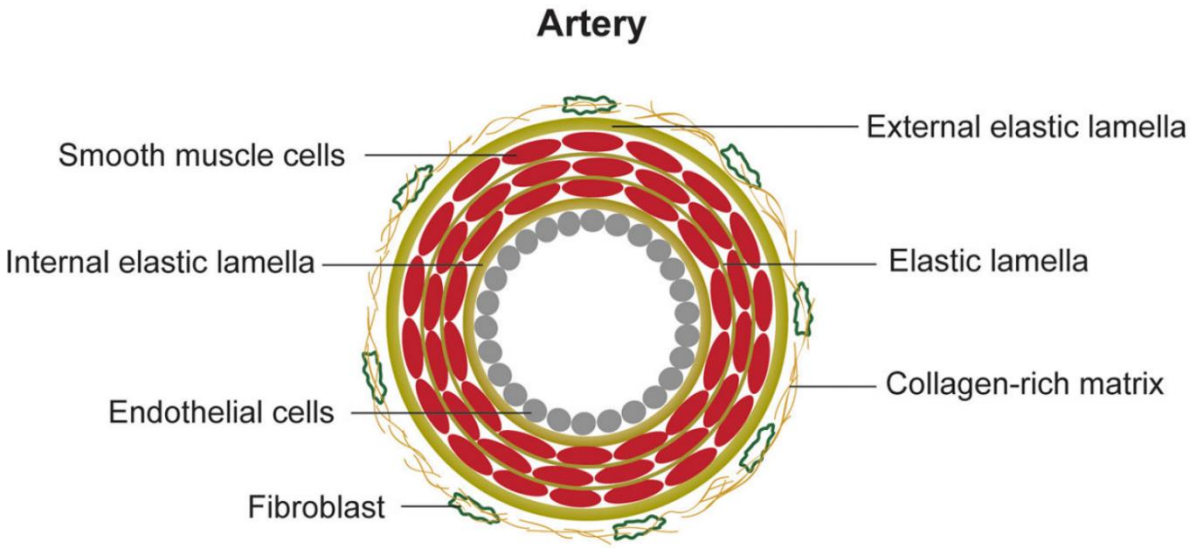

Figure 1. Schematic view of a transverse cross section of an artery.
The arterial walls contain three layers: the intima, media and adventitia. The intima is the region that is internal to elastic lamella, containing ECs and a basement membrane; the media is sandwiched between the internal and external elastic lamellae, containing VSMCs and ECM components, and is responsible for vascular tone and extracellular matrix. The adventitia is outside the external elastic lamella, containing fibroblasts, stem and immune cells and is responsible for trafficking immune cells and signalling molecules. Adapted from[24].

1.2 Endothelium-smooth muscle interplay in the cardiovascular system

Normal interactions between these three layers are important for the homeostasis of vascular circulation[35]. The communication between ECs and SMCs can be carried out in different ways. Mechanistically, the strategies of such a communication may be divided into two categories: via soluble and secreted molecule or via direct physical contact between different cell types. It

is well recognized that ECs can mediate differentiation and phenotypic plasticity of underlying VSMCs by paracrine signalling via secreted vasoactive molecules. In the mature vasculature, the close proximity of ECs and VSMCs allows efficient communication by secreted and diffusible factors. ECs release factors, such as nitric oxide (NO), prostacyclin and hyperpolarizing agents, which diffuse to VSMCs to cause vascular relaxation[36]. Oppositely, ECs factors may also stimulate contraction, such as entohelin-1(ET-1) and angiotensin II (Ang II), which are sensed by VSMCs and cause increased vascular contractility[36]. However, it appears that this paradigm might be an oversimplification of a much more nuanced story[37, 38]. In addition to the paracrine pathway, multiple other mechanisms of physical communication are critically involved in the cross-talk, such as myoendothelial gap junctions (MEJs), extracellular vesicles (EVs), heterotypic interactions[39, 40] and *vasa vasorum*. For example, a well-known heterotypic interaction is mediated by the Notch signalling pathway, in which membrane-bound receptors (Notch1-4) are activated by membrane-bound ligands (Jagged1,2 and Delta like 1,3 and 4) on adjacent cells[41]. Increasing evidence suggests that the non-paracrine systems also play a crucial role in regulating vessel morphogenesis and stability. Each of these mechanisms has unique features but acts in a coordinated manner, enabling a complicated and diversified mediation.

Understanding the cross-talk is imperative to decipher the mechanism of vascular remodelling. Therefore, it will be important to further characterize the roles of ECs in VSMCs formation and vascular wall integrity or *vice versa*. The TGFβ/BMP signalling is crucial for the interaction of these two cell types during development and beyond. The most convincing evidences come from the genetic knockout animal models, in which inactivation of several components of this signalling in ECs led to a failure of VSMC differentiation and proliferation[42-45]. However, several studies also showed that different receptors and ligands in this family are both expressed in ECs as well as in SMCs[44, 46]. Interestingly, a report demonstrated that deletion of the Smad4 in VSMCs resulted in decreased VSMC differentiation, proliferation and spreading[47], suggesting that the regulation of TGFβ/BMP signalling on VSMCs might by an endothelium independent manner.

1.3 SMCs display phenotypic plasticity

In contrast to cardiac and skeletal muscle cells, SMCs are not terminally differentiated and are still responsive to changes in the local environments even during adulthood. SMCs are capable of reversible switching along a spectrum from a quiescent, proliferation-arrested and contractile state and de-differentiate into a synthetic, proliferative and undifferentiated phenotype[1]. The contractile phenotype of SMCs is characterized by a highly functional contractile apparatus, which contains tightly bundled myofilaments and a small number of endoplasmic reticulum and Golgi[2, 3]. In adult vessels, VSMCs show low proliferative potential

with low rate of ECM synthesis, since they are fully committed to contractility. Contractile SMCs express several contractile proteins, including smooth muscle α-actin (also known as ACTA2), smooth muscle myosin heavy chains (also known as SMMHC), calponin, Transgelin/SM22a (also known as TAGLN) and smoothelin (also known as SMTN). Almost all of these SMC differentiation marker genes also expressed in some non-SMCs, with exception of SMMHC isoforms, which seem to be the most specific marker of differentiated SMCs. In contrast, at the synthetic extreme are fibroblast-like SMCs expressing low levels of contractile proteins, characterized by a cytoplasm devoid of contractile bundles but a major content of ribosome and Golgi apparatus[2, 3], that is able of extensive ECM synthesis. Several markers specific for synthetic SMC exist, including collagen type I, tropomyosin (also known as TPM4) and Vimentin (also known as VIM). Phenotypic plasticity from contractile to synthetic and *vice versa* provides the vessels with the necessary flexibility, required to perform efficiently under different conditions.

In mature vessels, alterations of nutrients and oxygen availability, shear stress, fluid pressure and metabolic requirement are the main factors promoting plasticity[48, 49]. For example, in some conditions, such as vascular injury, contractile VSMCs decrease expression of *Myh11* and *Acta2* and undergo modification toward a synthetic state in response to cues in the local microenvironmental[1, 50]. VSMCs undergoing such modification display increased proliferation, migration and synthesis of ECM components[51]. After injury, signals within the local environment promote the return of VSMCs to a normal state, in particular re-acquirement of contractile properties. Abnormal regulation of VSMC differentiation and function contributes to numerous vascular diseases, including hypertension, hereditary hemorrhagic telangiectasia (HHT), atherosclerosis, congenital heart diseases and restenosis after stent implantation[51]. The best known example of a disease caused by maladaptive VSMC phenotypic switching is atherosclerosis, a leading cause of morbidity and mortality worldwide[52]. During the development of atherosclerosis, macrophages are recruited to release growth factors and inflammatory mediators to induce VSMC dedifferentiation, which enables these VSMCs to migrate to the sub-intimal space where they contribute to the formation of a fibrous cap, where synthetic VSMCs secrete collagen to stabilize the plaque. In response to environmental signals, the synthetic state of VSMCs and macrophages within the fibrous cap promote apoptosis or lead to activation of various matrix metalloproteinases, which may induce rupture of the fibrous cap, leading to arterial thrombosis[53, 54].

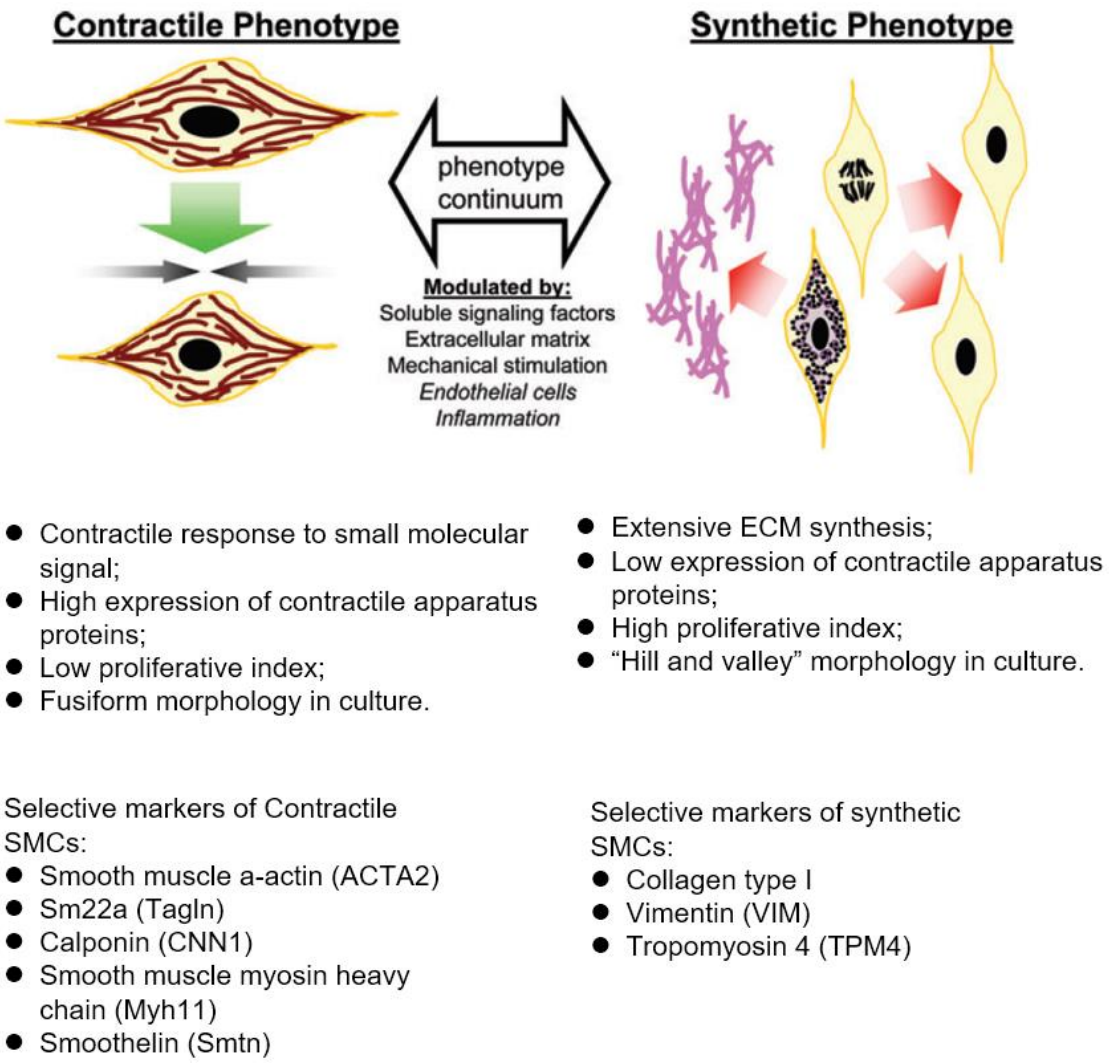

Figure 2. Characteristics of SMC plasticity between contractile and synthetic states. During vascular development or in the condition of injury, SMCs vary from a continuum from a contractile, quiescent state to a synthetic and proliferative phenotype, in which synthetic SMCs may synthesize proteins including collagen type I, VIM and TPM4. This is accompanied by the decreased expression of *Acta2, Tagln, Cnn1, Myh11* and *Smtn*, which is modulated by a variety of extracellular signals. Furthermore, contractile SMCs exhibit a more elongated morphology while the synthetic SMCs display a more roundish shape. Modified from[2].

The stimuli regulating VSMC phenotypic switching are numerous, including vascular injury, growth factors or inhibitors, mechanical force, inflammatory/oxidative stress as well as cell to cell or to matrix interactions [1, 50, 55]. Molecularly, these switches are mediated by a precisely coordinated molecular network, including the Myocd-SRF-CArG box complex, as well as components of TGFβ/BMP, Retinoid, Nox4-ROS, MicroRNAs, and Notch signaling pathways[51, 56, 57]. One of the most important and exciting findings of SMC phenotypic modulation is the discovery of myocardin (Myocd), a potent coactivator of serum response element (SRF), which

is exclusively expressed in cardiomyocytes and differentiated SMCs[58,59]. Virtually all smooth muscle specific genes contain at least two binding sites for SRF in the promoter regions. The Myocd-SRF regulatory module is a central component to mediate combinatorial interactions between activating and/or repressing factors that regulate most VSMC contractile genes[60]. Overexpression of Myocd in SMCs increases the expression of *Acta2* and calponin and is sufficient to induce the contractile phenotype of SMCs[61]. Blockade of SFR activity by a dominant negative SRF mutant resulted in decreased expression of SMC specific genes in proepicardial explants[62]. Besides the Myocd-SRF complex, accumulating evidences demonstrated that MicroRNAs (miRNAs) also play an essential role in SMC phenotypic switching. Several studies have indicated that some effects of these miRNAs on SMCs is mediated by suppression of pluripotency factors such as OCT4, SOX2 and KLF4 [63-65]. Our lab has demonstrated that pathways essential for promoting the VSMC contractile phenotype, such as Notch and Smad-signalling, act by stimulating expression of miRNA-143/-145, which play a crucial role for maintenance of the contractile phenotype[66-69]. Another study found that deletion of miRNA145 induced transdifferentiation of fibroblast into SMCs by derepression of Myocd. Furthermore, miRNA145 is sufficient to induce neural crest cells to differentiate into SMCs[63]. Loss of miRNA143 and miRAN145 results in reduced expression of contractile SMC genes and increased expression of synthetic genes[66]. Importantly, extensive studies have revealed that TGFβ strongly promotes SMC differentiation in several cell types, including mesenchymal and embryonic stem cells, lung fibroblasts as well as aortic SMCs[70-73]. These effects require Smad2/Smad3 and translocation of the Smad2/3/4 complex into the nucleus to initiate activation of several SMC specific genes by directly binding to the promoter region. In addition to such direct effects, TGFβ signaling indirectly regulates SMC phenotypic switching by modulating the expression of matrix remodeling proteins[74] and Myocd[75].

Taken together, SMCs represent a fascinating cell type. Our understanding of the mechanisms that modulate SMC phenotypic switching has been much improved over the past decades. However, processes that modulate the switch from a synthetic SMCs into a functional contractile state by circulating, hormone-like factors were not known. Investigation of the mechanisms responsible for VSMC phenotype switching is crucial to understand SMC-related vascular diseases to develop new therapeutics. It is clear that there are many important unanswered questions and challenges. Such questions and challenges highlight the importance of continued studies in this field.

1.4 VSMCs are intrinsically heterogeneous origin and function

The vascular system is heterogeneous and composed of arteries, veins, microvasculature and lymphatic vessels. It is increasing recognized that both in normal and disease conditions there is also a molecular, morphological and functional heterogeneity within the vasculature system. VSMC heterogeneity is reflected by differential expression of smooth muscle marker genes that vary between different vessel beds. Other types of heterogeneity include the stable difference in cell morphology, production of growth factors, organization at confluence as well as the ability of proliferation in serum- free medium, some of which may depend on the developmental stage and some may depend on conditions in the body[76].

The origin of VSMCs is far more diverse than originally thought. VSMCs originate from at least eight different sources of progenitors during embryonic development and exhibit sharp boundaries without intermixing of cells from different origins[77, 78]. Even within the same artery, distinct VSMC populations have been found in different segments, arising from distinct sources of progenitors[79]. For example, the descending aorta is different from the ascending aorta. Immunohistochemistry staining has revealed that in aortae, between adjacent VSMCs, there is a different expression of VSMC typical makers, adhesion molecules and gap junctional proteins[76, 80]. Fate mapping studies have suggested that VSMCs of the ascending aorta and aortic arch originate from neural crest, while mesoderm-derived VSMCs constitute the descending thoracic aorta, the abdominal aorta and distal portions of the internal carotid arteries[76]. The response of VSMC different signals also depends on the developmental origins[76]. For example, when exposed to TGFβ signalling, collagen production was enhanced in VSMCs derived from neural crest but did not change in VSMCs derived from the mesoderm. In another experiment, it was shown that DNA synthesis and cell proliferation were increased by TGFβ1 stimulation in neural crest-derived VSMCs, whereas in mesoderm-derived VSMCs, TGFβ1 inhibited cells growth[81]. It is essential to stress that the embryonic origin of VSMCs not only affects the expression of typical VSMC genes and response to stimuli but also affects predisposition to diseases[79, 82]. For example, atherosclerosis, aortic aneurysm and vascular calcification occur in specific locations in the vessel beds[83, 84]. The observed variation might result from the different developmental origins of VSMCs in different artery beds, as well as different vascular structures. The understanding of VSMCs heterogeneity is in its infancy and phenotypic heterogeneity as well as the origins and specific markers, are still largely unknown. Thus, new genetic tools will be valuable to target distinct subtype of VSMCs and a better understanding of the heterogeneity will provide an improved perspective for the identification of potential therapeutic, pharmacological targets or biomarkers that could act in the conditions of vascular heterogeneity.

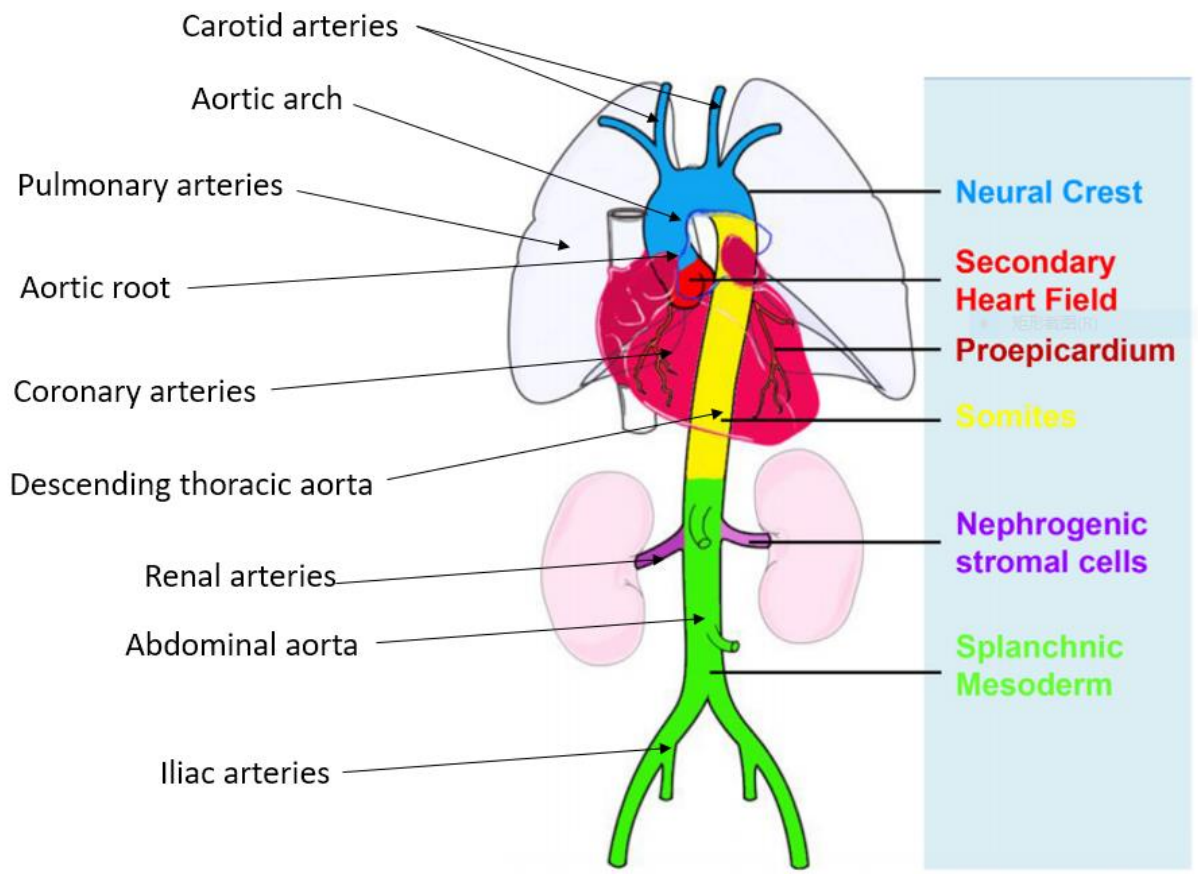

Figure 3. Developmental fate map of VSMCs.

VSMCs are originated from various origins, the different colors represent the different embryonic origins for VSMCs, as indicated in the figure. The yellow outline represents the local and systemic contributions by different sources of vascular stem cells. The fate map suggests a highly mosaic distribution of VSMC subpopulations in aorta and the major branch arteries. The lineage boundaries delineated are shown to approximation and may change with aging. Modified from[85].

1.5 BMP signalling pathway

The TGFβ and BMP signalling pathways elicits a number of cellular responses, such as differentiation, apoptosis, immune response, cell fate determination and growth arrest[86]. The past 20 years has witnessed a consistent set of researches in animal model and humans, which show the fundamental role played by TGFβ/BMPs signalling both in development and in maintaining homeostasis. Despite the knowledge gained, how the TGFβ/BMPs pathway intersects with other signallings and how this pathway regulates vascular developing remains enigmatic.

1.5.1 BMP family of ligands

The family of TGFβ ligands consists of more than 30 genes and over 20 molecules from the BMP subfamily. BMP ligands (some of them are also referred as growth and differentiation factors (GDFs)) are further subdivided into several groups based on sequence similarity, including BMP2/4, BMP5/6/7, GDF5/6/7 and BMP9/BMP10[87]. Among these ligands, 15 mammalian BMPs/GDFs have been identified as activators of typical BMP dependent responses, whereas others including BMP3 and Inhibin act as BMP antagonists because they inhibit BMP signalling by inactivation of BMP receptors[88,89]. Some ligands, including GDF1, GDF3 and GDF11, are essentially misnamed because they typically activate TGFβ signalling[90, 91]

BMP9 and BMP10 are members of the TGFβ superfamily and constitute a new BMP subgroup based on sequence homology. BMP9 was initially demonstrated to be involved in ectopic bone formation and later was shown to have roles in osteoblast differentiation and maintaining the neuronal cholinergic phenotype in the central nervous system[92]. BMP9 is secreted from the liver[93] and circulates as an activated protein. In contrast, *Bmp10* transcripts were found during mouse embryogenesis exclusively in the heart at E9.0, where it is expressed in the trabeculated part of ventricles and bulbus cordis but not in endocardial cells[94]. During later stages (E14.5), *Bmp10* expression is exclusively confined to the right atrium under physiological conditions[95-97]. Both proteins are present in the bloodstream with high concentration of approximately 0.5-15 ng/mL, which enable them to activate their receptors[96-98]. Receptor binding studies suggest that BMP9 and BMP10 serve as high-affinity ligands for the activin receptor-like kinase 1 (ALK1) and signal via the ALK1/BMPR2 complex, which also contains the accessory receptors endoglin and betaglycan to activate Smad1/5/8 signalling[99, 100].

1.5.2 BMP receptors and co-receptors

Signalling through the TGFβ receptor family occurs via ligand binding to heteromeric complexes consisting of type I and type II serine/threonine kinase receptors. The type I receptor determines signal specificity in the receptor complexes[101]. In vertebrates, seven type I receptors (termed activin receptor like kinases 1 through 7; ALK1-7), five type II receptors and two co-receptors exist. These receptors assemble in different combinations, which allow them to conduct signaling for all TGFβ superfamily members[87]. The type I receptors can be further divided structurally into three subgroups: ALK1/2 subfamily, ALK3/6 and ALK4/5/7 subfamily. ALK2, ALK3 and ALK6 are broadly expressed in various cell types, while *Alk1* has been described to be mainly expressed in ECs and in few other cell types[102, 103]. The ALK1/2 and ALK4/6/7 subfamily receptors phosphorylate Smad1/5/8, while ALK4/5/7 phosphorylate

Smad2/3 to activate TGFβ/Activin signalling [87]. The type I receptors including ALK1-4, ALK6 have a mass of approximately 55kD while type II receptors have a mass of 70-85kD and type III receptors of 200-400kD. Type III receptors contain two distinct members: a proteoglycan and a glycoprotein, known as betaglycan and endoglin respectively[104, 105]. Both type I and type II receptors share a similar structure and contain a short extracellular domain, a single transmembrane domain and an intracellular domain with serine-threonine kinase activity.

1.5.3 Smad and non-Smad signalling pathways

The serine/threonine kinase domain of type II receptors is activated by ligand binding, leading to phosphorylation of the glycine-serine domain of type I receptors, which activates their kinase activity[106]. Activation of type I receptors initiates intracellular signalling through phosphorylation of a set of receptor-regulated Smads (R-Smad), which subsequently form a complex with a Co-Smad (Smad4). The R-Smad/Co-Smad complex enters the nucleus, where it modulates the transcription of target genes by directly binding to Smad-binding elements[107], or indirectly through interacting with DNA-binding transcription factors, or by the association with co-activators/inhibitors and histone-modifying factors[108]. Depending on different type I receptors, different Smad signalling cascades are activated. In most cells, TGFβ signalling pathway involves the type I (TGFβR1/ALK5) and type II (TGFβR2) receptors, which induce Smad2/3 phosphorylation. In contrast, BMPs signal through ALK type I receptors and type II receptors, such as activin receptor type 2A (ACVR2A), ACVR2B and bone morphogenetic protein type 2 receptor (BMPR2), to phosphorylate of Smad1, 5 and 8[109]. Some BMPs are also suggested to bind to type II and type I receptors in a cooperative rather than in a step wise way[110]. It was also shown that receptors of type II and type I form homodimers, because the auto-phosphorylated type II receptor recruits type I receptor[111]. Smad complex activation is antagonized by inhibitory I-Smads (Smad6 and Smad7), which compete with R-Smads for type I receptor interaction and by recruiting specific ubiquitin ligases or phosphatases to the activated receptor complex, thereby targeting it for proteasomal degradation or dephosphorylation respectively. Smad7 inhibits all TGFβ/BMP superfamily members, while Smad6 is more prone to inhibit BMP family members[112, 113]. In addition to canonical signalling through Smad phosphorylation, the TGFβ/BMP pathway also involves Smad-independent regulation of cellular outcomes through the direct modulation of prototypical signalling mediators, including mitogen activated protein kinases (MAPKs), such as Erk5, Eer1/2, P38, SAPK/JNK or CREB[114]. These non-Smad pathways are important to create diversity and fine-tuning of signals in the TGFβ/BMP signaling pathway[115].

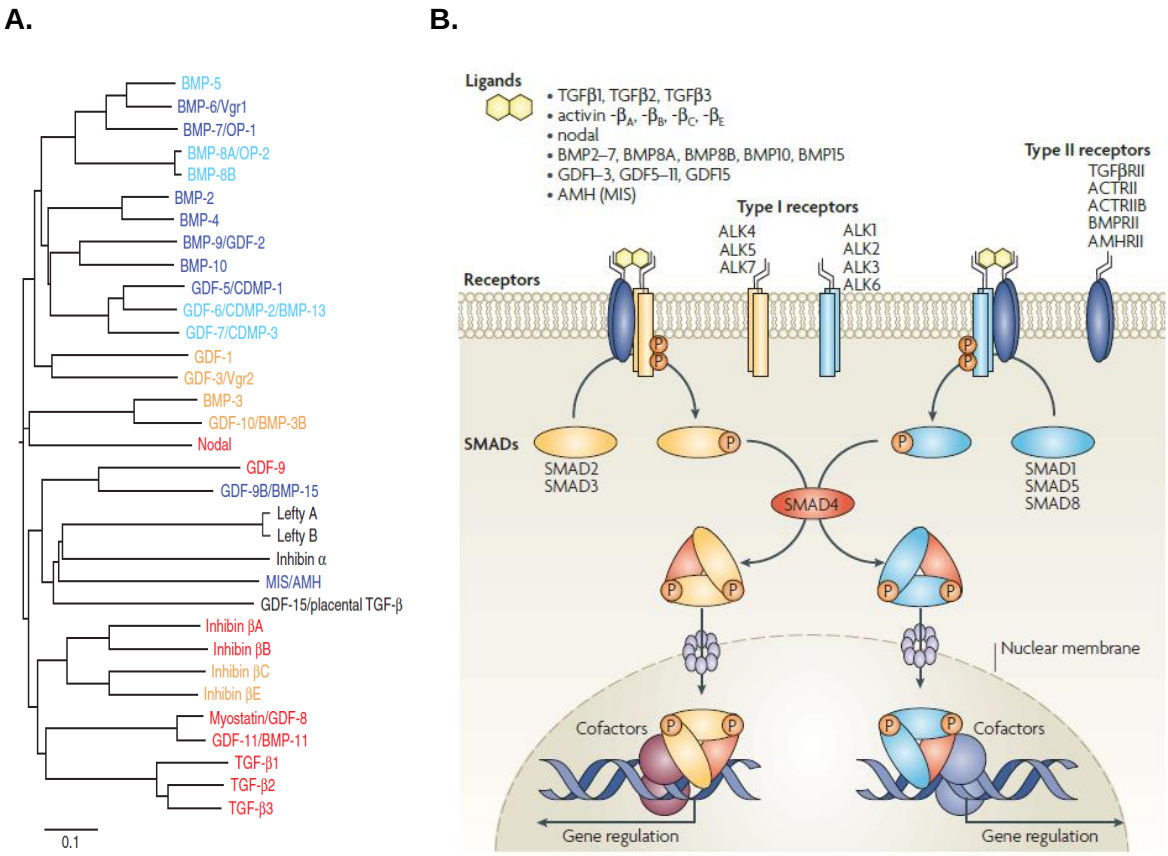

Figure 4. Phylogenetic tree of TGFβ/BMP family proteins and schematic representation of the TGF-β/BMP induced Smad signalling pathway.

(A.) Phylogenetic tree of the 33 TGFβ/BMP family polypeptides in human, revealing the high degree of sequence similarity between BMP9 and BMP10. Ligands that signal via activin or TGFβ activated R-Smads or BMP activated R-Smads are shown in red or blue, respectively. Ligands that activate two different R-Smads but receptors and Smad pathways have not fully understood are shown in orange or light blue. (B.) TGFβ or BMPs interact with surface receptors to induce heteromeric complex formation between type II and type I receptors. This process is mediated by type III receptors or co-receptors. After being phosphorylation by type II receptor, the type I receptors phosphorylate Smad1/5/8 or Smad2/3, which form heterodimeric complex with Smad4 and this complex translocates to the nucleus and regulates gene expression. Inhibitory Smad6 and Smad7 block receptor activation of Smad1/5/8 and Smad2/3. Modified from[116].

1.6 The role of BMP signalling in vascular homeostasis

Despite intense research efforts in the past, the role of TGFβ and BMP signalling for cardiovascular development, homeostasis and disease formation is still not clear. The importance of BMP pathway in ECs has been known for years and BMP signalling has been found to promote endothelial specification, venous differentiation and mediates shear and

oxidative stress[117]. Knockout of TGFβ type I receptor, TGFβ type II receptor[118], BMP type I receptor[7] or the signalling molecules Smads[119] results in embryonic lethality in part due to failure of differentiation of mesenchymal precursors into VSMCs. These findings underscore the essential and crucial roles of BMP signalling in regulating VSMC formation, maintenance and remodelling.

BMP9 and BMP10 proteins share 65% sequence identity[120]. It has been hypothesized that both proteins have overlapping functions during embryonic and postnatal angiogenesis. To study the potential role of these two proteins in angiogenesis, a BMP10 monoclonal neutralizing antibody was injected into BMP9 knockout pups to inactivate BMP10. The authors claim that the loss of BMP9 and BMP10 in neonatal mice results in delayed vascular plexus formation, reduced retinal vascular expansion, increased vascular density and enlarged vascular tubes compared to single BMP9 mutants[98]. Other studies suggested that BMP9 and BMP10 play redundant roles in retinal vascularization[16, 98] and proper closure of ductus arteriosus[17]. Although such approaches are informative, they do not address effects of the long lasting loss of BMP9/BMP10. Moreover, neutralization of BMP10 by antibody injection may result in unwanted side effects or suffer from problems with antibody specificity. To further address the overlapping function of these two proteins, one group generated a mouse strain in which the coding region of *Bmp10* was substituted by the coding region of *Bmp9* (*Bmp10*$^{9/9}$)[16]. Unlike the *Bmp10*$^{-/-}$ embryos, which developed severe angiogenic defects at E9.5, the *Bmp10*$^{9/9}$ embryos displayed no obvious defects by E14.5. However, from E14.5, the ventricular walls were thinned showing pericardial edema and by E17.5, some hearts had ventricular septal defects and altered shape, which resemble the hearts of *Bmp10*$^{-/-}$ embryos. Since in the early stage, no obvious defects were observed, they hypothesized that the later vascular symptom was a secondary effect of the cardiac defects. Taken together, previous research suggests that BMP9 and BMP10 are crucial for vascular remodeling and BMP9 is able to replace BMP10 but BMP10 still has a unique role in cardiac development, which could not be substituted by BMP9.

BMP9 and BMP10 bind ALK1 as well as the endoglin receptor with high affinity[95]. Genetic inactivation of *Alk1* in mice results in embryonic lethality at E11.5[121, 122]. ALK1 is a crucial receptor for vessel angiogenesis, as mice lacking ALK1 lack mature vessels and showing interconnected knots of similar sized endothelial tubes at E9.5. And at E10.5. Yolk sacs of *Alk1* mutants are avascular with few SMCs, displaying severe signs of vascular dilation[6, 7]. The expression of VSMC specific genes, such as *Acta2* and *Tagln*, is significantly reduced in tissues of ALK1 mutants where these genes are normally highly expressed, such as dorsal aorta, heart and somite. Moreover, SMCs are mislocalized in *Alk1* mutants and are not present in the perivascular region[6, 7]. Urness et al. attributed the drastic loss of SMCs to the downregulation of arterial specific markers, reduced attachment as well as reduced recruitment

of SMCs, which leads the vascular dilation and fusion of vessels causing arteriovenous shunts. Since constitutive knockout of *Alk1* causes embryonic lethality, a conditional knockout of *Alk1* was generated. The loss of *Alk1* at E15.5 led to similar phenotype observed in earlier *Alk1* mutants and the mice presented dilated and torturous vascular networks with signs of arteriovenous malformations (AVM)[123], indicating that arteries lost the arterial specification. When ALK1 was inactivated between E16.5-17.5, the pulmonary arteries displayed a disrupted mesh of dilated, fused arteries and ACTA2 staining suggested a reduction in the number of SMCs[123].

To figure out whether the loss of VSMC identity and specification is a direct consequence of cell autonomous malfunctions within VSMCs or a secondary effect caused by other cells, such as ECs, *Alk1* was specifically inactivated in ECs. The loss of ALK1 in ECs resulted in postnatal lethality at postnatal day 5 due to hemorrhagy, which was also observed in other *Alk1* mutants. Inactivation of ALK1 in ECs also showed vascular dilation and tortuous arteries, which displayed arteriovenous shunts and depleted SMCs identity[8]. The poor recruitment of SMC precursors caused by inactivation of *Alk1* indicated that the signalling in endothelium may be essential for initiation of SMC differentiation. However, *Alk1* transcripts have also been observed in VSMCs[121] and researches have reported that ALK1 regulated SMCs differentiation and recruitment directly *in vitro*. Along the same line, enhanced levels of *Alk1* correlate with increased expression of *Acta2*[124, 125]. Thus, it is likely that ALK1 signals in SMC precursors may be directly involved in the regulation of SMC proliferation and differentiation.

To better understand the role of ALK1 in adults after the establishment of vascular system, ALK1 was inactivated with a global and tamoxifen inducible Cre (*Alk1*^{iCre}), which resulted in a similar phenotype as observed in all previous *Alk1* loss-of-function models. The arteries were dilated with increased permeability and signs of AVM were observed[8]. In a wound healing model, which triggers *de novo* vascular remodeling, control mice could develop large number of growing vessels toward the wound. In contrast, the *Alk1*^{iCre} mice only formed few vessels. With other words: ALK1 has an essential role in SMC differentiation and vascular formation.

Unlike the type one and type two receptors, the type III receptors presented by betaglycan and endoglin(Eng) lack a signalling domain, although both play important roles in vascular development and diseases[126], in part by potentiating BMP signalling or exerting their action through preventing binding of ligands to receptors[100, 120, 127]. Betaglycan enhances BMP signalling by mediating trafficking and cell localization of interacting receptors[128], while it has also been shown to suppress BMP2 and BMP7 signalling by sequestrating BMPR2 into an inactive form[88]. Endoglin enhances BMP7 and BMP9 dependent Smad1/5/8 responses, although the mechanism behind is unknown[120, 129]. Constitutive *Eng* mutants possesses endothelial tubes lacking VSMC coverage by E8.5 in yolk sacs. Since endoglin regulates the

BMP/ALK1 but not TGFβ signalling[130], this finding further reiterates the involvement of BMP signalling in the maintenance of vascular homeostasis. Immunostaining revealed that the first organ system affected by the loss of endoglin was the vascular system. In particular, vascular development was disrupted by E9.5 as demonstrated by poor formation of VSMCs. Electron micrographs of E9.5 embryos demonstrated the absence of supporting cells, pericytes and VSMC precursors around the endothelium of capillary network[131]. Heterozygous knockout of endoglin in adult mice displayed signs of telangiectasia with recurring nose or mouth hemorrhage. Specific deletion of endoglin in ECs (*Eng*^{iECs}) led to denser capillary plexus and reduced vascular outgrowth in retina[132], recapitulating the defects observed by inactivation of BMP9 and BMP10. In retinas of *Eng*^{iECs} pups, AVMs were detected frequently and the vessels were ruptured with bleeding. It is evident that despite the absence of a signalling domain, betaglycan and engoglin play essential roles in SMC differentiation and vascular stability.

TGFβ and its receptors also play crucial roles in angiogenesis and vascular homeostasis. Mice lacking two alleles of TGFβ died around E10.5 due to abnormal vascular development in yolk sac, caused by the absence of mature differentiated VSMCs. In addition, when one allele of TGFβ was deleted, the levels of VSMC specific genes was strongly reduced[133]. In adult rats, expression of VSMC specific genes was correlated with TGFβ concentration, suggesting that TGFβ dynamically regulates the contractile state of VSMCs during adult stages[134]. TGFβ receptor II is essential for TGFβ signalling transduction, making it the best target to manipulate this signalling pathway. Specifically inactivation of this receptor in SMCs with *Sm22a-Cre* driver resulted in embryonic lethality with a significant decrease in the number of smooth muscle a-actin positive VSMCs[135]. Molecularly, studies had shown that Smad2/Smad3 interact with promoters of SMC-specific genes at putative Smad binding elements. Specifically, one group demonstrated that Smad3 recruited Myocd to *Tagln* promoter and directly regulated *Tagln* expression[75]. Other reports suggested a indirectly effect on VSMCs by promoting or suppressing expression of proteins exerting a secondary effects on VSMC differentiation, such as matrix remodelling proteins and reactive oxygen species[136, 137]. For example, one study showed that Smad3 physically interacted with SRF, which is the key player to regulate VSMC gene expression[73].

Smad4 is a central mediator of TGFβ/BMP signalling and a disruption of Smad4 in mice led to early embryonic lethality with defects in epiblast proliferation, egg cylinder formation and mesoderm induction[138]. EC specific deletion of Smad4 in mice also resulted in embryonic lethality at E10.5 with impaired tube formation and impaired development of VSMCs[139]. Importantly, inactivation of Smad4 in SMCs using highly specific *Sm22a-Cre* and *Smmhc-Cre* mice, without disturbing the endothelium, also resulted in reduced VSMC proliferation and attenuated differentiation, causing vascular leakage and embryonic lethality[47]. The structure of hearts was normal compared to controls and therefore embryonic lethality was likely caused

by the loss of VSMC identity. Vascular defects were observed before establishment of embryonic circulation whereas cardiogenesis was not affected. Thus, it was unlikely that the failed VSMC development and arrested angiogenesis were secondary to impaired blood flow[138]. There is a broad consensus that both TGFβ and BMP signalling directly participate in the complex mechanisms of mid-gestation VSMC formation. Since Smad4 is the regulator of both BMP and TGFβ activated signalling, the relative role of Smad4 in mediating BMP and TGFβ dependent effects in vascular system is unknown.

Constitutive *Smad5* mutants died early in gestation with defects in vascular organization and VSMC recruitment, which resembles defects observed in ALK1, ENG null mice and BMPR2 knockout embryos, suggesting that Smad5 may function in the same way[119, 140]. However, conditional deletion of Smad5 in ECs or SMCs using *Tie2-Cre* or *Sm22a-Cre* respectively demonstrated that the vessel wall was normal during embryonic vascular development and that adult mice are fertile and healthy[141]. This result suggests a functional compensation for the loss of Smad5 during later developmental stages. Unlike the constitutive Smad5 knockout mouse, Smad1 null mouse only displayed minor defects in the yolk sack vasculature, which might be a secondary effect from chorioallantoic membrane fusion[142]. Furthermore, Smad8 null mice were also viable without obvious defects in vasculature[143], suggesting that Smad1 and Smad8 possess a redundant role in embryonic vascular development. Taken together, these Smad1, Smad5 and Smad8 own non-redundant roles at different stage of vascular development and should not be considered as exchangeable.

In summary, TGFβ/BMPs and their downstream signalling molecules are irreplaceable for VSMC differentiation during vascular formation and maintenance, which has been demonstrated by numerous of studies. However, many critical biological questions pertaining to BMP signalling still need to be answered. For example, it has not been fully explored whether TGFβ/BMPs directly affect the fate of VSMC *in vivo* or act indirectly via signals from ECs. Similarly, the Smad complex may bind directly to promoters of typical SMC genes or regulate expression of such gene indirectly by binding to additional regulators, such as SRF. In addition, the extensive cross-talk with other signalling pathways, such as the Notch and Hippo pathways, needs to be fully elucidated. In the end, a better understanding of BMP signalling should facilitate the treatment of associated diseases and may lead to the development of efficient therapies.

1.7 The role of BMP signalling in pulmonary arterial hypertension

Pulmonary hypertension (PH) is a severe life-threatening disease characterized by progressive increase of pulmonary vascular resistance. PH was initially grouped as an idiopathic disease but more recent classifications define five different categories, based on similarities in

pathophysiological mechanisms, clinical presentation and therapeutic options[5]. One category, named pulmonary arterial hypertension (PAH), has an unclear aetiology and includes both familial and sporadic forms of the disease. The pathogenic mechanisms underlying PAH are only partially understood, but it is assumed that imbalances of vascular and environmental factors, including hypoxia, anorexigens, central nervous system (CNS) stimulants and associated conditions play crucial roles[144]. Such an imbalance results in excessive proliferation of PASMCs, adventitial fibroblasts, ECs as well as increased resistance to apoptosis. Thus, pulmonary circulation pressure will increase and the increased pressure enhances right ventricle afterload, leading to maladaptive right ventricle hypertrophy (RVH)[145] and regional ischemia, dedifferentiation of cardiomyocytes, accumulation of inflammatory[146] and ultimately right ventricle failure[5].

It is commonly assumed that endothelial dysfunction resulting in decreased production of endothelium-derived vasodilators and increased expression of vasoconstrictors, leads to pulmonary vasoconstriction and contributes to VSMC and adventitial cell hypertrophy[147]. Therapies to PAH are limited and are mainly targeting vasoconstriction and reversal of vascular cell proliferation to decrease blood pressure and reduce afterload. Although these treatments slow down the progression of the disease, they do not provide a cure. Unfortunately, no therapies are capable to completely reverse PAH[148]. There are some potential anti-proliferative inhibitors to treat PAH[149]. However, in clinic, only few have been approved because of toxicity or lack of efficacy. The median survival of PAH is only 2.8 years without treatment and in the past 20 years, even with new developed drugs, the 3 year survival is still below 60%[150]. The exact molecular mechanisms contributing to progression of PAH are still poorly understood. Deciphering the mechanisms that balance pulmonary vasodilatation and vasoconstriction represents an essential component for the development of new therapeutic approaches for the treatment of PAH and right ventricle hypertrophy.

TGFβ/BMPs signalling controls and regulates numerous biological processes, including cellular proliferation, migration, apoptosis and differentiation. Genetic deletion of several components of this signalling pathway results in embryonic lethality due to abnormal vascular formation and cardiovascular dysfunction. It is not surprising that perturbation of this signalling is associated with PAH. Patients with heritable forms of PAH often have mutations in genes encoding receptors of the TGFβ/BMP receptor superfamily, in particular BMPR2, ALK1, ENG. Familiar forms of PAH are often associated with mutations in BMPR2 gene[151, 152] , suggesting that this family plays a central role in the onset and progression of PAH. In fact, the first link between BMP signalling and PAH was the observation that heterozygous germline mutants of *Bmpr2* gene are prone to PAH[145, 152]. Around 70% of patients with familial and 20% with idiopathic PAH possess mutants in *Bmpr2*[153]. Recently, one study from China based on whole exome or whole genome sequencing of DNA from 331 idiopathic PAH patients compared to

10508 controls, revealed that mutants in BMPR2 (19.5%) were the most common mutation associated with PAH[154]. In animal models, BMPR2 mutation mice present increased arterial blood pressure and increased vascular resistance, resulting from increased VSMC recruitment[155]. In addition, these mice exhibited a severe inflammatory response and were more susceptible to hypoxia-induced PAH[156]. *Bmpr2* is highly expressed in both ECs and VSMCs and studies found that genetic ablation of BMPR2 in pulmonary artery endothelial cells (PAECs) or PASMCs predisposed mice to develop PAH[157, 158]. In the past 20 years, the protective roles of BMPR2 on pulmonary vascular have been well studied. Recent studies indicate that manipulation of BMPR2 at different levels including genetic therapies, translational regulation, protein delivery and modulation downstream signalling represents a promising approach to restore normal vascular function[159-161].

Besides BMPR2 mutations, other variants in the TGFβ/BMP family genes also contribute to familial PAH. In mouse models, ALK1 and ENG mutants develop PAH with signs of increased right ventricle systole pressure, right ventricle hypertrophy and decreased pulmonary artery density[162, 163]. Moreover, mutations in either of these two receptors are found in HHT-associated PAH[164]. Importantly, ALK1 mutation carriers are strikingly younger at PAH diagnosis and show lower survival with rapid disease development compared to BMPR2 mutations[165]. Although ALK1 mutation carriers only account for a rare subset of PAH patients, the poor prognosis makes it necessary to identify affected patients earlier when medical administration may be more efficient[165].

Bmp9 is expressed in the liver while *Bmp10* is mainly expressed in the right atrium, directly serving the pulmonary artery and the lung. Since BMP9 and BMP10 are found in blood circulation with high concentration, it seems likely that BMP9 and BMP10 might play a role in PAH. Researches have shown that BMP9 and BMP10 inhibits human mammary EC proliferation as well as migration via ALK1 signalling[100, 120]. Indeed, the study by Wang[154] identified of heterozygous mutations in BMP9 in 6.7% of PAH cases, making BMP9 the second most common cause of PAH in the Chinese cohort. This report suggests that BMP9 mutations is a major culprit for PAH and raises the possibility that BMP10 mutations may also cause PAH. At present, it is not clear whether ALK1 and its corresponding ligands BMP9 and BMP10 protect or promote adverse vascular remodeling during onset and progression of PAH.

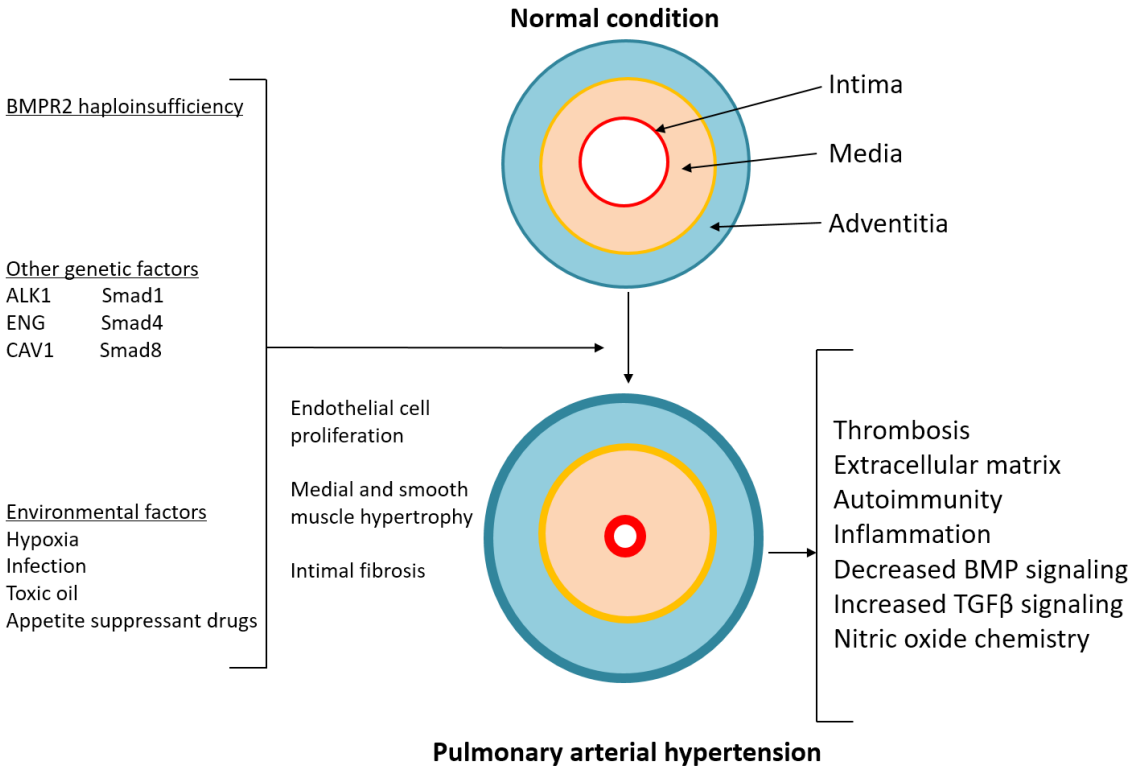

Figure 5. Causes and effects of pulmonary arterial hypertension.
Schematic representing the genetic and environmental factors that lead to PAH and the biochemical readouts associated with PAH. BMPR2 haploinsufficiency is the major genetic hallmark of PAH, although other proteins such as ALK1, Smad1, Smad4, Smad8, ENG and CAV1 fall into the same category. PAH is characterized by vascular tone imbalance, increased proliferation of PASMCs, adventitial fibroblasts and PAECs. Adverse remodeling includes thrombosis, ECM deposit, autoimmunity, decreased in BMP signalling and increased in TGFβ signalling.

It is assumed that endothelial dysfunction (decreased synthesis of vasodilators and increased expression of vasoconstrictors) results in severe pulmonary vasoconstriction and contributes to VSMC and adventitial fibroblast hypertrophy[5]. Several studies have highlighted the potential roles of the BMP signalling in regulation of the vascular tone and contractile/synthetic states of VSMCs via regulation of apelin in the endothelium, which is considered as a vasoreactive mediator of pulmonary vasculature[12, 166, 167]. Apelin is a catalytic substrate for Ang II and activates APJ, a seven-transmembrane G protein-coupled receptor, which shows significant homology with the Ang II type 1 receptor (AT1R). Apelin is localized in vascular ECs and *Apj* is expressed in both ECs and SMCs. Several studies suggested that apelin is regulated by hypoxia inducible factor -1α (HIF1a) and BMPR2[159, 160]. The apelin-APJ system represents a novel neurohormonal signalling pathway of modulating PAH by regulating several critical factors involved in the pathogenesis of PAH, such as Krűppel-like factor 2 (KLF2), endothelial

nitric oxide synthase (eNOS), and microRNAs (miRNAs)[168], *In vivo,* apelin knockout mice displayed remarkable loss of microvasculature and developed more severe PAH symptom compared to controls when subjected to hypoxia treatment[169]. Furthermore, disruption of apeln-APJ signalling in PAECs was observed in PAH patients as well as in rodent PAH models based on monocrotaline (MCT), chronic hypoxia, and SU5416/hypoxia treatment[168, 170]. Recently, it was shown that apelin deficiency in PAECs resulted in increased expression of *Fgf2* and its receptor *Fgfr1*[171]. FGF2 and FGFR1 promote hyper-proliferation of PAECs and PASMCs, which are hallmarks of aberrant vascular remodeling and PAH progression[172]. Taken together, these studies underscore the potential important role of apelin-APJ in vascular integrity. Disruption of this signalling may lead to progressive vascular remodeling.

It has been also suggested that up-regulation of endothelin (ET-1), another vasoconstrictor mediators, contributes to PAH progression due to regulation of EC migration[12, 173]. Studies showed that TGFβ induced *endothelin* expression via the ALK5/Smad5 axis and that parts of the anti-migration and anti-proliferation effects of TGFβ on ECs are mediated by ET-1. Furthermore, BMP9 has been shown to increase levels of ET-1 via the canonical Smad1/5/8 axis in human pulmonary microvascular ECs[12, 174]. In addition, BMPR2 dysfunction perturbs the level of ET-1 in pathogenesis of PAH[175]. Thus, the TGFβ/BMP signalling as well as several downstream genes, such as apelin, APJ and ET-1, are attractive therapeutic targets for PAH. Unfortunately, our current understanding of the molecular mechanisms regulated by BMPs and their exact pathogenic roles during PAH progression is still incomplete.

1.8 Thesis aim and overview

VSMCs show a remarkable phenotypic plasticity reflecting their ability to acquire contractile or synthetic states. To date, little is known about the role of BMP9 and BMP10 in vascular development and how they control vessel tone. Since *Bmp10*$^{-/-}$ mice die during embryonic development, it is impossible to study the functional role of BMP10 in adults using germline mutant mice. Conditionally inactivation of BMP10 in adult mice on a BMP9 mutant genetic background provides the opportunity to disclose the main function of BMP9/BMP10 in the cardiovascular system.

The aim of this thesis was to use different mouse strains and *in vitro* experiments to uncover the role of BMP9 and BMP10 in VSMC differentiation and maintenance of the contractile state. To achieve this goal, I wanted to investigate the vasculature of mice, lacking BMP9 and BMP10, or ALK1 in SMCs. In a complementary approach, I wanted to evaluate mice that overexpress *Bmp10* in ECs and *Smad7* in SMCs. A further aim was to study the molecular mechanisms underlying the action of BMP9/BMP10, for which I used dedifferentiated PASMCs that were treated with BMP9/BMP10 and analyzed by RNA-seq and ATAC-seq. With these readouts, I

aimed to explore novel roles of BMP9 and BMP10 signalling in VSMC differentiation and vascular tone modulation. Specifically, I pursued the following questions:

- how BMP9/BMP10 regulate VSMC differentiation?
- is there a synergism of BMP9 and BMP10 during this process?
- does BMP9 and/or BMP10 protect or promote PAH?
- does BMP9/BMP10/ALK1 signalling promote vascular contractility?
- are there direct versus indirect effects of BMP9/BMP10 on VSMCs?
- what is the impact of YAP/TAZ/TEADs signalling on the BMP9/BMP10/ALK1 pathway in the regulation of VSMC plasticity?

2 Materials and Methods

2.1 Generation of transgenic mice

All animal experiments were done in accordance with German animal protection laws and were approved by the local governmental animal protection committee. The *Bmp10*-lacZ reporter mice were generated via BAC transgenesis. A *Bmp10* containing BAC (bMQ438F3) from the mouse bMQ BAC library[176] was modified by insertion of a lacZ-polyA|FRT-PGK-Em7-neo-FRT cassette immediately behind the BMP10 start codon by homologous recombination in E. coli SW102. The FRT-flanked neomycin cassette was deleted in 294-Flp bacteria (Gene Bridges). All sequences were verified by sequencing or restriction enzyme digestion. Genotyping was performed on DNA from tail biopsies, using lacZ specific primers (lacZ fwd1: 5'-CCGACGGCACGCTGATTGAAG-3', lacZ rev1: 5'-ATACTGCACCGGGCGGGAAGGAT-3'). The *Bmp10-LacZ* reporter strain was generated by Dr. Sandra Swist, Max Planck Institute for Heart and Lung Research.

To generate the conditional *Bmp10* allele, a *Bmp10* targeting vector containing loxP sites flanking exon 2, which encodes for the active mature BMP10 peptide, was introduced into ES cells. The BMP9 gene was targeted using a vector obtained from the EUCOMM consortium. *Bmp9* and *Bmp10* mutant ES cells were injected into blastocysts using standard procedure. Resulting chimeras were crossed to C57BL/6 mice. Heterozygous mutant animals were identified by Southern blot and PCR analysis. BMP9 and BMP10 double knockout mice were generated by crossing *Anf-Cre^{pos}/Bmp10$^{loxP/loxP}$* with *Bmp9$^{-/-}$* mice on a C57/BL6 background to yield *Anf-Cre^{pos}/Bmp10$^{loxP/loxP}$/Bmp9$^{-/-}$* (*Bmp9/10^{dko}*) mice. *Bmp9/10^{dko}* mutants were backcrossed to C57BL/6 mice for 5 generations. . The conditional *Bmp10* allele as well as the constitutive *Bmp9* allele strain were generated by Dr. Sandra Swist, Max Planck Institute for Heart and Lung Research.

Transgenic mice conditionally overexpressing murine *Bmp10* and human V5-tagged Smad7 were generated using a modified *Rosa26* targeting vector in which the SA-site of pBigT was replaced by a synthetic CAG promoter. cDNAs encoding the open reading frames were PCR amplified to add NheI and NotI sites, introduced into the pBigT-CAG vector and subsequently into the pRosa26-PA construct using PacI and AscI restriction sites. Correctly targeted ES cells were identified by Southern blotting and injected into C57BL/6 blastocysts. Conditional Cre-mediated overexpression of 1. *Bmp10* in the endothelium, 2. *Smad7* in SMCs and 3. *Atoh8* in SMCs and all tissues was achieved by breeding 1. *Rosa26^{iBmp10}* mice with endothelial specific *Cdh5-CreERT2, 2. Rosa26^{iSmad7}* with SMC specific *Sm22-Cre* as well as *Smmhc-CreERT2* strains and 3. *Rosa26^{iATOH8}* with *Sma22-Cre* and *Cmv-Cre*, respectivlely. The *Rosa26^{iBmp10}, Rosa26^{iSmad7}* and *Rosa26^{iATtoh8}* alleles were kept heterozygous in all experiments. Aged-matched wildtype littermates expressing Cre-recombinase were used as controls. The *Bmp10,*

Smad7 and *Atoh8* overexpression strains were generated by Dr. Andre Schneider, Max Planck Institute for Heart and Lung Research.

Tamoxifen was dissolved in corn oil at a concentration of 20mg/mL. Mice were injected intraperitoneally with 0.75mg tamoxifen/10g body weight. To inactive BMP10 in BMP9 mutants (*Bmp9*$^{-/-}$*/Bmp10*^{iMhc}), tamoxifen was injected daily for 7 continuous days. Mice were analyzed 3 weeks later (day 28 after the first injection). To activate *Bmp10* in ECs (*Rosa26*^{iBmp10}), tamoxifen was injected once and samples were analyzed 10-14 days later. To activate Smad7 in SMCs (*Rosa26*$^{Smmhc\text{-}iSmad7}$ mice), tamoxifen was injected daily for 10 days and samples were analyzed 45 days later from first injection.

2.2 Telemetric blood pressure measurements

Blood pressure was measured using implantable telemetric transmitters (DSI, TA11PA-C10) inserted into the left carotid artery. Data was set to record every 15 minutes for 3 minutes. Blood pressure was recorded 7 days before and 14 days after tamoxifen injection. Data were sampled with Dataquest A.R.T. 4.0 with a sample rate of 500 Hz and with a filter cut-off of 100 Hz. Data reduction was performed using Dataquest A.R.T. 4.0 by calculating the reduced mean for the sampled signals.

2.3 Right ventricle systolic pressure (RVSP) measurements

RVSP was measured as previously described[177]. Briefly, mice were anesthetized, intubated, and placed in a supine position on a homeothermic plate (AD Instruments, Spechbach, Germany), connected to an animal ventilator (MiniVent type 845, Hugo Sachs Elektronik, March-Hugstetten, Germany). Body temperature was kept at 37°C and controlled by an anal probe. Right ventricles were exposed and catheterized through a small tunnel created by a 25 G needle with a high-fidelity 1.4F micromanometer/Mikro-Tip Pressure catheter (Millar Instruments, Houston, TX). Data were collected and analyzed using the PowerLab data acquisition system (MPVS-Ultra Single Segment Foundation System, AD Instruments) and LabChart 7 for Windows software.

2.4 Isolation of mouse embryos

After mating, female mice were checked for the vaginal plug formation for continuous 3 days. The day of the plug formation is considered as embryonic day E0.5. *Rosa26*$^{Sm22\text{-}iSmad7}$ embryos were isolated at E10.5 by cervical dislocation of the pregnant female. The abdominal cavity was opened and the uteri was removed and transferred to PBS. A small part of tails was used for genotyping.

2.5 Pressure myography

Pressure myography experiments were performed as described by Luo F et, al[178]. Mesenteric arteries were removed from the third or fourth branch by gently peeling away the adventitia and placed into ice-cold Krebs buffer (1% BSA, 118.1 mM NaCl, 2.5 mM $CaCl_2$, 4.8 mM KCl, 1.2 mM $MgSO_4$, 1.2 mM KH_2PO_4, 25 mM $NaHCO_3$, 9.3 mM glucose, and 0.026 mM EDTA, pH 7.4).Mesentery arteries were attached to two glass micropipettes, mounted onto a myograph (DMT, Denmark) and secured with a 10.0 nylon suture at both sides. The external diameter of the mesenteric artery was visualized and recorded with a camera using MyoView software (Danish Myo Technology A/S). The temperature of the chamber was constantly kept at 37°C. Perfusion was initiated with Krebs buffer at ≤5 uL/minute to remove any residual blood. The artery was pressurized to 20 mmHg under no-flow conditions and incubated for 30 minutes followed by perfusion for 1 hour with Krebs buffer with or without BMP9 and BMP10 at a concentration of 1 ng/mL and 5 ng/mL, respectively. After perfusion, arteries were fixed in 4% PFA for 20 minutes and embedded in OCT.

2.6 Cell culture

2.6.1 Isolation of adult pulmonary arterial smooth muscle cells (PASMCs)

PASMCs were isolated according to the protocol described by[179]. Anaeestetise and heparinise the animal interperitoneally and place one incision into the right heart ventricle and insert the catheter into the pulmonary artery and another incision into the left ventricle for drainage. Lung perfusion was performed with 3 mL PBS followed by instillation with 3 mL Iron-Agarose (0.5% Iron III Oxide and 0.5% Agarose in Medium 199). Subsequently, agarose (1% Agarose in Medium 199) was instilled into the trachea until the lung is completely filled. After a short time the catheter was pulled out, the ligature was closed and the lung was removed from the thorax and incubate in the cold PBS for 10 minutes. After removal of the heart, aorta, oesophagus and connective 1-2 mL PBS was added to the lung lobes and mince the lobes into small pieces with scalpels. Pipette the minced lung slurry into sterile 50 mL conical tube, wash with 10-30 mL PBS and place the tube into the magnetic holder (Invitrogen, MPC-1 Magnet, 12001D). Wait shortly and aspirate and discard the liquid. After washing, resuspend the lung pellet into 3 mL Collagenase type 2 (80 U/mL in Medium 199 + 1% Pen/Strep) and incubate pellets for 1 hour at 37°C. After incubation, homogenize the tissue-Collagenase solution by aspirating and releasing several times through 15G needles and 18G needles. Wash via magnetic holder 3 times with PromoCell medium (C-22062) containing supplements (C-39267) and pour the pellet into a culture dish. Four days later, pour the supernatant into a new conical tube and wash the pellet via magnetic holder 3 times with PBS and culture the iron-containing pellet with PromoCell medium containing supplements. Once there are cells grown around the particles, the iron can be washed off and either seeded again or thrown away. After iron particle removal

media will be changed every 2 days.

To starve these PASMCs, the media was changed to Promocell medium without supplements for 24 hours. For RT-qPCR analysis, PASMCs were stimulated in supplement-free Promocell medium with BMP9 (R&D 5566-BP-010) and BMP10 (R&D 6038-BP) at 1 ng/mL and 5 ng/mL respectively for 6 hours (for the expression of *Acta2* and *Tagln*) and 24 hours (for the expression of *Myh11* and *Smtn*). Before immunofluorescence staining for ACTA2, TAGLN, MYH11 and SMTN, PASMCs were stimulated with BMP9/BMP10 for 48 hours using the same concentrations as for the RT-qPCR analysis.

2.6.2 Adenoviral infection

Sub-confluent primary PASMCs, cultured in PromoCell medium containing supplements, were infected with adenoviruses expressing Cre or lacZ for 48 hours. The adenoviruses were washed out with PBS and afterwards primary PASMCs were incubated with PromoCell medium containing supplements for 48 hours and then starved in PromoCell medium without supplements for 24 hours. Next, cells were treated with 1ng/mL BMP9 and 5ng/mL BMP10 in PromoCell medium without supplements for 6 hours to study the expression of *Acta2* and *Tagln* by RT-qPCR or 24 hours for the expression of *Myh11* and *Smtn*. To study the phosphorylation of Smad1/5/8, Smad2 and Smad3, the PASMCs were stimulated for 1 hour with BMP9 and BMP10 at 1 ng/mL and 5 ng/mL, respectively.

2.7 RNA-seq analysis of BMP9/BMP10 stimulated PASMCs

Starved PASMCs were stimulated with BMP9 and BMP10 in Promocell medium without supplements for 6 hours. After that, the medium was washed out and followed by PBS washing. TRIzol (Invitrogen™ 15596026) was added and RNA was extracted from cultured PASMCs using the miRNeasy micro kit (Qiagen) combined with DNase digestion (DNase-Free DNase Set, Qiagen) to remove contaminating genomic DNA. Total RNA and library integrity were verified using the LabChip Gx Touch 24 (Perkin Elmer). 400ng of total RNA was used as input for Truseq Stranded mRNA Library preparation, following the low sample protocol (Illumina). Sequencing was done on the NextSeq 500 instrument (Illumina) using v2 chemistry, which resulted in an average of 38M reads per library with 1×75 bp single-end setup. Raw reads were assessed for quality, adapter content and duplication rates. Reaper version 13-100 was used to trim reads, which were aligned to Ensemble mouse genome version mm10 (GRCm38) with STAR 2.4.0a using the parameter “--outFilterMismatchNoverLmax 0.1” to increase the maximum ratio of mismatches to mapped length to 10%. The number of reads aligning to genes was counted with featureCounts 1.4.5-p1 tool from the Subread package. Reads mapping at least partially inside exons were admitted and aggregated per gene. Reads overlapping multiple genes or aligning to multiple regions were excluded. Quantification and

identification of differentially expressed genes were carried out using DEseq2. Only genes with a minimum log2-fold change of ± 0.585 (1.5-fold), a maximum Benjamini-Hochberg corrected p-value of 0.05, and a minimum combined mean of 5 reads were deemed to be significantly differentially expressed. The Ensemble annotation was enriched with UniProt data (release 06.06.2014) based on Ensembl gene identifiers (Activities at the Universal Protein Resource (UniProt)). Bioinformatics and differential gene expression analyses were performed as described in detail previously[180].

2.8 ATAC-seq analysis of BMP9/BMP10 stimulated PASMCs

The starved PASMCs were stimulated with BMP9 and BMP10 in Promocell medium without supplements for 6 hours. Then the cells were washed with PBS for two times and were trypsinized (Sigam Aldrich, T1426). After that, spin the cells down and wash cells with cold PBS two times. Around 50,000 cultured PASMCs were used for ATAC-seq. Cells were resuspended in 50 uL cold lysis buffer (10 mM Tris-HCl pH 7.4, 10 mM NaCl, 3 mM $MgCl_2$, 0.1% Igepal CA-630). Afterwards, cell pellets were resuspended in transposition reaction mix (25 µL TD-Buffer, 22.5 µL water) together with 2.5 µL TN5 Transposase from Nextera DNA Library Prep Kit (Illumina #1502811) and incubated for 30 minutes at 37 °C. After the transposition reaction, purification was performed using MinElute PCR Purification Kit (Qiagen #28004). Amplification of Library together with indexing was carried out as described previously[181]. Sequencing was performed on the NextSeq 500 instrument (Illumina) using v2 chemistry.

Trimmomatic version 0.38 was employed to trim reads after a quality drop below a mean of Q15 in a window of 5 nucleotides[182]. Only reads longer than 15 nucleotides were cleared for further analyses. Trimmed and filtered reads were aligned versus the mouse genome version mm10 (GRCm38) using STAR 2.6.0c with the parameters "--outFilterMismatchNoverLmax 0.2—outFilterMatchNmin 20—alignIntronMax 1 --outFilterMultimapNmax 1"[183] and retaining only unique alignments to exclude reads of uncertain origin. Reads were further deduplicated using Picard 2.18.16 (Picard: A set of tools (in Java) for working with next generation sequencing data in the BAM format) to mitigate PCR artefacts leading to multiple copies of the same original fragment. Reads aligning to the mitochondrial chromosome were removed. The Macs2 peak caller version 2.1.1 was employed to accommodate for the range of peak widths typically expected for ATAC-Seq[184]. Minimum qvalue was set to -4 and FDR was changed to 0.0001. Peaks overlapping ENCODE blacklisted regions (known misassemblies, satellite repeats) were excluded. In order to be able to compare peaks in different samples and to assess reproducibility, the resulting lists of significant peaks were overlapped and unified to represent identical regions. Sample counts for union peaks were produced using bigWigAverageOverBed (UCSC Toolkit) and normalized with DESeq2 1.18.1 to compensate

for differences in sequencing depth, library composition, and ATAC-Seq efficiency[185]. Peaks were annotated with the promoter of the nearest gene in range (TSS +- 5000 nt) based on reference data of GENCODE vM15.

Genes with differential peaks were tested for gene set overrepresentation using KOBAS[186]. Two tests were performed per contrast to separate the direction of the change (up/down). Locus plots were generated by "Gviz" R package[187] and usage of library size normalized bigwig files for each sample. Averaging of bigwig files was performed by wigmath in java-genomics-toolkit. Annotation track was generated by bimaRt package[188]. Heatmap and density plots were generated with computeMatrix followed by plotHeatmap or plotProfile from deepTools2. Size factors produced by edgeR based on unified peak counts were used to scale samples to account for differences in sequencing depth, library composition, and ATAC-Seq efficiency. To compare transcription factor binding between BMP/noBMP stimulation, footprinting analysis was performed using the TOBIAS framework (https://github.com/loosolab/TOBIAS). First, reads from all replicates were merged per condition and corrected for Tn5 bias within peaks using standard parameters. Footprinting tracks were likewise calculated per condition. Thereafter, differential footprinting scores were calculated for 763 transcription factor motifs obtained from the JASPAR motif database (jaspar.genereg.net). The differential binding plot was produced by the "TOBIAS BINDetect" submodule with the p-value threshold set at the 95th quantile of all motifs.

2.9 DNA-microarray analysis of aortae and HUVECs stimulated by BMP9/BMP10

Human Umbilical Vein Endothelial Cell (HUVECs) were obtained from Lonza (CC-2519) and were cultured in Endothelial Basal Medium (CC-3121) with 10% fetal calf serum (FCS) and EGM™ SingleQuots™ (CC-4133). To starve HUVECs, the medium was changed to Endothelial Basal Medium without FCS and EGM™ SingleQuots™ but with 0.1 % BSA and the cells were cultured for 12 hours. Stimulation was done with BMP9 and BMP10 at a concentration of 1 ng/mL and 5ng/mL respectively for 6 hours. RNA from aortae or HUVECs was isolated using TRIzol (Invitrogen) according to the manufacturer's protocol and was labeled and hybridized to MTA1.0 arrays and Affymetrix HuGene 2.0_st arrays, respectively, following the manufacturer's instructions. Data were analyzed using DNAStar ArrayStar with RMA algorithm and evaluated using students t-test to determine statistical significance of changes in gene expression. The False Discovery Rate (FDR) procedure according to Benjamini-Hochberg was used to correct for multiple testing. A corrected p-value of 0.05 was considered to be significant. For unbiased identification of regulated biological processes, GSEA was performed using the GSEA Java desktop software application v4.0.2 with default parameters based on the permutation type gene set[189]. GSEAs with FDR and Familywise Error Rate (FWER) corrected p-values of <0.05 were assumed to be significant.

2.10 Molecular biology

2.10.1 Genomic DNA isolation

A small tail biopsy was cut and digested in 500 uL TENS Buffer (100 mM EDTA, pH 8.0; 100 mM NaCl, 50 mM Tris-hydrochloric acid, pH8.0 and 1%SDS) with 200ug/mL proteinase K at 56 ℃ over night. The following day, samples were centrifuged at 12000g for 5 minutes and the supernatant was transferred into a new tube. Then 500 uL isopropanol was added to precipitate the DNA. Spin down the DNA at 12000g for 5 minutes and the pellet was washed with 1 mL 75% ethanol. Spin the pellet down again at 12,000g for 5 minutes and dry for 5 minutes before adding 300 uL autoclaved water. The tube was incubated at 56℃ for 1 hour or longer to elute and re-suspend the DNA.

2.10.2 Polymerase Chain Reaction and Genotyping

Polymerase chain reaction (PCR) was performed to determine mice genotypes. For each setup, 10 uL 2× Taq Master Mix (Vazyme biotech co,Ltd.), 1 uL 10mM forward primer, 1 uL 10 mM reverse primer, 5 uL molecular level water and 3 uL genomic DNA were mixed. PCRs were performed in a Thermocycler PCR machine at a cycle program corresponding to the PCR conditions.

Table 1. The primer list and protocols used for each reaction were listed as follows:

Genotype	Forward Primer	Reverse Primer
αMhc MCM	CAACAT GAA ATG CAA GAA CG	GGAAACCATTTCCGGTTATTC
Anf Cre	GAC AGC AAA CAT CAG ATC G	CTA GAG CCT GTT TTGCACGTT
Alk1 mutant	CCTGGACAGCGACTGTACTAC	GCCCCATTGCTCTCCTCAAAC
Apelin Mutant	ATG TCT GGG TGT AGG TCC ATA AAG G	GACAGTTTCTCTAACTCAAAGGGCC
Apelin Wild Type	ATG TCT GGG TGT AGG TCC ATA AAG G	GCTTCCTTCTTCTAGTCCTGTTCCA
Bmp10 mutant	AAC AGG CCC GCA TCA TTT AT	TGG CCC AGG GGC CTA TTC TTT G
Bmp9 Mutant	CTG TGG TCC ACC AGG ATA CG	ACACCG GGATTCTCCCAATC
Bmp9 Wild Type	GTCACTGTTCCCCCACTAGC	GAAAGGGGAAGTCCTCCGTG
Atoh8 Wild	CGTCCTCGCCATGAAGCACATC	AACGGTTGTGTCCTGTCCCGAAGC

Type	C	
Atoh8 mutant	CGTCCTCGCCATGAAGCACATCC	CCATTCAGGCTGCGCAAACTGTTGG
General Cre	CCAGGCTAAGTGCCTTCTCTACA	AATGCTTCTGTCCGTTTGCCGGT
iCdh5 Cre	GCCTGCATTACCGGTCGATGCAAC GA	GTGGCAGATGGCGCGGCAACACCATT
Rosa26-Cag Mutant	CTTGCTCTCCCAAAGTCGCTCTGAG	ACCGTAAGTTATGTAACGCGGAACTCC
Rosa26-Cag Wild type	CTTTAAGCCTGCCCAGAAGACTCCC	CTTGCTCTCCCAAAGTCGCTCTGAG

The following Thermocycler conditions were used for the genotyping of:

Bmp10$^{loxP/loxP}$

Steps	Temperature (°C)	time	Repeat
1. Initialization	94	3 min	
2. Denaturation	94	30 sec	
3. Annealing	58	30 sec	Step 2 to 4
4. Elongation	72	30 sec	35 times
5. Final elongation	72	5 min	
6. Final hold	12	∞	

Bmp9$^{-/-}$

Steps	Temperature (°C)	time	Repeat
1. Initialization	94	3 min	
2. Denaturation	94	30 sec	
3. Annealing	50	30 sec	Step 2 to 4
4. Elongation	72	45 sec	35 times
5. Final elongation	72	5 min	
6. Final hold	12	∞	

Bmp9 wild type

Steps	Temperature (°C)	time	Repeat
1. Initialization	94	3 min	
2. Denaturation	94	30 sec	
3. Annealing	65	30 sec	Step 2 to 4

4. Elongation	72	45 sec	35 times
5. Final elongation	72	5 min	
6. Final hold	12	∞	

Alk1$^{loxP/loxP}$

Steps	Temperature (°C)	time	Repeat
1. Initialization	94	3 min	
2. Denaturation	94	30 sec	
3. Annealing	55	30 sec	Step 2 to 4
4. Elongation	72	40 sec	30 times
5. Final elongation	72	5 min	
6. Final hold	12	∞	

Anf-Cre

Steps	Temperature (°C)	time	Repeat
1. Initialization	94	3 min	
2. Denaturation	94	30 sec	
3. Annealing	58	30 sec	Step 2 to 4
4. Elongation	72	60sec	35 times
5. Final elongation	72	5 min	
6. Final hold	12	∞	

General Cre

Steps	Temperature (°C)	time	Repeat
1. Initialization	94	3 min	
2. Denaturation	94	60 sec	
3. Annealing	67	60 sec	Step 2 to 4
4. Elongation	72	60 sec	30 times
5. Final elongation	72	5 min	
6. Final hold	12	∞	

Atoh8 wild type and mutant, *Rosa26*-CAG wild type and mutant

Steps	Temperature (°C)	time	Repeat
1. Initialization	94	3 min	
2. Denaturation	94	45 sec	
3. Annealing	57	45 sec	Step 2 to 4
4. Elongation	72	45 sec	35 times
5. Final elongation	72	5 min	

6. Final hold	12	∞	

iCdh5-Cre

Steps	Temperature (°C)	time	Repeat
1. Initialization	94	3 min	
2. Denaturation	94	45 sec	
3. Annealing	70	45 sec	Step 2 to 4
4. Elongation	72	60 sec	35 times
5. Final elongation	72	5 min	
6. Final hold	12	∞	

Rosa26-CAG

Steps	Temperature (°C)	time	Repeat
1. Initialization	94	3 min	
2. Denaturation	94	45 sec	
3. Annealing	57	45 sec	Step 2 to 4
4. Elongation	72	45 sec	38 times
5. Final elongation	72	5 min	
6. Final hold	12	∞	

2.10.3 RNA preparation and cDNA synthesis

RNA was isolated from cells or tissues using the Trizol reagent (life technologies) according to the manufacturer's protocol. For tissue samples, samples were placed in a 2 mL tube with 1 sterile grinding ball (grinding balls 5 mm – Retsch, 22.455.0003). 1 mL Trizol was added and the tube was placed in a tissue homogenizer (Retsch, MM301) for 5 minutes with frequency of 30/second for homogenization. For cultured cells, cells were firstly washed with PBS and then 1 mL Trizol was added directly to the dish. Using a cell scraper (Sarstedt, 83.1830) to harvest the cells and cells were transferred into a fresh 1.5 mL tube. 200 uL chloroform was added to the tube and incubated for 5 minutes at room temperature. Samples were centrifuged at 4°C for 15 minutes at 12,000 x g. After centrifugation, the aqueous phase was transferred into a fresh tube and 500 uL isopropanol was added. Samples were incubated at room temperate for 10 minutes and centrifuged at 4°C for 10 minutes at 12,000 x g. The pellet was washed twice with 1 mL 75% ethanol. Finally, the pellet was resuspended with 15-25 uL DEPC water (0.1% v/v DEPC in water). To determine the concentration, samples were measured with a spectrophotometer (NanoDrop ND-2000c Spectrophotometer).

5 µg of purified RNA was reversely transcribed with the Superscript II Reverse Transcriptase (life technologies) following the standard protocol as follows:

Volume	Components
X µL (0.5 µg)	RNA
1 µL	Oligo(dT)15 Primer (Promega; C110A)
1 µL	dNTP (Fermentas; R0186)
10 –x µL	MilliQ H2O

Reactions were adjusted to 65°C for 5 minutes.

After cooling down, 8 µL of synthesis mixture were added.

Synthesis mixture setup:

Volume	Components
4 µL	5 X first strand buffer (Invitrogen; P/N y02321)
2 µL	0.1 M DTT (Invitrogen; P/N y00147)
1 µL	RNasin RNase Inhibitor (Promega; N261B)
1 µL	SuperScript®II reverse transcriptase (Invitrogen; P/N 100004925)

Reactions were adjusted to 42°C for 1 hour and followed by 70°C for 15 minutes. After the reaction, samples were diluted with 180 uL water and stored in -20°C until further use.

2.10.4 Quantitative real-time polymerase chain reaction using TaqMan® Gene Expression Assay

RT-qPCR was performed using Taqman assay with the following probes： *Acta2*: Mm00725412_s1, *Tagln*: Mm00441660_m1, *Myh11*: Mm00443013_m1, *Smtn*: Mm00449973_m1, *vimentin* Mm01333430_m1, *Tpm4*: Mm01245298_m1, *Bmp10*: Mm01183889_m1, *Alk1*: Mm00437432_m1, *Atoh8*: Mm00464055_m1. And *Gapdh*: Mm999999915_g1 was used for normalization under standard conditions. RT-qPCR was carried out using the StepOnePlus real-time PCR system (Applied Biosystems). The master mix for each reaction was prepared as follows:

Volume	Components
5 µL	TaqMan Gene Expression Master Mix (2x)
0.5 µL	Specific TaqMan Gene Expression Assay (20x)
0.5 µL	GAPDH TaqMan Gene Expression Assay (20x)
4 µL	cDNA Template

Thermocycler conditions were used as follows:

Steps	Temperature (°C)	Time	Number of cycles
1	50	2 min	
2	95	10 min	40 times

3	95	15 sec
4	60	1 min

RT-qPCR was performed with a qPCR thermocycler (Step OnePlus Real-Time PCR Cycler – Applied Biosystems).

2.10.5 Quantitative real-time polymerase chain reaction using SYBR Assay

The mix for each reaction was prepared as follows:

Volume	Components
12.5uL	2 x SYBR Green
5.5uL	Water
1uL	Forward primer
1uL	Reverse primer
5uL	cDNA Template

Thermocycler conditions were used as follows:

Steps	Temperature (°C)	time	Repeat
1. Initialization	94	30 sec	
2. Denaturation	94	10 sec	
3. Annealing	70	20 sec	Step 2 to 4
4. Elongation	72	05 sec	40 times
5. Final elongation	72	10 sec	
6. Final hold	12	∞	

The PCR was performed with a qPCR thermocycler (Step OnePlus Real-Time PCR Cycler – Applied Biosystems).

2.11 Western blot

2.11.1 Protein isolation from tissues

Tissue samples excised from mice were snap freezed with liquid nitrogen and crushed using a mortar and pestle into powder, which was transferred into a fresh 1.5 mL tube and 500 uL protein extraction buffer (0.1 M Tris/HCl pH 8.0, 0.01 M EDTA, 10 % SDS) supplemented with protease inhibitor (4 µg/mL aprotinin, 500 µg/mL benzamidine, 4 µg/mL leupeptin, 1 mM Na_3VO_4, 20 mM NaF and 2 mM PMSF) was added to homogenized the samples. Sonication was performed for 20 seconds with 5 cycles. After that, samples were centrifuged at 12000 rpm for 10 minutes to remove the debris. The supernatant containing the protein lysate was transferred to a fresh tube and concentration was measured using Bio-Rad assay (BioRad; Reagent A - 500-0113; Reagent B - 500-0114) in 96 well plate according to the manufacturer instruction. In brief, samples for a standard regression curve were prepared by using different

standard concentrations of bovine serum albumin (BSA) shown as below. Protein concentration was calculated based on the standard curve.

							Blank	Sample
BSA(uL)	1	2	5	10	15	20	0	5
H_20(uL)	19	18	15	10	5	0	20	15

Add 200 uL of Solution B (Bio-Rad, Protein Assay Reagent B, 5000114) and 25 uL of Solution A (Bio-Rad, Protein Assay Reagent A, 5000113) were mixed with samples or BSA solution. Wait for 5 minutes and measure the concentration.

2.11.2 Protein isolation from cultured cells

To harvest proteins from cultured cells, the dish was washed two times with PBS and cell lysate was prepared in 300uL protein extraction buffer supplemented with protease inhibitor. Samples were scraped and transferred into a fresh 1.5 mL tube. Sonication was performed for 20 seconds with 5 cycles and samples were centrifuged for 10 minutes at 12000 rpm to remove the debris. The supernatant was transferred into a fresh tube and 0.04 M DTT was added. Samples were incubated in 95℃ for 5 minutes before loading.

2.11.3 Sodium Dodecyl Sulfate-Polyacrylamide Gel Electrophoresis

Sodium Dodecyl Sulfate-Polyacrylamide Gel Electrophoresis for western blot were self-made according to (Table 2). Fill the resolving gel in around 80% of the NOVEX Cassettes (1 mm – Invitrogen, NC2010) and wait 20-30 minutes until it was set. Then the cassette was filled with the stacking gel and inserted with a comb. To separate the protein by their mass, the electrophoresis was performed in a running chamber (NOVEXElectrophoresis Mini-Cell - Invitrogen, EI001) using the MES (2.5 mM MES, 2.5 mM Tris, 0.05 % SDS, 50 mM EDTA) buffer for 2 to 3 hours at 120 volts until the samples were separated accordingly. Protein location was detected with the Protein-Marker VI (Peqlab, 27-2311).

Table 2. Composition of gel electrophoresis 10% Bis-Tris polyacrylamide gel.

Resolving gel	**10%**
Rotiphorese® Gel 30 (37.5:1) (Roth, 3029.1)	2.3 mL
3.5 x bis-Tris pH 6.5 – 6.8	2 mL
Milli-Q H2O	2.7 mL
10 % Ammoniumperoxodisulfat (APS – Merck, 1.01201)	25 uL
TEMED (Roth, 2367.1)	7 uL
Stacking gel	**5%**
Rotiphorese® Gel 30 (37.5:1) (Roth, 3029.1)	0.29 mL

3.5 x bis-Tris pH 6.5 – 6.8	0.5 mL
Milli-Q H_2O	0.96 mL
10 % Ammoniumperoxodisulfat (APS – Merck, 1.01201)	8 uL
TEMED (Roth, 2367.1)	3 uL

2.11.4 Protein immunoblotting

In brief, wet transfer was used to transfer the proteins from the gel onto a nitrocellulose (AmershamTM ProtranTM 0.45 µm NC – GE Healthcare, 10600002). The protein transfer was achieved with transfer buffer (12.5 mM Bicine, 12.5 mM Bis-Tris, 0.8 mM EDTA, 20 % Methanol). The transfer chamber (NOVEX X Cell II Blot Module - Invitrogen; EI9051) was filled with sponges that had been soaked in transfer buffer. Next Whatman filter paper was placed followed by the gel and then the membrane. Another Whatman filter paper and soaked sponges were then added. This chamber was filled with transfer buffer and run at 30 volts for 1.5 hour. To visualize the loading and a proper transfer, the blots were later stained with Red Alert (RedAlert™ Western Blot Stain – Millipore, 71078-50ML) staining solution on a shaker for 10 minutes. The Red Alert staining was then removed by washing in PBST. To stain the membrane for the specific antibody, the unstained membrane was firstly blocked with 3% skim milk powder in TBST at room temperate for 1 hour. After blocking, the membrane was incubated with primary antibodies as listed in (Table 3) diluted in 3% skimmed milk in TBST overnight at 4°C on a shaker. After the incubation, the membrane was washed 3 times by TBST on a shaker for 5 minutes. Next the membrane was incubated with a horse-radish-peroxidase (HRP-) coupled secondary antibody diluted in 3% skimmed milk at room temperate for 1 hour on a shaker. In the end, the membrane was washed in TBST for 5 minutes and 5 times. For signal detection, the membrane was incubated with Super Signal West Femto Maximum Sensitivity Substrate (Thermo Scientific; 34096), according to the manufacturer instructions. And exposed in the Chemiluminescence Analyzer (ChemiDoc™ MP Imaging System – BioRad, 731BR01764) to detect the protein signal. Quantification of band intensities was carried out using the Image J software.

Table 3. List of primary antibodies for Western Blot.

Antibody	Company	Source	Catalog No.	Dilution
pSmad1/5/8	Cell Signalling	Rabbit	9511	1:1000
pSmad3(Ser423/425)Smad1 (463/465)	Cell signalling	Rabbit	9514	1:1000
pSmad2(Ser465/467)	Cell signalling	Rabbit	3101	1:1000
pSmad2 (Ser245/250/255)	Cell signalling	Rabbit	3104	1:1000
pSmad3 (Ser423/425)	Cell signalling	Rabbit	9520	1:1000

pErk5	Cell signalling	Rabbit	3371	1:1000
pErk1/2	Cell signalling	Rabbit	3840	1:1000
pP38	Cell signalling	Rabbit	9215	1:1000
Psapk/JUK	Cell signalling	Rabbit	9251	1:1000
pCREB	Cell signalling	Rabbit	9196	1:1000

2.12 Co-Immunoprecipitation

Cultured PASMCs were stimulated with BMP9 and BMP10 for 6 hours. Then the medium was removed and cells were washed with PBS in plate. 500uL PIPA (50 mM Tris-Hcl, 150 mM Nacl, 1% NP40, 0.25% Na deoxycolate) buffer was added with protease inhibitor and cells were scraped. Re-suspend the cells in 5mL of PBS for washing and spin them down at 1250 rpm for 5 minutes. The supernatant was removed and cells were resuspended with 500uL RIPA buffer containing protease inhibitor. A brief sonication with 3 rounds of 10 seconds at 30% energy was performed and samples were centrifuged with maximum speed for 15 minutes to get rid of the cell debris. Then adjust the volume to 300uL of RIPA buffer with protease inhibitor. Take 60 uL of Protein A beads per sample and wash 3 times in RIPA buffer and spin the beads down at 3000g for 1 minute. Beads were dissolved in original volume with RIPA buffer. 30 uL beads were transferred into a fresh tube and tubes were kept at 4°C in rotating wheel for 1 hour to pre-clear the beads. The remaining beads were blocked in RIPA buffer with 5% BSA overnight at 4 °C in a rotating wheel. After the pre-clearing, spin down the samples and the supernatant was collected in a fresh tube and 2ug of primary antibody was added to samples, which was rotated in a wheel at 4 °C overnight. In the next day, blocked beads were washed in PBS for 3 times. And afterwards 30 uL of blocked beads were added to each sample and mix them at 4°C in a rotating wheel for 3 hours. Later, spin down the beads at 300g for 1 minute and the supernatant was discarded. The bead was washed in RIPA buffer 3 times for 10 minutes in a rotating wheel at 4 °C. Then 20 uL of extraction buffer with glycerol, DTT, bromophenol blue was added to each sample and samples were incubated at 95 °C for 5 minutes. In the end, spin down the samples and collect the supernatant and ready to run the Western Blot.

2.13 Histology

2.13.1 Preparation of OCT embedded samples

For lung samples, perfuse the lung with PBS from the right ventricle. After PBS perfusion, the lung was perfused again with 30 mL 4% PFA and incubated in 4% PFA overnight at 4°C. For aortae from adult mice and embryos isolated from pregnant mice, samples were fixed with 4% PFA overnight night without perfusion. After washing with PBS 3 times, samples of lung, aorta and embryo were dehydrated through 15% saccharose at room temperate for 1 hour followed

by 30% saccharose at 4°C overnight. In the following day, samples were embedded in Tissue-Tek® O.C.T. Polyfreeze™ on dry ice. For cultured cells seeded in chamber slides, the medium was moved out and washed with PBS for 5 minutes. Cells were fixed in 4% PFA for 15 minutes and washed again with PBS and stored in 4°C or proceed to staining. Heart samples isolated from mice were washed with PBS and directly embedded in OCT on dry ice without fixation.

The embedded samples were fixed on a metal holder followed by cryosection with a Leica cryotome (Leica CM1950). Sectioning was performed at -23°C and cryosections were mounted on a slide (Superfrost ultra plus – Thermo scientific, J3800AMNZ). Shortly dried and stored at -20 °C or directly proceed to staining.

2.13.2 Immunofluorescence staining

To perform the staining, slides were fixed with cold acetone for 5 minutes and followed by washing of three times with PBS. Afterwards, slides were blocked for 1 hour with blocking solution (5% FCS, 1% BSA, 0.1%Triton in 1x Gold Buffer [20 mM Tris, 0.155 M NaCl, 2 mM EGTA, 2 mM $MgCl_2$ at pH 7.5]) at room temperature. The primary antibodies listed in the (Table4) were diluted in 1% BSA, 0.1% Triton in 1×Gold buffer and slides were incubated with diluted antibodies at 4 °C overnight in a humidified chamber. The following day, primary antibodies were washed out with PBS 3 times for 5 minutes each and the sections were incubated with corresponding secondary antibodies listed in (Table 5). Secondary antibodies were diluted in 1%BSA, 0.1%Triton in 1×Gold buffer and slides were incubated at room temperate for 1 hour. After that, secondary antibodies were washed out and nuclei were stained with DAPI (Molecular ProbesTM, Thermo Fisher, D1306) diluted in 1%BSA, 0.1%Triton in 1×Gold buffer for 10 minutes at room temperature in the humidified chamber. Finally, slides were washed again 3 times in PBS and mounted using a glass cover and Mowiol. Images were acquired with Leica SP8 LIGHTNING confocal microscope.

Table 4. List of primary antibodies for immunofluorescence

Antibody	Company	Source	Catalog No.	Dilution
Pecam	BD Pharmingen	Rat	550274	1:100
alpha Smooth Muscle Actin Cy3	Sigma-Aldrich	Mouse	C6198	1:500
Vimentin	Abcam	Rabbit	ab92547	1:500
Transgelin/SM22	proteintech	Rabbit	Invitrogen	1:200
pSmad1/5/8	Cell Signalling	Rabbit	9511	1:500
Acvr1(ALK2)	Sigma-Aldrich	Rabbit	SAB1306388	1:500
BMPR1a(ALK3)	Thermo Fisher	Rabbit	38-6000	1:500

	Scientific			
ALK1	Santa Cruze Biotechnology	Rabbit	SC-28976	1:500

Table 5. List of secondary antibodies for immunofluorescence

Antibody	Company	Source	Catalog No.	Dilution
anti-rabbit Alexa 594	Invitrogen	goat	A11012	1:500
anti-rat Alexa 594	Invitrogen	Goat	A11007	1:500
anti-rat Alexa 488	Invitrogen	Goat	A11006	1:500
Anti-rabbit Alexa 488	Invitrogen	Goat	A11070	1:500
DAPI	Roche		10236276001	1:1000

2.13.3 Fluorescence *in situ hybridization*

The florescent RNA hybridization was performed using ViewRNA ISH Assays (ThermoFisher Scientific Cat# QVT0013) according to the manufacturer's instructions. The following probes were used: *Alk1*: VB1-3028698-VT(mouse), *ALK1*: VA1-13227(human), *Alk1*：VB1-13719-VT (mouse)， *Alk3:* VB1-13718-VT (mouse), *Alk6*: VB1-3028975-VT (mouse), *Bmpr2*: VB1-3028976-VT (mouse). To quantify the level of gene expression for individual genes, at least 30 images were taken and the ratio of RNA dots to nuclei numbers was calculated. Images were acquired with Leica SP8 Lightning confocal microscope.

2.13.4 Preparation of paraffin embedded samples

The organ was washed 3 times in PBS and then fixed in 4% PFA at 4°C overnight. After fixation, samples were washed twice in PBS and then processed in the dehydration series of 50%, 70%, 90%, 100%, 100% ethanol for 2 hours each step at room temperature. The sample was incubated in xylene for 30 minutes at room temperature followed by incubation with 50% xylene: 50% paraffin overnight at 65°C overnight. In the following day, samples were further incubated with 100% paraffin at 65°C for 2 hours. In the end, samples were embedded in paraffin with an embedding machine (Leica RM2125RT). Sections were obtained using a microtome (Leica RM2125RT) and collected with a glass slide (Superfrost Ultra Plus -Thermo Scientific, J3800AMNZ). Sections were dried overnight on a hot plate (42°C; HI1220–Leica) and stored at room temperature.

2.13.5 Hematoxylin and Eosin staining

Slides were deparaffinized by placing the samples twice in Xylene for 10 minutes each round and rehydrated in an ethanol series from 100%, 100%, 90%, 70%, 50% of ethanol to water. Afterwards, the slides were stained firstly with Meyer's Hematoxylin (Haemalaum, acidic Mayer – WALDECK, 2E-038) for 10 minutes. Thereafter, slides were dipped twice in water and rinsed in running tap water for 10 minutes. Sections were stained in Eosin (Eosine Solution– WALDECK, 2C-140) for 10 minutes and then were dehydrated in increasing ethanol series (50%, 70%, 90%, 100%, 100% of ethanol each for 10 minutes). Afterwards, slides were incubated in 100% xylene twice for 10 minutes each. In the end, slides were mounted in Entellan (Merck-Millipore, 1.07961.0100) and photographed with a Keyence (Keyence BZ-9000).

2.13.6 Trichrome staining

Trichrome staining was performed according to standard protocol. In short, sections were deparaffined twice in xylene and rehydrated by a series in 100%, 90%, 70%, 50% ethanol followed by ddH_2O. Slides were exposed to Bouin'S solution at 56°C for 15 minutes and then rinsed in running tap water until the yellow color disappeared. Slides were stained with Hematoxylin for 5 minutes, thereafter were washed in running tap water for 5 minutes. Afterwards, sections were exposed to Biebrich Scarlet-Acid Fuchsin solution for 5 minutes and slides were dipped 10 times in water and transferred to phosphotungstic/phosphomolybdic acid for 5 minutes. Then slides were exposed to Anilin Blue solution for 5 minutes and followed by 1% acetic acid for 2 minutes. Slides were then dehydrated by 96%, 100% ethanol for 10 minutes each and were incubated in xylene for 20 minutes. Finally, slides were mounted with Entellan and coverslips. All the steps were performed at room temperature. Images were acquired with Keyence microscope (Keyence BZ-9000).

2.13.7 Beta galactosidase (LacZ) staining

Cryosections were fixed in Fixing Solution (0.4% glutaraldehyde, 2 mmol/L $MgCl_2$, 5 mmol/L EGTA (pH 7.5), in SPP buffer (77.4 mmol/L Na_2HPO_4, 22.6 mmol/L NaH_2PO_4)) for 5 minutes at room temperature and rinsed with Wash Solution (2 mmol/L $MgCl_2$, 0.01 % Na-desoxycholate, 0.02% NP-40, in SPP buffer) for 15 minutes at room temperature. After that, slides were incubated in Staining Solution (5 mmol/L K_3FeCN_6, 5 mmol/L K_4FeCN_6, 0.1 % X-Gal) at 37°C overnight, in the dark. Thereafter, sections were rinsed with Wash Solution for 10 minutes at room temperature and were stained with Eosin. After eosin staining, the sections were dehydrated in 70%, 80%, 90% and 100 % ethanol series followed by 10 minutes 100% xylene incubation. In the end, sections were mounted in Entellan. Images were acquired with Keyence microscope (Keyence BZ-9000).

2.14 Statistical analysis

Statistical analysis was performed by unpaired, two-tailed Student's t-test, or by paired, one-tailed Student's t-test when a normal distribution was assumed, or by one-way ANOVA followed by Bonferroni's multiple comparison test. For all bar graphs, data are represented as mean ± S.E.M, P values < 0.05 were considered significant. n represents the number of independent experiments. All calculations were performed using GraphPad Prism 8.0 software.

Table 6. List of reagents in this study

Reagents	Source	Catalog No.
Proteinase K	Carl Roth	7528.2
SuperScript® II Reverse transcriptase	Invitrogen	P/N 100004925
Oligo(dT)15 Primer	Promega	C110A
dNTP	Fermentas	R0186
RNasin RNase Inhibitor	Promega	N261B
Collagenase II	Worthington	LS004176
Trypsin	Sigma	T0303
truChIPä Chromatin Shearing Reagent Kit	Covaris	520154
Magna ChIP™ Protein A+G Magnetic Beads	Millipore	16-663
QuantiGene ViewRNA ISH Tissue 1-Plex Assay Kit	Thermo	QVT0050
QuantiGene ViewRNA Chromogenic Signal Ampification Kit	Thermo	QVT0200
1,4-Dithiothreit (DTT)	Carl Roth	6908.2
10 x RedAlert™ Western Blot Stain	Millipore	71078-50ML
16 % Formaldyhyde Solution, Methanol free	ThermoScientific	28906
Acetic acid	Roth	3738.5
BisTris	AppliChem	A1025,0500
Bovine Serum Albumin (BSA) solution	Sigma	A9576
Dimethyl sulfoxide (DMSO)	Sigma	D-4540
Dimethylformamide	Sigma	319937-500ml
DPBS, no calcium, no magnesium	Gibco™	14190144
EDTA	Roth	8040.3
Ethanol	Roth	9065.4
Fetal bovine serum (FBS)	Sigma	F7524
Glucose	Roth	X997.2
Haemalaum, acidic Mayer	WALDECK	2E-038
Ammoniumperoxodisulfat (APS)	Merck	101.201
Eosine Solution	WALDECK	2C-140
Isopropanol	Roth	6752.4
Medium 199 (Earle’s salt)	Gibco	31153
Methanol	Roth	4627.5
Mowiol	Millipore	475904100GM

Paraformaldehyde	Roth	0335.4
Penicillin/Streptomycin/Glutamine	Sigma	G6784
RotiphoreseR Gel 30 (37.5:1)	Roth	3029.1
SDS	Roth	2326.3
Sodium chloride (NaCl)	Roth	3957.2
Sodium hydroxide (NaOH)	Roth	6771.2
Sucrose	Carl Roth	9097.1
Super SignalR West Femto Maximum Sensitivity Substrate	ThermoScientific	34096
TaqMan Gene Expression Master Mix (2x)	Applied Biosystems	10525395
Triton X-100	Roth	6683.1
Sodium chloride (NaCl)	Roth	3957.2
Tween 20	Roth	9127.2
FSC 22R clear Frozen Section Compound	Leica	3801480
protease inhibitors (cOmplete ULTRA Tablets,Mini, EASYpack)	Roche	05892970001
Ad-CMV-iCre	VECTOR BIOLABS	1045N
Smooth Muscle Cell Medium 2	Promocell	C-22062
Smooth Muscle Cell Medium 2 Supplement Mix	Promocell	C-39267
Iron II-III Oxid Pulver	Sigma	31006-9
Collagen Solution	Sigma	C8919
Protein Assay Reagent A	Bio-Rad	5000114
Protein Assay Reagent B	Bio-Rad	5000113

3 Results

3.1. *Bmp9*$^{-/-}$ and *Bmp10*^{Anf} mutants do not display morphological alterations in the vascular system.

Since germline deletion of *Bmp10* leads to embryonic lethality at E10.5, a conditional *Bmp10* allele in which exon2 of *Bmp10* was flanked by loxP sites (*Bmp10*$^{loxP/loxP}$) was generated. To confirm a functional loss of BMP10 in mice, *Bmp10*$^{loxP/loxP}$ mice were crossed with a germline deleter strain (*Cmv-Cre*), which results in a constitutive BMP10 knockout in all tissues. Consistent with previous reports, constitutive loss of BMP10 led to embryonic lethality around E10.5. Mutants displayed thin ventricle walls and arrested cardiac development. Newly generated *Bmp10*-LacZ report mice and fluorescence *in situ hybridization* (RNA-FISH) staining (data not shown), revealed that the broad expression of *Bmp10* in the early embryonic myocardium becomes restricted to the right atrium during late fetal stages under physiological conditions (Figure 6A), which corroborated previous reports[915, 94]. Thus, it was assumed that deletion of BMP10 specifically in the atria might overcome embryonic lethality. Since ANF (also known as Natriuretic Peptide A) is specifically expressed in right atria, *Bmp10*^{Anf} mice were generated by crossing the *Bmp10*$^{loxP/loxP}$ strain to *Anf-Cre* mice to delete BMP10 specifically in right atria. Western blot analysis confirmed that BMP10 protein expression was completely lost in right atria of *Bmp10*^{Anf} mutants (Figure 6B). The cardiovascular system appeared grossly normal and did not reveal any obvious morphological alterations both in germ line BMP9 mutants (*Bmp9*$^{-/-}$) and *Bmp10*^{Anf} mutants (Figure 6C). BMP9 and BMP10 are released from different organs (BMP9 from liver and BMP10 from the right atrium) to the blood stream, where they presumably form BMP9-BMP10 heterodimers to achieve full biological BMP activity[190]. To avoid a potential functional redundancy of BMP9 and BMP10, conditional double knockout mutants were generated by crossing *Bmp9*$^{-/-}$ mutants with the atrial specific *Bmp10*^{Anf} knock out strain (*Bmp9*$^{-/-}$*/Bmp10*^{Anf}, hereafter called *Bmp9/10*^{dko}).

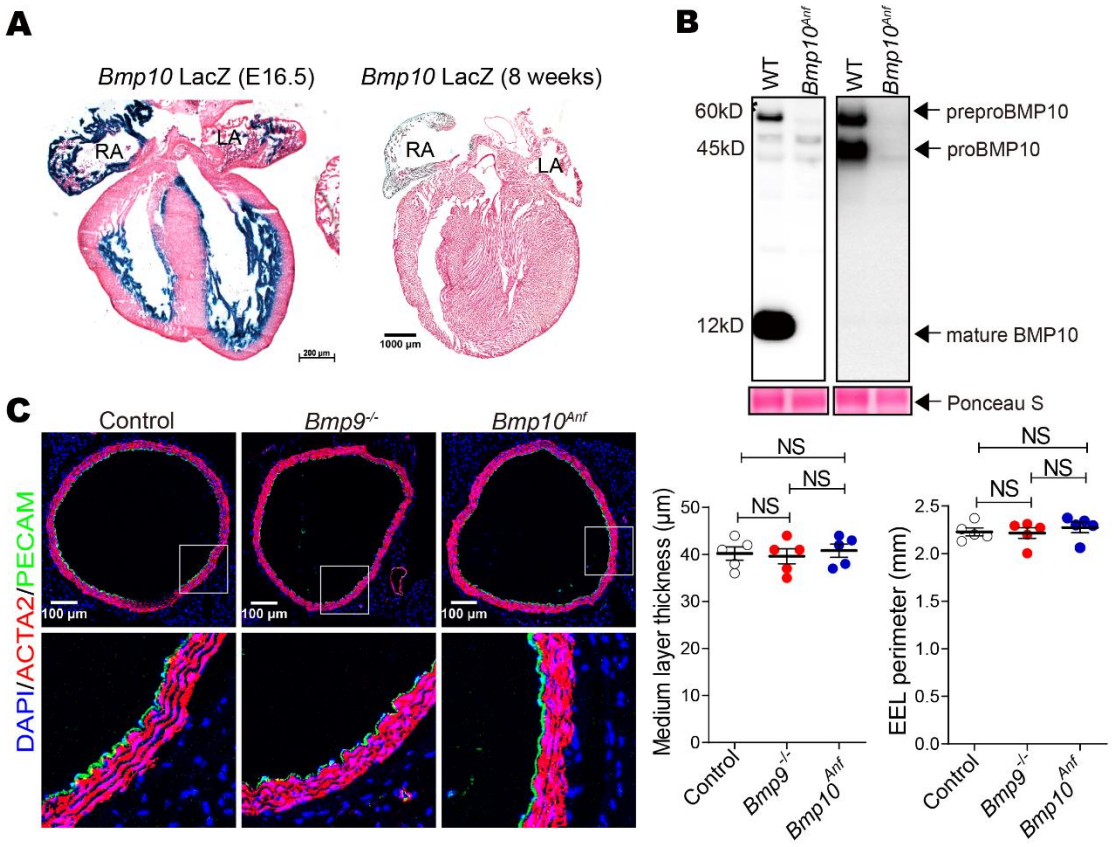

Figure 6. Analysis of vascular system in *Bmp9*$^{-/-}$ and *Bmp10*^{Anf} mutant mice.

A. LacZ staining of *Bmp10*-LacZ reporter mice at E16.5 embryos and in 8 weeks old adults (RA, right atria; LA, left atria, n=5). In adult mice *Bmp10* expression is confined to the right atrium. **B.** Western blot analysis of BMP10 expression in right atria of wild type and *Bmp10*^{Anf} mice. The antibody used for the panel on the left detects mature, processed BMP10, while the antibody used for the panel on the right recognizes pro-BMP10. **C.** Immunofluorescence staining of aortae from 8 weeks old control, *Bmp9*$^{-/-}$ and *Bmp10*^{Anf} mice for ACTA2 and PECAM. Quantification of medial layer thickness and external elastic lamina (EEL) (data are mean±SEM; one-way ANOVA: NS P >0.05, n=3). Primary data of Figure6A and Figure6B were generated by Dr. Sandra Swist, Max Planck Institute for Heart and Lung Research.

3.2 BMP9 and BMP10 are required for formation of contractile VSMCs and normal vessel contractility.

Bmp9/10^{dko} mice showed a dramatic phenotype in the cardiovascular system. Immunofluorescence staining for ACTA2 and PECAM showed massively reduced coverage of arteries with loss of contractile VSMCs. The muscular layer of aortae was thinner as indicated by a 33% reduction of medial layer thickness (n=8, unpaired two-tailed Student's t-test: P<0.0001) (Figure 7A). Furthermore, the perimeter of external elastic layer (EEL) of aortae was increased by 24% (n=8, unpaired two-tailed Student's t-test: P<0.0001) (Figure 7A).

Similar defects were observed in cardiac vessels, where the number of vessels with diameter smaller than 20 um decreased significantly while the number of larger vessels (diameter more than 70um) increased, due to vessel dilation (Figure 7B). DNA-microarray of aortae from 8 weeks old *Bmp9/10^{dko}* mice followed by gene set enrichment analysis (GSEA) revealed a strong up-regulation of genes involved in fatty acid metabolism, structural constituents of ribosome, TAC cycle and electron transport chain (Figure 7C), which further indicates the switching of VSMCs to a synthetic state[191]. This result mirrors the appearance of less mature, more synthetic and a lower number of VSMCs observed by immunofluorescence staining (Figure 7A-B). Furthermore, RT-qPCR analysis of aortae corroborated the microarray data and confirmed decreased expression of typical contractile VSMC genes including *Acta2, Tagln, Myh11 and Smtn*, further suggesting that contractility was compromised (Figure 7D). Staining against viminten (VIM*)*, a VSMC synthetic marker, demonstrated a strong up-regulation of the synthetic protein in VSMCs (Figure 7E). Expression of the synthetic genes *Vim* and *Tpm4* was increased in VSMCs of *Bmp9/10^{dko}* mice (Figure 7F). Taken together, my results suggest that BMP9/BMP10 are crucial and essential to the contractile state of VSMCs and loss of these two proteins prevents recruitment and subsequent maturation of VSMCs.

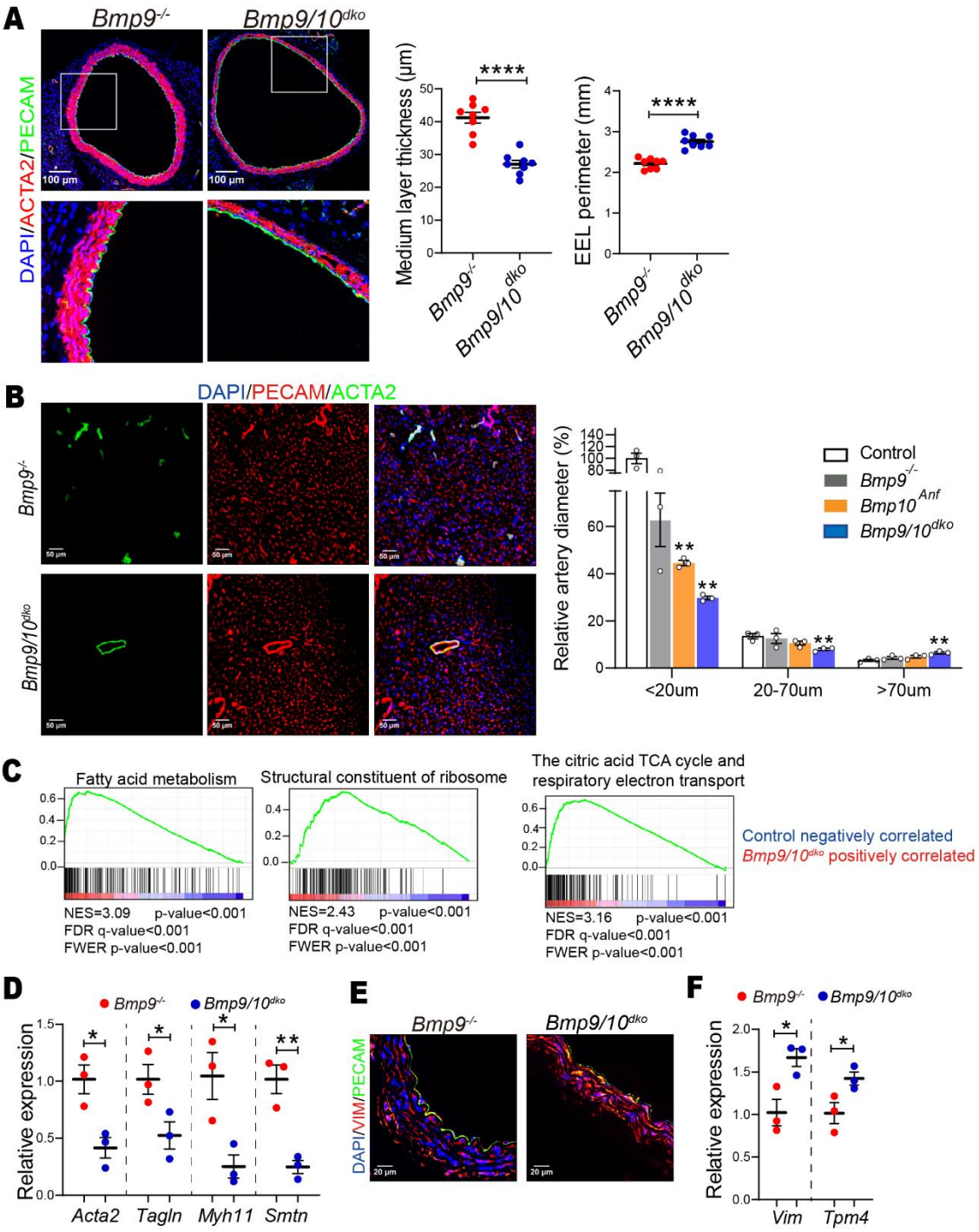

Figure 7. BMP9 and BMP10 are instrumental for formation of contractile VSMCs.

A. Immunofluorescence staining of aortae from 8 weeks old *Bmp9*$^{-/-}$ and *Bmp9/10*^{dko} mice for ACTA2 and PECAM. Quantification of medial layer thickness and external elastic lamina (data are mean±SEM; two tailed t-test: ***P<0.001, n=8). **B.** Immunofluorescence staining of hearts from 8 weeks old *Bmp9*$^{-/-}$ and *Bmp9/10*^{dko} mice for ACTA2 and PECAM. Quantification of relative artery diameter (data are mean±SEM; two tailed t-test: **P<0.01, n=3). **C.** Gene set enrichment analysis (GSEA) of aortae from 8 weeks old control and *Bmp9/10*^{dko} mice (n=2. y-axis: enrichment score; NES: Normalized Enrichment Score; FDR: False Discovery Rate;

FWER: Familywise Error Rate). **D.** RT-qPCR analysis of VSMC gene expression in aortae of *Bmp9*$^{-/-}$ and *Bmp9/10*^{dko} mice (data represent mean±SEM; two tailed t-test: *P <0.05, **P <0.01, n=3). **E.** Immunofluorescence staining of aortae from 8 weeks old *Bmp9*$^{-/-}$ and *Bmp9/10*^{dko} mutants for vimentin (VIM) (n=3). **F.** RT-qPCR analysis of synthetic gene expression in aortae of 8 weeks old *Bmp9*$^{-/-}$ and *Bmp9/10*^{dko} mice (data represent mean±SEM; two tailed t-test: *P <0.05, **P<0.01, n=3).

3.3 Acute deletion of *Bmp10* in adult *Bmp9* mutants recapitulates the *Bmp9/10*^{dko} phenotype.

Bmp9$^{-/-}$*/Bmp10*^{Anf} mutants show a strong attenuated contractile state of VSMCs. However, inactivation of *Bmp10* expression by *Anf-Cre*, which occurs during fetal development might generate a developmental phenotype, which might obscure potential functions of BMP9/BMP10 for maintaining the contractile state of VSMCs in adult mice. In order to rule out such a possibility, the tamoxifen-inducible alpha myosin-heavy chain *MerCreMer* strain was employed to inactivate BMP10 in adult BMP9 mutants (*Bmp9*$^{-/-}$*/Bmp10*^{iMhc}, hereafter called *Bmp9/10*^{iMhc}). The MerCreMer strain proved to be as efficient as the *Anf-Cre* mice to inactivate *Bmp10* in right atria as suggested by RT-PCR analysis after 7 times tamoxifen injection (Figure 8A, 8B). Exactly the same phenotype in *Bmp9*$^{-/-}$*/Bmp10*^{iMhc} as in *Bmp9*$^{-/-}$*/Bmp10*^{Anf} mutants was observed. Staining against ACTA2 and PECAM revealed that aortae were massively dilated as indicated by the increase of the external elastic lamina perimeter by 37% (n=6; unpaired two-tailed Student's t-test: P<0.0001) and thickness of the muscular layer was reduced by 32% (n=6; unpaired two-tailed Student's t-test: P<0.0001) (Figure 8C). RT-qPCR showed that expression of typical contractile VSMC genes including *Acta2, Tagln, Myh11 and Smtn* was strongly down-regulated in aortae (Figure 8D). In contrast, the synthetic marker VIM was more abundant as indicated by immunofluorescence staining (Figure 8E). Expression of synthetic VSMC genes including *Vim* and *Tpm4* increased significantly (Figure 8F). My results demonstrate that BMP9 and BMP10 are instrumental for acquisition and maintenance of contractile VSMCs identity. The strong changes of VSMCs in BMP9 and BMP10 compound mutants, which were not apparent in single mutant mice, indicated that BMP9 and BMP10 play partially redundant functions *in vivo*.

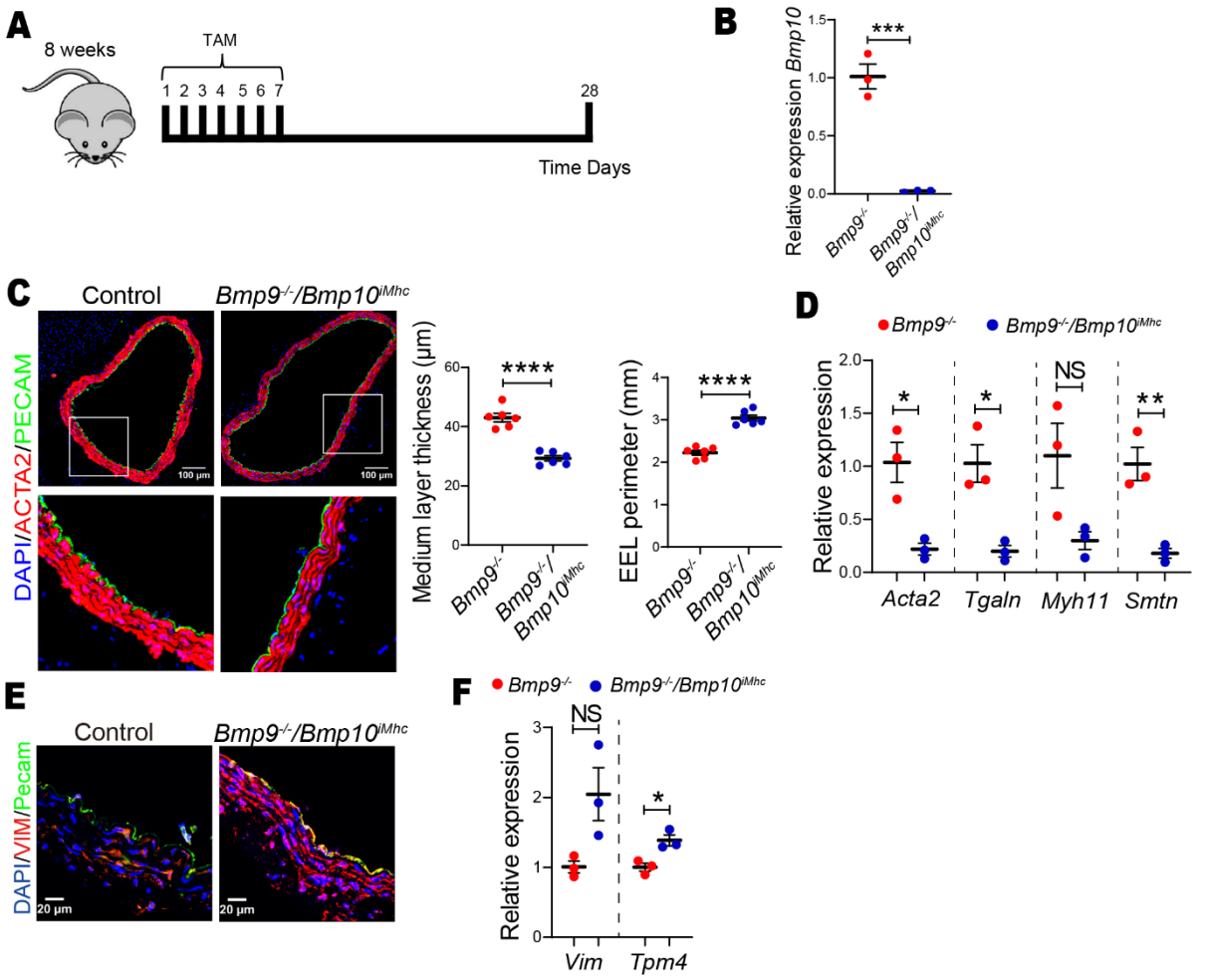

Figure 8. Acute deletion of BMP10 in adult mice results in loss of contractile VSMCs.

A. Schematic depiction of the timeline for tamoxifen treatment and tissue analysis. TAM, tamoxifen. **B.** RT-qPCR analysis of *Bmp10* expression in the right atrium after tamoxifen injection in *Bmp9*$^{-/-}$/*Bmp10*^{iMhc} mice (data represent mean±SEM; two tailed t test: ***P< 0.001, n=3). **C.** Immunofluorescence staining of aortae from *Bmp9*$^{-/-}$/*Bmp10*^{iMhc} mice for ACTA2 and PECAM (n=6). Quantification of medial layer thickness and external elastic lamina perimeter (EEL) (data represent mean±SEM; two tailed t-test: ****P<0.0001, n=6, *iMhc-Cre* negative mice were used as control). **D.** RT-qPCR analysis of SMC gene expression in aortae from control and *Bmp9*$^{-/-}$/*Bmp10*^{iMhc} mice after tamoxifen injection (data represent mean±SEM; two tailed t test: *P<0.05, **P<0.01, NS P>0.05, n=3). **E.** Immunofluorescence staining for Vimentin (VIM) in aortae from control and *Bmp9*$^{-/-}$/*Bmp10*^{iMhc} mutants (n=3). **F.** RT-qPCR analysis of synthetic gene expression in aortae from control and *Bmp9*$^{-/-}$/*Bmp10*^{iMhc} mice (data represent mean±SEM; two tailed t test: *P<0.05, NS P>0.05, n=3).

3.4 Inactivation of BMP9/BMP10 are partially protected against hypoxia-induced PH.

The severe reduction in contractile VSMCs in *Bmp9/10*^{dko} mutants suggested a potential

protection against hypoxia-induced PH. Hence, we investigated the impact of BMP9 and BMP10 on pulmonary hemodynamics and right ventricle function under normoxia and 10% hypoxia for 28 days. Chronic hypoxia is a strong inducer of PH and pulmonary vascular remodeling, characterized by SMC, EC and fibroblast proliferation, leading to lumen obliteration[192]. Exposure to hypoxia revealed an improvement of hemodynamic parameters and right ventricle function in *Bmp9/10^{dko}* mutants. To study the right ventricle function, Tricuspid Annular Plane Systolic Excursion (TAPSE), a parameter used to evaluate global right ventricle function, was calculated[193]. The result revealed that TAPSE was reduced in control and single knockout mice after hypoxia treatment but did not change dramatically in *Bmp9/10^{dko}* mutants (Figure 9A), suggesting the right ventricle function was maintained. Pulmonary acceleration time (PAT) was only slightly lower in *Bmp9/10^{dko}* after treatment but it was remarkably decreased in control and BMP10 single mutants, suggesting a poor blood flow in those mice (Figure 9B). Moreover, calculation of the Fulton index (right ventricular weight to left ventricular plus septal weight) revealed that *Bmp9/10^{dko}* mutants developed much milder right ventricle hypertrophy than *Bmp9$^{-/-}$* and *Bmp10^{Anf}* single mutants or controls (Figure 9C). Finally, right ventricular systolic pressure (RVSP) was significantly increased in control and *Bmp10^{Anf}* mice, suggesting the mice developed symptoms of PH. In contrast, RVSP was much lower in hypoxia-treated *Bmp9$^{-/-}$* and *Bmp9/10^{dko}* (Figure 9D). Taken together, it seems valid to conclude that the loss of BMP9 and BMP10 partially protects mice from hypoxia-induced PH.

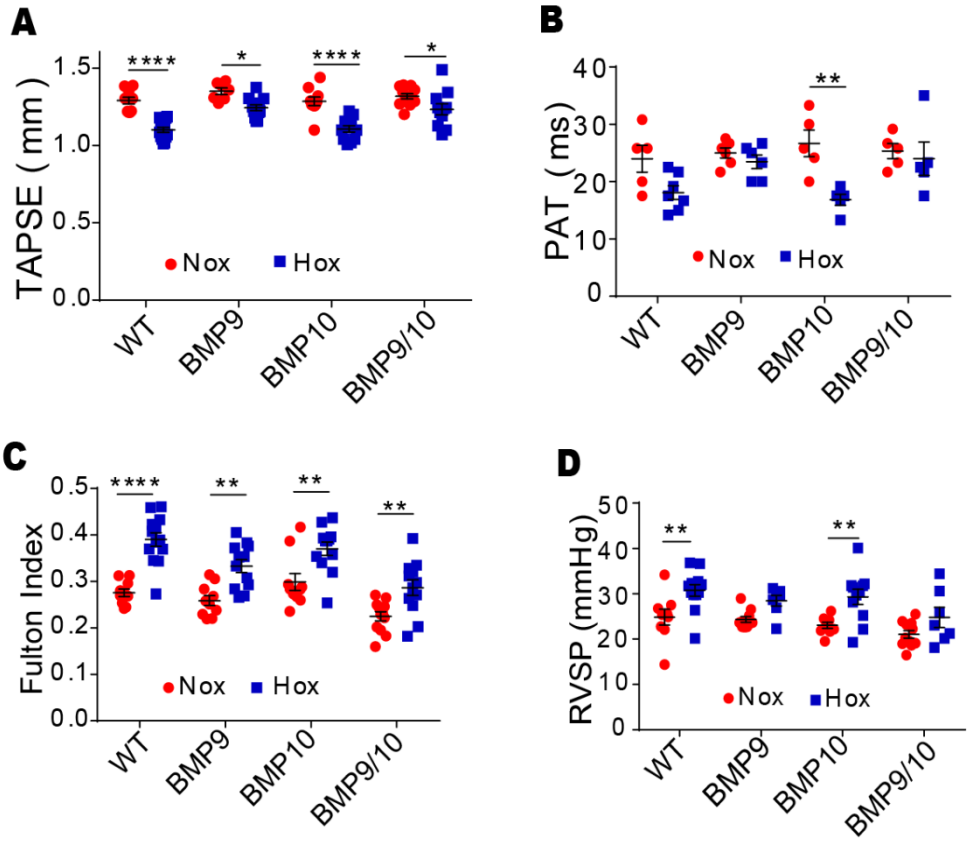

Figure 9. Loss of BMP9 and BMP10 protect mice against hypoxia-induced PH.
A. TAPSE in the right ventricle measured by right heart catheterization (data represent mean±SEM; two tailed t-test: *P<0.05, ****P<0.0001, n=12)**. B.** PAT measured by pulmonary artery catheter (data represent mean±SEM; two tailed t-test: **P<0.01, n=12). **C.** Right ventricle hypertrophy was calculated by Fulton index as the weight ratio of right ventricle and (left ventricle + septum) (data represent mean±SEM; two tailed t-test: **P<0.01, ****P<0.0001, n=12). **D.** Right ventricle systolic pressure (RVSP) in mmHg measured by right heart catheterization (data represent mean±SEM; two tailed t-test: **P<0.01, n=12). Primary data were generated by Dr. Simone Kraut, University of Giessen.

3.5 Overexpression of *Bmp10* induces a major phenotypic shift in VSMCs and leads to acquisition of a hyper-contractile state.

The concomitant absence of BMP9 and BMP10 leads to a profound loss of contractile VSMCs and increased vessel diameter. To investigate whether elevated levels of BMP10 have opposite effects, a Cre-inducible BMP10 gain-of-function mouse model was generated, in which a BMP10 cDNA is overexpressed from the *Rosa26* gene locus under the control of the ubiquitously active cytomegalovirus enhancer-chicken beta-actin (CAG) promoter after Cre-mediated excision of a flox-stop-flox cassette(*Rosa26*^{Bmp10}) (Figure 10A). Crossing of the strain with mice expressing either the constitutively active *Tie2-Cre* or tamoxifen-inducible *Cdh5-Cre-ERT2* allowed specific expression of BMP10 in ECs during embryonic development or in adult mice. Overexpression of *Bmp10* during fetal development strongly increased formation of contractile VSMCs, severely disrupting angiogenesis and causing early embryonic lethality around E8.5 (data not shown). To analyze effects of increased *Bmp10* expression in adult mice, I administrated tamoxifen to *Cdh5-Cre-ERT2/Rosa26*^{iBmp10} (thereafter called *Rosa26*^{iBmp10}) mice, which resulted in strong induction of *Bmp10* expression in ECs of aortae (Figure 10C). The data showed a strong increase of smooth muscle coverage reflected by increased medium wall thickness by 47% (n=7, unpaired two-tailed Student's t-test: P<0.0001) (Figure 10D). Additionally, immunofluorescence staining showed increased expression of *Acta2* (Figure 10D). Furthermore, decreased diameters of aortic lumens were observed as indicated by a decrease of EEL perimeter by 20% in aortae (n=7, unpaired two-tailed Student's t-test: P<0.0001). The phenotype was also observed in other vessel beds including pulmonary arteries and cardiac arteries (data not shown). Moreover, RT-qPCR analysis of aortae revealed that typical VSMC markers including *Acta2, Tagln, Myh11* and *Smtn* were significantly increased (Figure 10E). Immunofluorescence staining demonstrated reduced presence of VIM in aortae (Figure 10F). In addition, RT-qPCR showed lower expression of synthetic marker including *Vim* and *Tpm4*, corroborating a profound shift of VSMCs from synthetic to hyper-contractile state when concentrations of BMP10 were increased (Figure 10G). Interestingly, the increased thickness of arterial muscular layers was accompanied by dilation of right ventricles, and the right

ventricle wall thickness was reduced significantly (Figure10 H). Hemodynamic measurements revealed a strong increase of the RVSP in *Rosa26*^{iBmp10} mice, which explains the right ventricular dilation (Figure 2I). Likewise, we observed a substantial elevation of systemic blood pressure in *Rosa26*^{iBmp10} after initiation of increased *Bmp10* expression both during day time and night time (Figure 10J). Taken together, the findings clearly demonstrate that enhanced availability of BMP10 within arteries is sufficient to increase the number of contractile VSMCs, blood pressure and reduce vessel diameter.

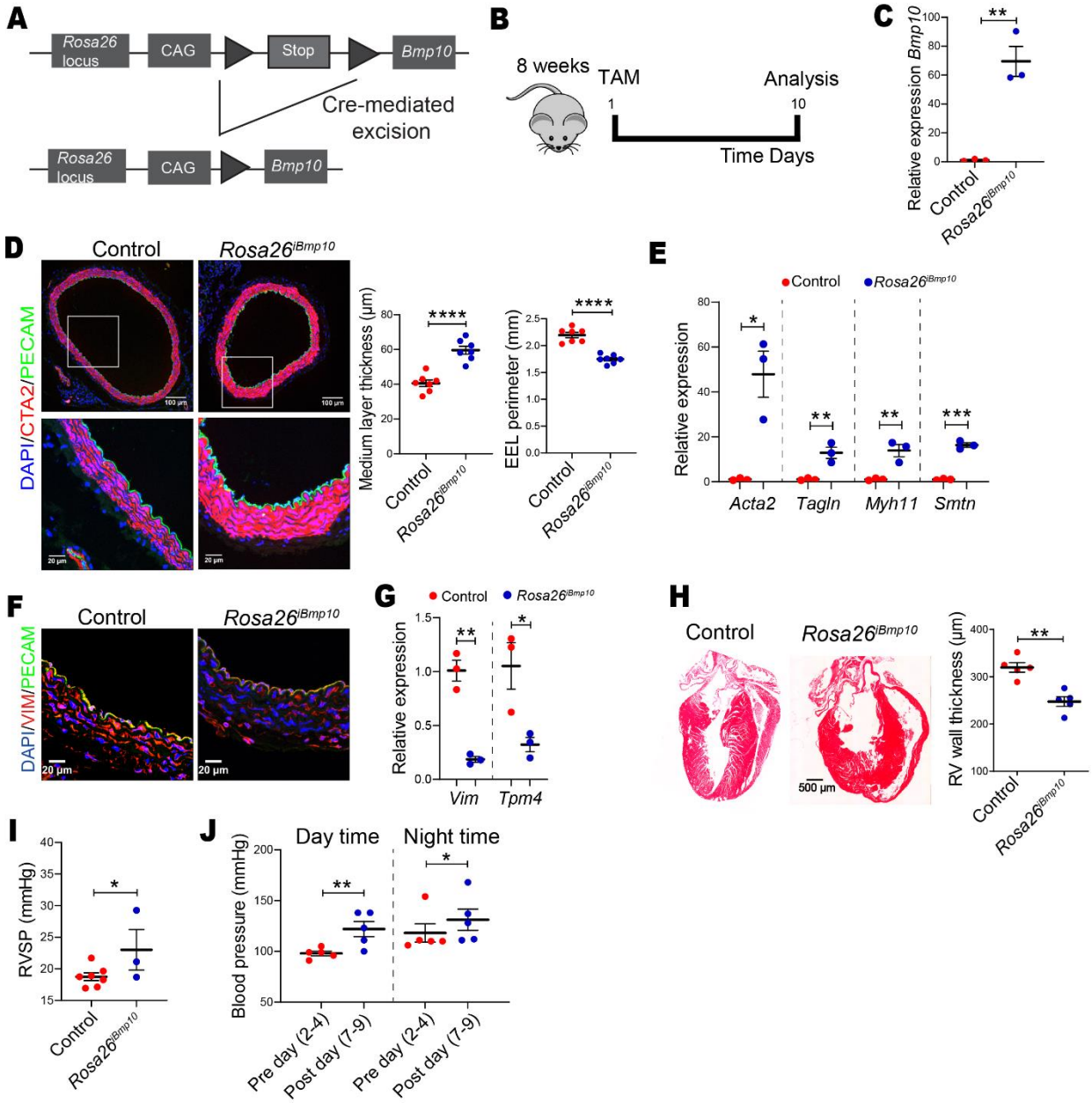

Figure 10. Overexpression of *Bmp10* in endothelial cells leads to excessive formation of contractile VSMCs.

A. Schematic representation of the strategy to generate the *Bmp10* overexpression allele. **B.** Schematic representation of the timeline for tamoxifen treatment and tissue analysis. **C.**RT-

qPCR analysis of *Bmp10* expression in aortae of control and *Rosa26*^{iBmp10} mice after tamoxifen injection (data represent mean±SEM; two tailed t-test: **P<0.01, n=3). **D.** Immunofluorescence staining of aortae from control and *Rosa26*^{iBmp10} mice for ACTA2 and PECAM. Quantification of medial layer thickness and external elastic lamina (data are mean±SEM; two tailed t-test: ****P<0.0001, n=7). **E.** RT-qPCR analysis of SMC gene expression in aortae from control and *Rosa26*^{iBmp10} mice (data represent mean±SEM; two tailed t-test: *P<0.05, **P<0.01, ***P< 0.001, n=3). **F.** Immunofluorescence staining of aortae from control and *Rosa26*^{iBmp10} mice for VIM after tamoxifen injection (n=3). **G.** RT-qPCR analysis of synthetic gene expression in aortae from control and *Rosa26*^{iBmp10} mice (data represent mean±SEM; two tailed t-test: *P<0.05, **P<0.01, n=3). **H.** H&E staining of hearts of control and *Rosa26*^{iBmp10} two weeks after tamoxifen injection (data represent mean±SEM; two tailed t-test: **P<0.01, n=5). **I.** Right ventricle systolic pressure (PVSP) measurements of 8-weeks-old control (n=6) and *Rosa26*^{iBmp10} (n=3) mice 7 days after tamoxifen induction (data represent mean±SEM; *P<0.05). **J.** Average telemetric blood pressure measurements of *Rosa26*^{iBmp10} mice 2-4 days pre-and 7-9 days post-tamoxifen induction (data represent mean±SEM; paired, one-tailed Student's t-test: *P<0.05, **P<0.01, n=5).

3.6 Increased apelin signaling from the endothelium plays a negligible role for VSMC homeostasis.

So far the data showed that inactivation of BMP9/BMP10 results in a phenotypic shift of VSMCs from a contractile to a synthetic state, while overexpression of *Bmp10* stimulates formation of contractile VSMCs. The effects of BMP9/BMP10 on VSMCs might be mediated by ECs, which might release signals and cause VSMC phenotypic switching and vessel dilation. Indeed, evidence was obtained that BMP9/BMP10 exert effects on ECs, which may act on VSMCs and stimulate the phenotype observed in *Bmp9/10*^{dko} mutants. BMP9/BMP10 treatment strongly down-regulated the vasodilatory factor apelin in human umbilical vein endothelial cells (HUVECs) (Figure 11A, 11B) and RT-qPCR revealed up-regulation of apelin in hearts of *Bmp9/10*^{dko} mice (Figure11C). These findings are in line with previous observations demonstrating higher levels of apelin and adrenomedullin in *Bmp9*$^{-/-}$ mice chronically exposed to hypoxia[12]. Therefore, it was assumed that inactivation of apelin in the *Bmp9/10*^{dko} mice might rescue the loss of contractile VSMC phenotype and the increased vessel dilation. To analyze this possibility, apelin/BMP9/BMP10 triple mutant mice (*Bmp9/Bmp10*^{dko}*/apelin*$^{-/-}$, thereafter called TKO) were generated by breeding *Bmp9/10*^{dko} mice with *apelin*$^{-/-}$ mice. RT-qPCR show that apelin was efficiently decreased in TKO mice (Figure 11C). Surprisingly, the phenotype of TKO mice did not differ from *Bmp9/10*^{dko} mice. PCR-qPCR showed that there was no increase of *Acta2* expression in aortae compared to *Bmp9/10*^{dko} mice (Figure 11D). A comparable loss of contractile VSMCs and vasodilation as in *Bmp9/10*^{dko} mice (Figure 11E) was observed. Thus, the up-regulation of apelin is not decisive for the VSMC phenotype of *Bmp9/10*^{dko} mice,

although BMP9/BMP10 mediated regulation of apelin and other vasoactive molecules might be relevant in a different physiological context. However, it is possible that the failed rescue is due to the presence of second ligand for APJ, i.e. apela[194], which also binds to the apelin receptor APJ and might compensate for the loss of apelin.

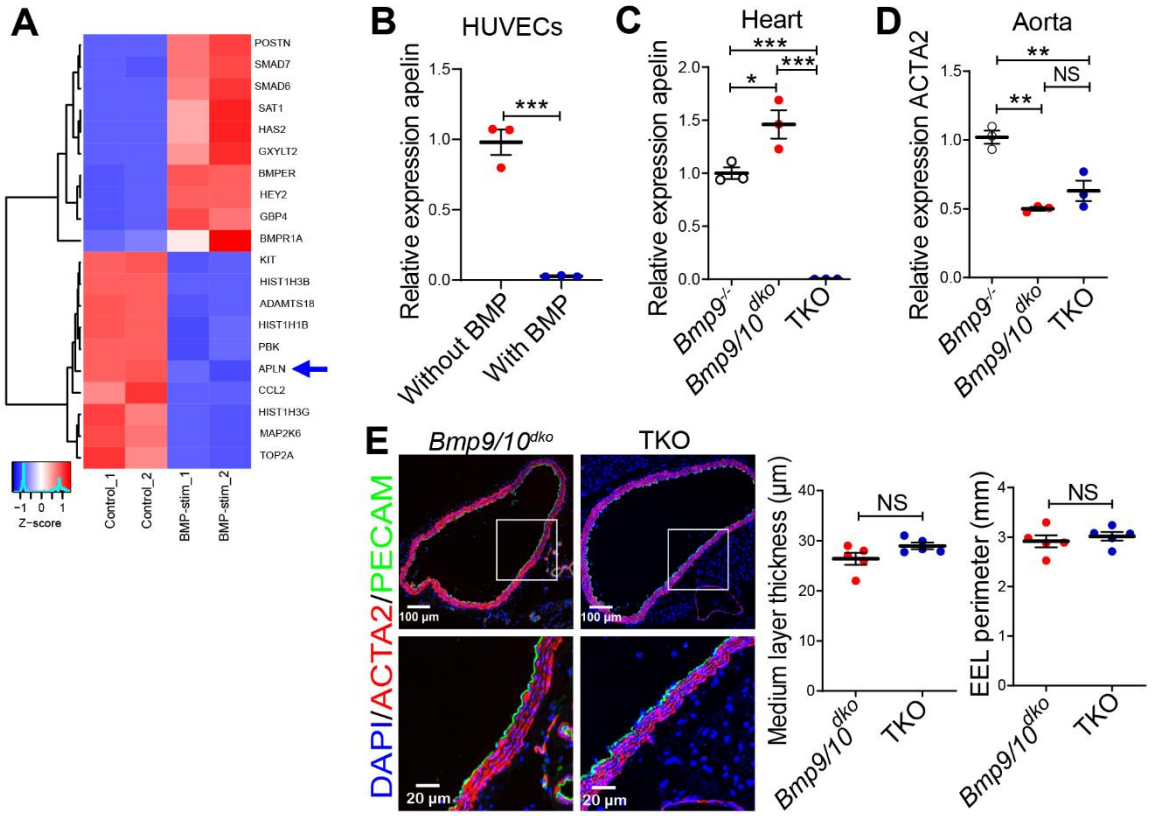

Figure 11. The up-regulation of *apelin* in *Bmp9/10^{dko}* mice does not play a crucial role for vasodilatation and the loss of contractile VSMCs.

A. RNA-seq analysis of HUVECs treated with BMP9/BMP10 for 6 hours. The heatmap displays top 20 differentially expressed genes. **B.** RT-qPCR analysis of *apelin* expression in HUVECs after treatment with BMP9/BMP10 for 6 hours (data represent mean±SEM; two tailed t-test: ***P<0.001, n=3). **C.** RT-qPCR analysis of apelin expression in hearts of *Bmp9$^{-/-}$*, *Bmp9/10^{dko}* and *Bmp9/10^{dko}/apelin$^{-/-}$* mice (data represent mean±SEM; one-way ANOVA: *P<0.05, ***P<0.001, n=3). **D.** RT-qPCR analysis of *Acta2* in aortae of *Bmp9$^{-/-}$*, *Bmp9/10^{dko}* and *Bmp9/10^{dko}/apelin$^{-/-}$* mice (data represent mean±SEM; one-way ANOVA: *P< 0.05, **P<0.01, n=3). **E.** Immunofluorescence staining for ACTA2 and PECAM in aortae from 8 weeks old *Bmp9/10^{dko}* and *Bmp9/10^{dko}/apelin$^{-/-}$* mice. Quantification of medial layer thickness and external elastic lamina (data represent mean±SEM; two tailed t-test: NS P>0.05, n=5).

3.7 Overexpression of *Smad7* with *Sm22a-Cre* suppresses VSMC formation during embryonic development.

The results indicated that increased apelin signaling from the endothelium plays a negligible

role to confer effects of the absence of BMP9/10 to VSMCs. It seems more likely that BMP9 and BMP10 act directly on VSMCs by passing through the EC layer or by the microcirculation serving larger muscularized vessels. To understand whether inhibition of BMP-Smad signalling in VSMCs prevents formation of contractile VSMCs, the inhibitory *Smad7* was specifically overexpressed in SMCs. Smad7 is a general antagonist of TGF-β signaling that forms a stable complex with type I receptors, therefore leading to inhibition of R-Smad phosphorylation and the hetero-complex formation between R-Smads and Co-Smad. It also recruits the E3 ubiquitin ligases, Smurf1 and Smurf2 to the activated type I receptor leading to degradation of the receptor through the proteasomal pathway and interferes with the R-Smad-Smad4-DNA complex formation by binding to DNA in the nucleus[188, 189]. Following the same strategy as for *Bmp10* overexpression, mice that conditionally expressed *Smad7* from the ROSA26 locus under control of CAG promoter were generated (*Rosa26*^{Smad7}) (Figure 12A). Firstly, to specifically overexpress *Smad7* in SMCs, the *Rosa26*^{Smad7} strain was crossed with *Sm22-Cre*, a Cre-expressing strain that is constitutively active during embryonic development (*Rosa26*$^{Sm22\text{-}Smad7}$). Overexpression of *Smad7* in SMCs resulted in embryonic lethality at E10.5 (Figure 12B) and dramatically reduced coverage of SMCs within vessels, which nearly completely lacked expression of SMC specific markers ACTA2 and TAGLN (Figure 12C, 12D). I therefore concluded that the embryonic lethality was most likely caused by the loss of SMC proliferation, migration and differentiation. Because vascular defects in *Smad7* overexpression mice were observed before embryonic circulation was established and cardiogenesis was not affected, it was unlikely that failed VSMC development and arrested angiogenesis were secondary to impaired blood flow. In other words, the nearly complete absence of VSMCs in mice overexpressing *Smad7* clearly indicates that BMP/Smad signalling is essential for differentiation of VSMCs.

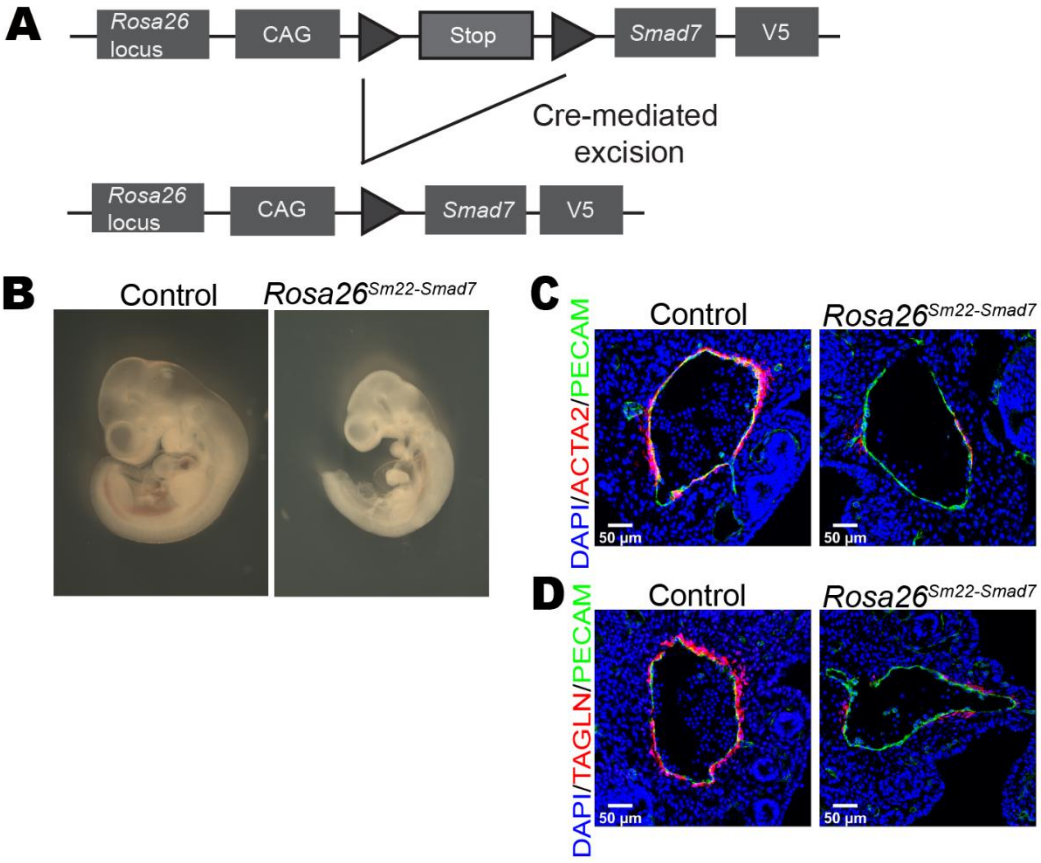

Figure 12. Overexpression of *Smad7* suppresses VSMC differentiation during embryonic development.

A. Schematic depiction of the strategy to overexpress *Smad7* in SMCs, using a SMC specific driver. **B.** The development of embryos of *Rosa26*$^{Sm22\text{-}Smad7}$ was delayed with smaller body size (n=4). **C, D.** Immunofluorescence staining for ACTA2 (C) and TAGLN (D) in control and *Rosa26*$^{Sm22\text{-}Smad7}$ embryonic vessels at E10.5 (*Sm22-Cre* negative mice were used as control, n=6).

3.8 Overexpression of *Samd7* with *Smmhc-Cre* in adult mice causes loss of contractile VSMCs and vessel dilation.

Smad7 was also expressed specifically in SMCs of adult mice by crossing an inducible *Smmhc-Cre* driver with adult *Rosa26*^{Smad7} mice (*Rosa26*$^{Smmhc\text{-}iSmad7}$), which will not result in Smad7 expression in the heart. Conditional expression of *Smad7* in SMCs of adult mice strongly decreased the coverage of arterial vessels in ACTA2-expressing VSMCs, reducing the thickness of the muscular layer by 34% (n=6; unpaired two-tailed Student's t-test: P<0.0001) and causing vessel dilation, as indicated by increase of the EEL perimeter by 31% (n=6; unpaired two-tailed Student's t-test: P<0.001) (Figure 13B). Accordingly, expression of specific markers for contractile VSMCs in aortae was lower as indicated by RT-qPCR (Figure 13C), while immunofluorescence staining revealed increased expression of VIM in aortae (Figure

13D). In addition, RT-qPCR using samples from aortae showed increased synthetic gene expression including *Vim* and *Tpm4* (Figure13E). These data supported the hypothesis that BMP/Smad signalling in SMCs was required for normal VSMC development and maintenance. Additionally, these findings corroborate the observation from Mao[47], who described that the deletion of Smad4 specific in SMCs resulted in decreased VSMC differentiation, migration as well as attachment and spreading. Taken together, these experiments reveal that suppression of BMP signalling in VSMCs, without disturbing endothelium, prevents VSMC differentiation, proliferation and contractility maintenance.

The direct effects of BMP9/BMP10 on VSMCs *in vivo* suggested that circulating BMP9/BMP10 might reach the SMC layer either by *vaso vasorum* or by active or passive transport through the endothelial barrier. To explore the underlying mechanisms, mesenteric arteries were isolated from wild type mice and perfused in a pressure myograph system, which mimics blood circulation *in vivo*[195]. Mesenteric arteries were perfused with BMP9/BMP10 for 1 hour and a strong Smad1/5/8 phosphorylation was observed in the VSMC layer while no Smad1/5/8 phosphorylation was observed in control-perfused arteries (Figure 13F). Since BMP9/BMP10 cannot reach the VSMC layer via capillary *vasa vasorum* in arteries mounted in a pressure myograph, this result strongly indicates that circulating BMP9/BMP10 reach VSMCs through the endothelial barrier.

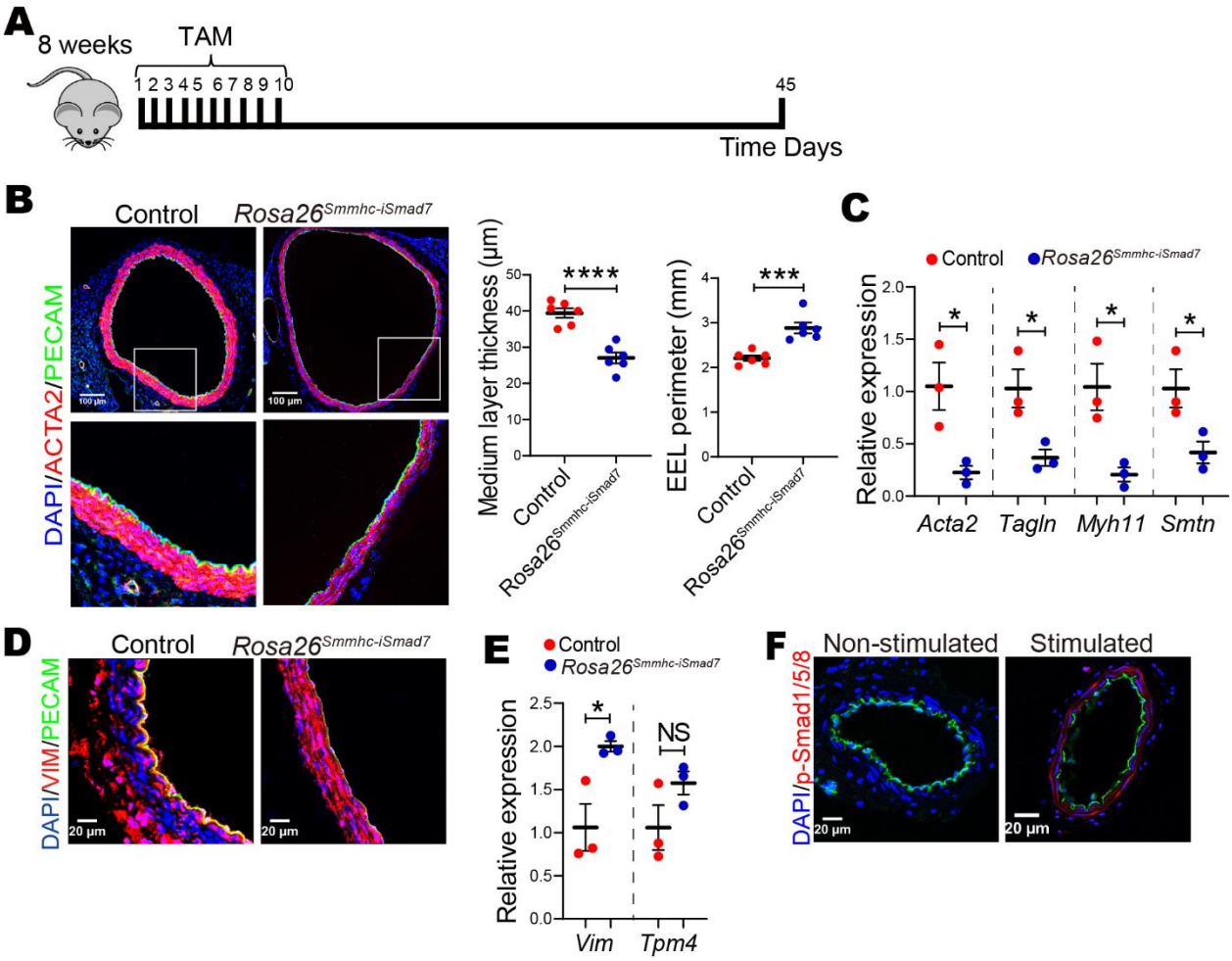

Figure 13. Enhanced *Smad7* expression suppresses formation of contractile VSMCs. **A.** Schematic depiction of the timeline for tamoxifen treatment and tissue analysis. TAM, tamoxifen**. B.** Immunofluorescence staining of control and *Rosa26*$^{Smmhc\text{-}iSmad7}$ aortae for ACTA2 and PECAM after tamoxifen injection. Quantification of medial layer thickness and external elastic lamina (data represent mean±SEM; two tailed t test: ****P<0.001, n=6). **C.** RT-qPCR analysis of SMC gene expression in control and *Rosa26*$^{Smmhc\text{-}iSmad7}$ aortae (data represent mean±SEM; two tailed t test: *P<0.05, n=3). **D.** Immunofluorescence staining of control and *Rosa26*$^{Smmhc\text{-}iSmad7}$ aortae for VIM after tamoxifen injection (n=5). **E.** RT-qPCR analysis of synthetic gene expression in control and *Rosa26*$^{Smmhc\text{-}iSmad7}$ aortae (data represent mean±SEM; two tailed t test: *P<0.05, NS P>0.05, n=3). **F.** Immunofluorescence staining of phosphorylated Smad1/5/8 after perfusion of myograph-mounted mesenteric arteries with BMP9/BMP10 for 1 hour (n=4).

3.9 The regulation of ATOH8 by BMP9/BMP10 does not play a decisive role for contractile state of VSMCs.

To gain further insights into how BMP9/BMP10 control the fate of VSMCs, RNA-seq analysis with cultured PASMCs stimulated with BMP9/BMP10 was performed. Interestingly, within the

top genes that were up-regulated was the basic helix-loop-helix transcription factor *Atoh8* (also known as Math6 or Hath6)[196], which to date has not been described as a downstream target of BMP9/BMP10 signalling. Interestingly, a publication identified ATOH8 as a shear-stress-responsive transcription factor and ATOH8 was the up-stream regulator of eNOS, which generates NO and causes vessel dilation[197]. Consistent with the RNA-seq result, BMP9/BMP10 treatment of PASMCs resulted in a significant up-regulation of *Atoh8* suggested by RT-qPCR (Figure 14A), while *Atoh8* expression was significantly reduced in *Bmp9/10*^{dko} mutants (data not shown). These results suggested that ATOH8 is a bona fide downstream target of BMP signalling in VSMCs. To further investigate the role of ATOH8 in VSMC differentiation and contraction, *Atoh8* overexpression mice were generated (*Rosa26*^{iAtoh8}), following the same strategy as for *Bmp10* and *Smad7* overexpression strains (Figure 14B). We firstly employed *Sm22*-Cre driver to specifically increase the expression of *Atoh8* in SMCs (*Rosa26*$^{Sm22\text{-}iAtoh8}$). Western blot confirmed that the protein level of ATOH8 was significantly increased in SMCs (Figure 14C). However, similar to ATOH8 knockout mice, overexpression of *Atoh8* did not lead to embryonic lethality. ATOH8 mutant mice were healthy and fertile and the vessel morphology in adult animals appeared normal. Neither the vessel diameter nor VSMC coverage was changed (Figure 14D). Therefore, a *Cmv-Cre* deleter was employed to overexpress *Atoh8* (*Rosa26*$^{Cmv\text{-}iAtoh8}$) in all tissues. Again, staining against ACTA2 and PECAM suggested that vessel diameter and VSMC coverage were not affected (Figure 14D). In summary, the data indicate that ATOH8 is a downstream target of BMP signalling in VSMCs but plays a negligible role for differentiation and the contractile state of VSMCs.

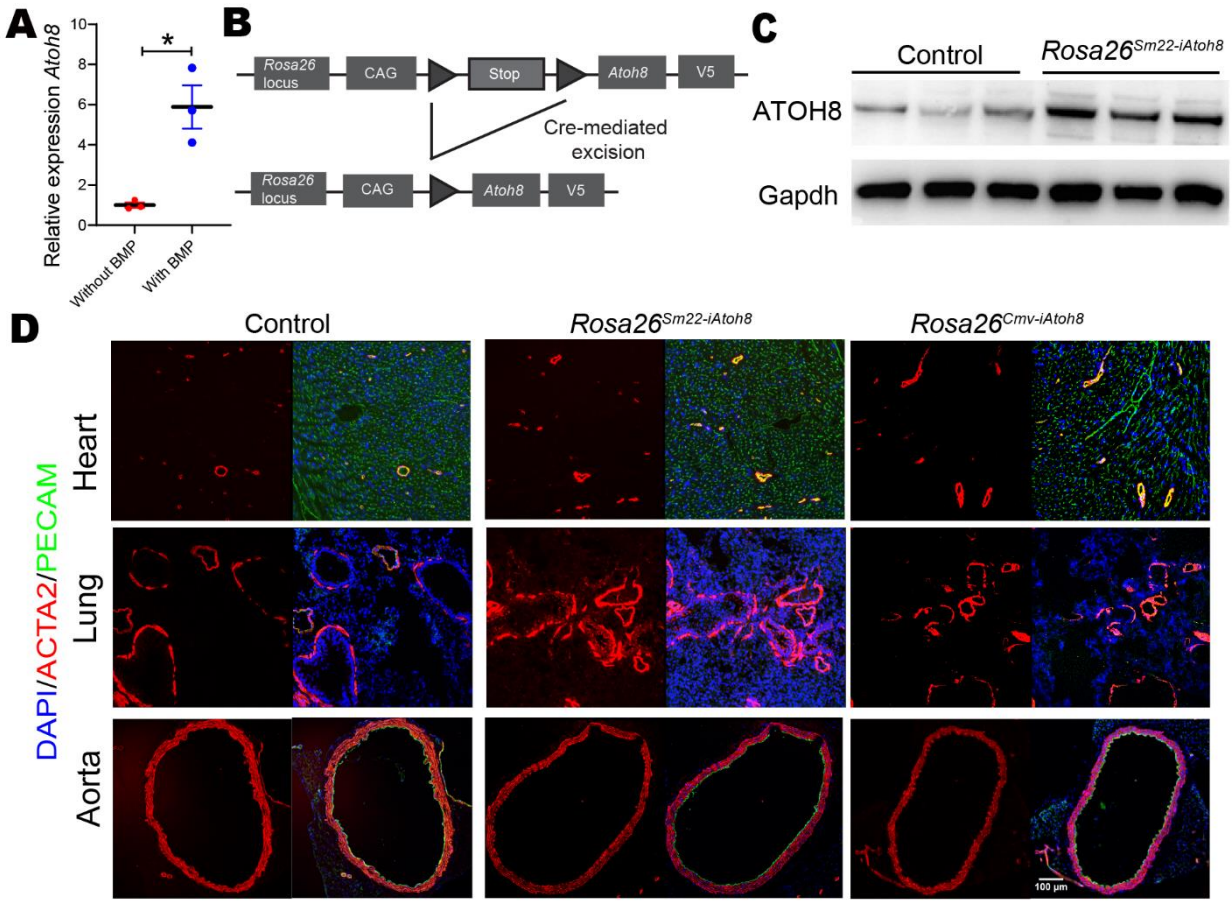

Figure 14. ATOH8 has a negligible role in differentiation and the contractile state of VSMCs.

A. RT-qPCR of *Atoh8* expression in cultured PASMCs treated with BMP9 and BMP10 (data presented as mean±SEM; two tailed t test: *P<0.05, n=3). **B.** Schematic depiction of the overexpression strategy for *Atoh8*. **C.** Western blot analysis of ATOH8 in aortae of 8 weeks old control and *Rosa26*$^{Sm22\text{-}iAtoh8}$ mice (n=3). **D.** Immunofluorescence staining of ACTA2 and PECAM of heart, lung and aortae of 8 weeks old control, *Rosa26*$^{Sm22\text{-}iAtoh8}$ and *Rosa26*$^{Cmv\text{-}iAtoh8}$ mice (n=5 in each strain).

3.10 BMP9/BMP10 act directly on VSMCs via the ALK1/Smad signalling pathway to induce VSMC differentiation *in vitro*.

To further answer the question whether BMP9/BMP10 exert effects directly on VSMCs, PASMCs from wild type mice were isolated and cultured. Cultured cells rapidly lost the contractile phenotype and acquired synthetic characteristics. Stimulation of de-differentiated PASMCs with BMP9/BMP10 for 48 hours resulted in a remarkable increase of *Acta2, Tagln, Myh11* and *Smtn* expression as suggested by immunofluorescence staining (Figure 15A). 12 hours stimulation with BMP9/BMP10 induced the expression of *Acta2* and *Tagln* and 24 hours stimulation induced the expression of mature contractile genes *Myh11* and *Smtn* as measured by RT-qPCR compared to non-stimulated cells, indicating a shift from de-differentiated,

synthetic to a differentiated, contractile state (Figure 15B). As indicated by RNA-seq analysis, BMP9/BMP10 treated PASMCs showed a strong up-regulation of genes required for VSMC contraction including *Acta2, Cald1, Smtn* and *Myl9, Myl12* (Figure 15C). Furthermore, increased expression of typical BMP-target genes such as the type II receptor *Bmpr2, Smurf, Fstl1* and others was found (Figure 15C). Gene set enrichment analysis (GSEA) showed enrichment of terms related to elastic fiber formation, smooth muscle cell contraction, extracellular matrix organization and vesicle mediated transport, suggesting PASMCs became mature and differentiated upon BMP9/BMP10 stimulation (Figure 15D). Accordingly, I observed increased expression of typical genes within the terms “Smooth muscle contraction” and “Signalling by BMP” (Figure 15E, 15F). Interestingly, a concomitant up-regulation of the inhibitory *Smad7* was observed, which may represent a cellular counter-measure to prevent excessive BMP-Smad-signalling after BMP9/BMP10 stimulation (Figure 15C, 15F). The dramatic changes in the transcriptional profile of BMP9/BMP10 treated VSMCs suggest that cellular processes related to contractile state of VSMCs depend on the presence BMP9 and BMP10.

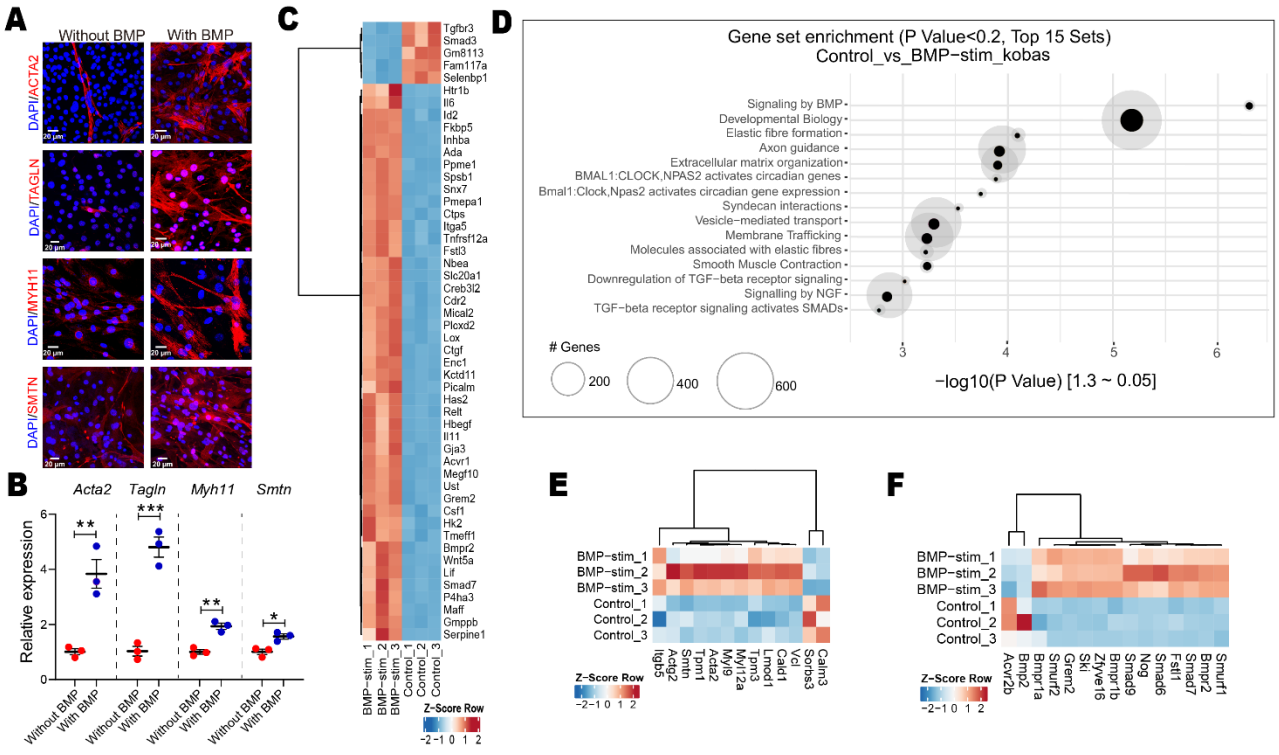

Figure 15. BMP9/BMP10 act directly on VSMCs to induce contractile state of VSMCs.
A. Immunofluorescence staining for ACTA2, TAGLN, MYH11 and SMTN in cultured PASMCs treated with BMP9/BMP10 for 48 hours. **B.** RT-qPCR analysis of *Acta2*, *Tagln*, *Myh11* and *Smtn* expression in PASMCs, following treatment with BMP9/BMP10 (data represent mean±SEM; two tailed t-test: *P<0.05, **P<0.01, ***P<0.001 n=3). **C.** RNA-sequencing analysis of BMP9/10-treated PASMCs 6 hours after BMP9/BMP10 stimulation. The heatmap

displays the top 50 differentially expressed genes (DEGs) based on significance (FDR). **D.** GSEA pathway enrichment analysis of genes up-regulated in PASMCs treated with BMP9/BMP10 for 6 hours compared to non-stimulated cells. The top 15 pathways based on p-values are displayed. Circle sizes represent the scale. Centered circles represent the number of up-regulated genes in different pathways (cutoff: FDR < 5%, BaseMean > 5, log2FC > 0.585). **E.** Heatmap for RNA-sequencing analysis of BMP9/10-treated PASMCs with DEGs matching to enriched term “Smooth muscle contraction” of Reactome database (n=3). **F.** Heatmap for RNA-sequencing analysis of BMP9/10-treated PASMCs with DEGs matching to enriched term “Signaling by BMP” of Reactome database (n=3).

3.11 BMP9 and BMP10 stimulation increases chromatin accessibility of VSMC genes.

Besides RNA-seq, Assay for Transposase-Accessible Chromatin coupled with deep sequencing (ATAC-seq) of BMP9/BMP10 stimulated PASMCs was performed as well. ATAC-seq analysis identified numerous potential target genes with increased chromatin accessibility (Figure 16A). GSEA revealed enrichment of terms related to elastic fiber formation, Wnt ligand biogenesis, extracellular matrix organization and gap junction formation, while terms related to PDGF, EGF and VEGF-signalling were greatly depleted (Figure 16B). Since previous studies have suggested that these signalling pathways induce VSMC proliferation, migration and negatively regulate VSMC differentiation[198, 199], this result suggests that the PASMCs became differentiated and maturate upon BMP9/BMP10 stimulation. The dramatic changes in the transcriptional profile of BMP9/BMP10 treated VSMCs suggest that cellular processes related to maturation of the muscular layer depend on BMP9/BMP10. Furthermore, a combined analysis of RNA-seq and ATAC-seq signals identified several SMC differentiated genes such as, *Acta2* and *Tagln*, showing that transcriptional levels were increased and chromatin were accessible upon BMP9/BMP10 treatment (Figure 16C, 16D).

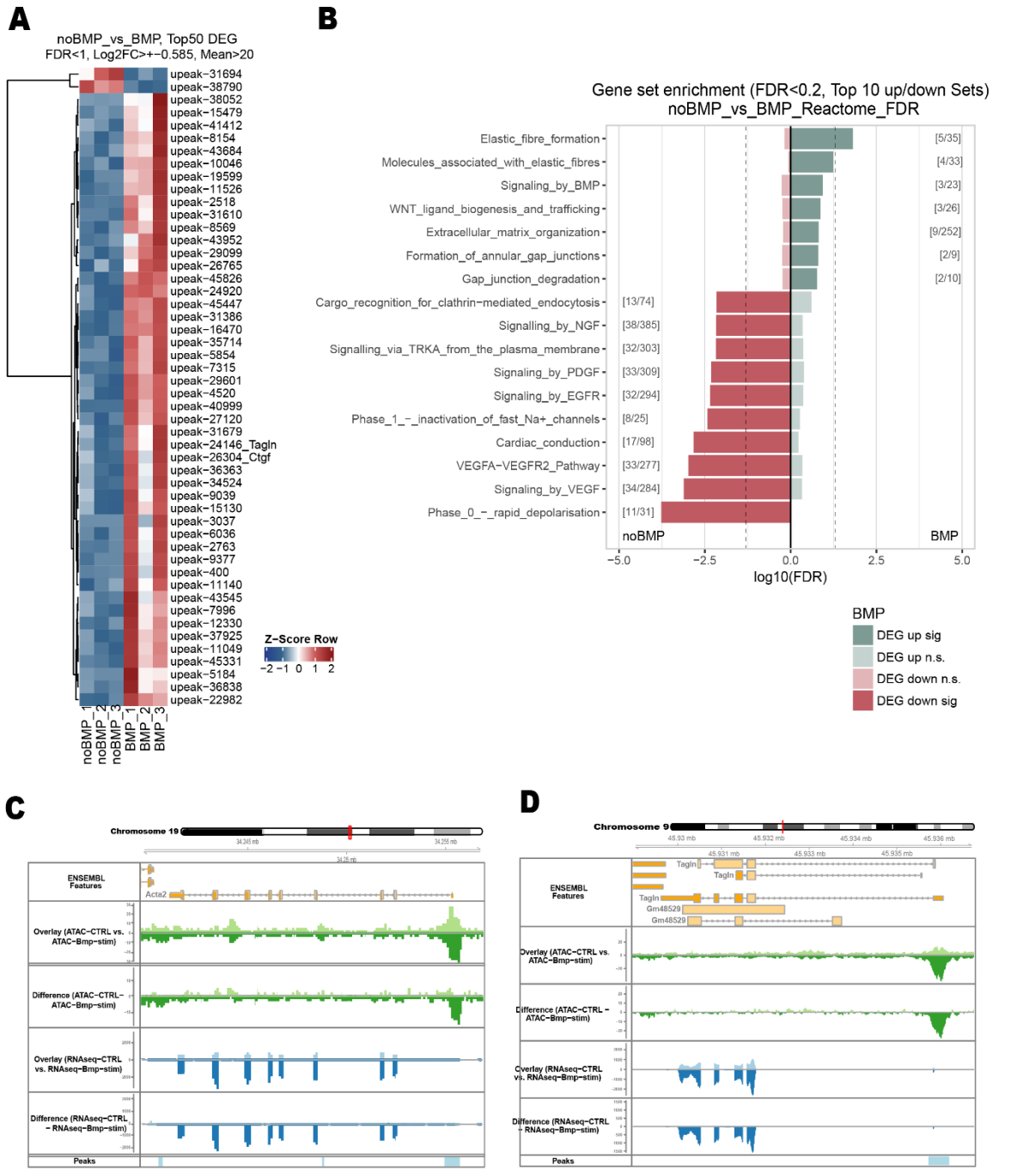

Figure 16. ATAC-seq reveals that BMP9/BMP10 stimulation increases chromatin accessibility of VSMC genes.

A. ATAC-seq analysis of BMP9/BMP10-treated PASMCs. The heatmap displays the top 50 differentially accessible genes by ATAC-seq. **B.** GSEA pathway enrichment analysis of gene chromatin accessibility increased and decreased in PASMCs treated with BMP9/BMP10 compared to non-stimulated cells. The top 17 pathways based on p-values are displayed. The dashed line marks a p-value of 0.05. Bars of green color represent chromatin of genes, which is more accessible and bars of red color represent of chromatin of genes, which is less accessible in different pathways. **C-D.** Integrated Genome Browser view of RNA-seq and

ATAC-seq data for *Acta2* (A.) and *Tagln* (B.) obtained from cultured PASMCs stimulated with or without BMP9/BMP10 for 6 hours. The deep color represents PASMCs treated with BMP9/BMP10.

3.12 Enhanced expression of *Smad7* inhibits BMP/Smad1/5/8 signalling in PASMCs.

To gain further insights into the intracellular signalling pathways initiated by BMP9 and BMP10, we determined the phosphorylation levels of Smad1, 5, 8; Smad2, 3 and proteins of non-canonical BMP signaling including Erk5; Erk1, 2, p38; SAPK/JNK and CREB. Both BMP9 or BMP10 strongly induced phosphorylation of Smad1, 5, 8 but not of Smad2, 3, while TGF-β1 phosphorylated Smad2, 3 but not Smad1, 5, 8. In contrast to activation of canonical BMP-signalling, no phosphorylation of proteins in non-canonical BMPs signalling axis including Erk1/2, P38, SAPK/JNK or CREB was observed after BMP9, BMP10 or TGF-β1 stimulation (Figure 17A). Since Oncostain M (OSM) activates the non-canonical BMPs signaling[200, 201], OSM was used as a positive control.

As mentioned previously, Smad7 is a general antagonist of TGFβ/BMP signalling. Since overexpression of the inhibitory *Smad7* in SMCs strongly suppressed formation of contractile VSMCs *in vivo*, I wondered whether Smad7 does inhibit Smad1, 5, 8 and Smad2, 3 in cultured cells to a similar extent. PASMCs from *Rosa26*^{iSmad7} mice were isolated and infected with an adenovirus expressing Cre recombinase to remove the stop codon and to activate *Smad7* expression. Recombined PASMCs were exposed to BMP9/BMP10 or TGFβ1 stimulation and subjected to western blot analysis to assess Smad phosphorylation levels. Interestingly, Smad7 inhibited phosphorylation of Smad1, 5, 8 more efficiently than Smad2, 3, resulting in reduced VSMC gene expression (Figure 17B). Although expression of SMC genes including *Acta2, Tagln, Myh11* and *Smtn* was reduced after addition of TGF-β1 in *Smad7* expressing PASMCs, the effects on BMP9/BMP10-treated cells were clearly more stronger. Overexpressing *Smad7* completely prevented expression of VSMC specific genes after BMP9/BMP10 treatment. These results suggested that the strong effects of *Smad7* overexpression on VSMC formation and differentiation are primarily mediated by inhibition of the Smad1/5/8 signalling axis (Figure 17C, D).

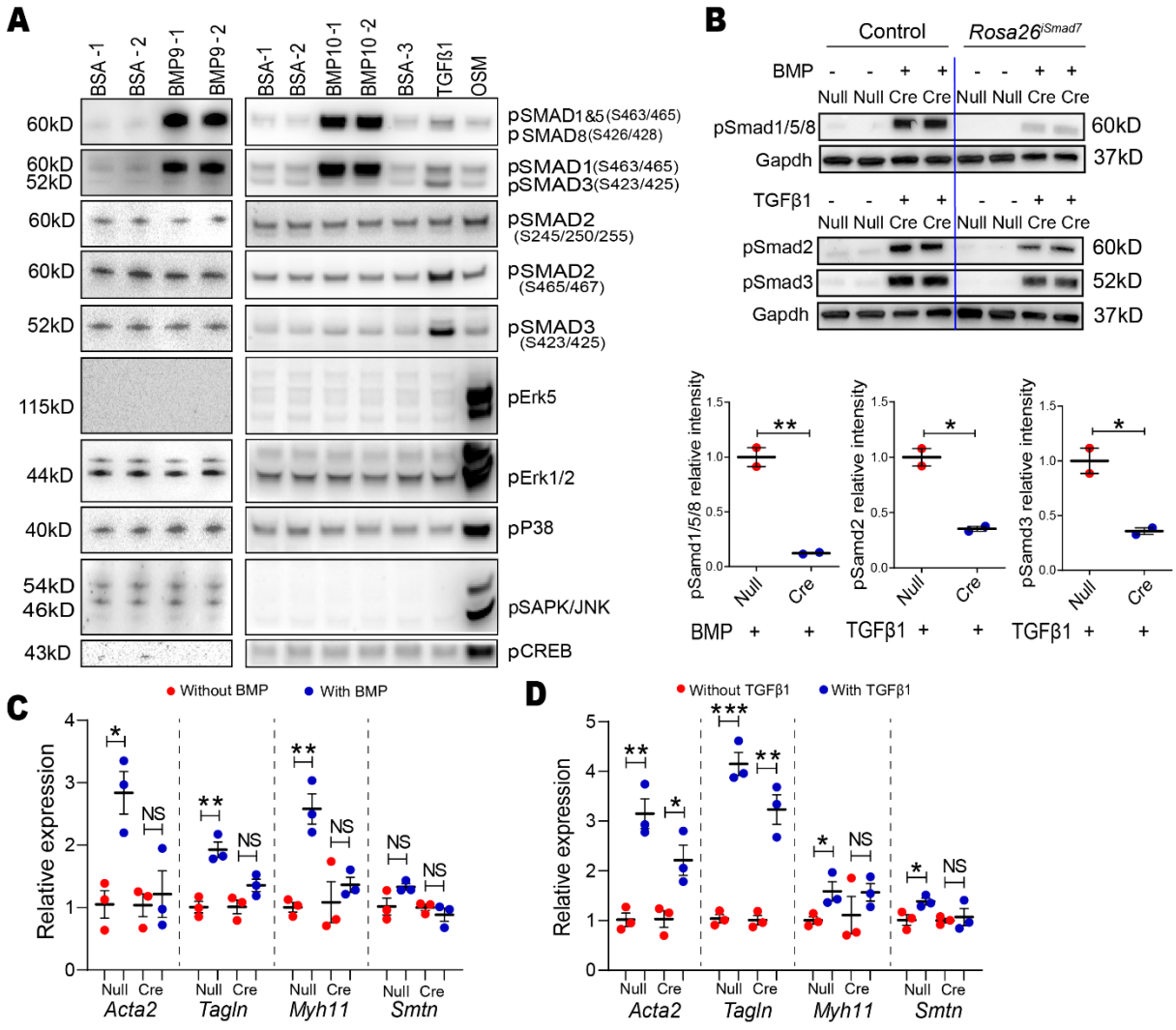

Figure 17. BMP9/BMP10 induce differentiation of VSMCs via the canonical Smad1/5/8 signalling pathway.

A. Western blot analysis of cultured PASMCs treated with BMP9, BMP10, TGFβ1, Oncostatin M (OSM) and BSA for 1 hour. **B.** Western blot analysis and quantification of pSmad1/5/8, pSmad2 and pSmad3 in PASMCs isolated from *Rosa26*^{iSmad7} after adenoviral transduction of Cre recombinase and treatment with BMP9/BMP10 or TGFβ1 for 1hour (data represent mean±SEM; two tailed t-test: *P<0.05, **P< 0.01, n=2). **C, D.** RT-qPCR analysis of SMC gene expression in PASMCs after adenoviral transduction of Cre recombinase and treatment with BMP9/BMP10 (C.) and TGFβ1 (D.) (data represent mean±SEM; two tailed t-test: *P<0.05, **P < 0.01, ***P<0.001, NS P>0.05, n=3).

3.13 VSMCs express BMP type I receptor *Alk1* and type II receptor *Bmpr2*.

The BMP9/BMP10's receptor ALK1 had been described mainly as an endothelial receptor. Intriguingly, in contrast to previous reports that *Alk1* expression is restricted to ECs, re-assessment of *Alk1* expression revealed high expression levels in ECs and SMCs but not in

cardiomyocytes (CMs) (Figure 18A). Antibody staining with isolated PASMCs validated that *Alk1* is expressed in SMCs from wild type mice but not in PASMCs isolated from *Sm22-Cre/Alk1*$^{\Delta loxP/\Delta loxP}$ mice, where *Alk1* was specifically deleted (Figure 18B). Further analysis by fluorescence *in situ hybridization* (FISH) demonstrated that ALK1 is present in VSMCs of different vessel beds including aortae (Figure 18C), coronary and pulmonary arteries (data not shown). Interestingly, FISH also showed that the BMPR2 is highly expressed in all SMC beds studied (Figure 18D).

To test whether BMP9/BMP10 signals exclusively via ALK1 on PASMCs or employ other receptors to transmit the BMP signaling, we generated SMC-specific knockout of ALK1 mice using *Sm22-Cre* mice (*Sm22-Cre/Alk1*$^{\Delta loxP/\Delta loxP}$). Immunofluorescence staining revealed that ALK1-mutant PASMCs did not respond to BMP9/BMP10 stimulation, since stimulation was unable to up-regulate *Acta2* expression and stimulate Smad1/5/8 phosphorylation. Similar results were obtained by RT-qPCR analysis indicating that PASMCs critically rely on ALK1 for BMP9/BMP10-dependent acquisition of the contractile state (Figure 18E-G), demonstrating that, at least in PASMCs, BMP9/BMP10 act on VSMCs in an ALK1 dependent manner.

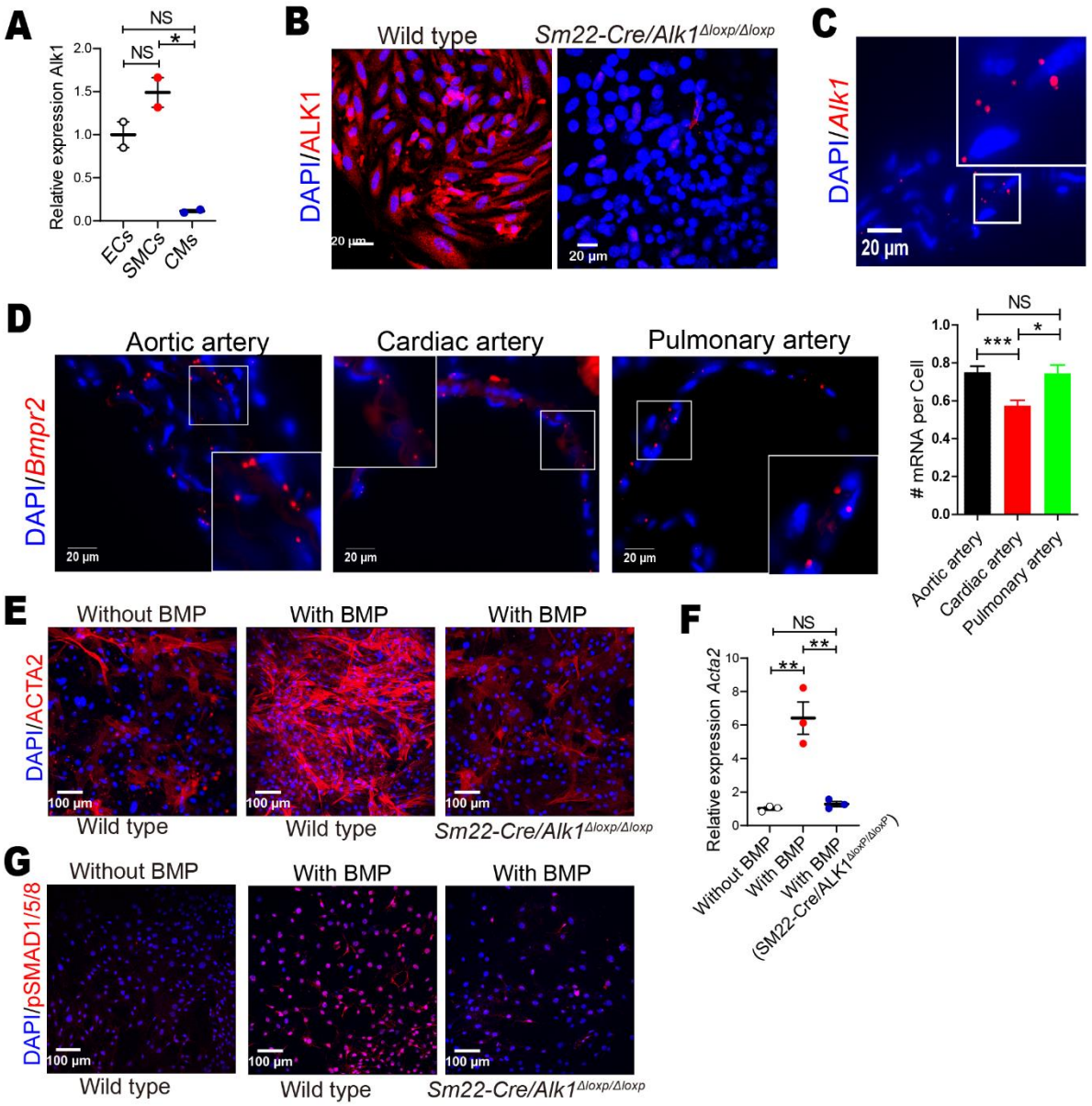

Figure 18. BMP9/BMP10 act directly on SMCs via an ALK1 dependent manner *in vitro*.
A. RT-qPCR analysis of *Alk1* expression in ECs, VSMCs and cardiomyocytes (CMs) (data represent mean±SEM; one-way ANOVA: *P< 0.05, NS P>0.05, n=2). **B.** Immunofluorescence staining for ALK1 in cultured PASMCs isolated from wild type or *Sm22-Cre/Alk1*$^{\Delta loxP/\Delta loxP}$ mice. **C.** FISH staining of *Alk1* on aortae sections (n=5 biological replicates). **D.** FISH staining of BMPR2 in aortic, cardiac and pulmonary arteries (data presented as mean±SEM; one-way ANOVA: *P< 0.05, ***P<0.001, NS P>0.05, n=3). **E.** Immunofluorescence staining of ACTA2 after BMP9/BMP10 stimulation in PASMCs isolated from wild type and *Sm22-Cre/Alk1*$^{\Delta loxP/\Delta loxP}$ mice (n=3). **F.** RT-qPCR analysis of *Acta2* expression after BMP9/BMP10 stimulation in PASMCs isolated from wild type and *Sm22-Cre/Alk1*$^{\Delta loxP/\Delta loxP}$ mice (data represent mean±SEM; one-way ANOVA: **P<0.01, NS P>0.05, n=3). **G.** Immunofluorescence staining of phosphorylated Smad1/5/8 after BMP9/BMP10 stimulation in PASMCs isolated from wild type

and *Sm22-Cre/Alk1*$^{\Delta loxP/\Delta loxP}$ mice (n=3).

3.14 BMP9 and BMP10 are strong inducers of the contractile phenotype in VSMCs.

The result revealed a striking effect of BMP9/BMP10 on the phenotypic shift of PASMCs from a synthetic to a contractile state. Next effects of BMP9, BMP10, TGF-β1, Activin A, retinoic acid (RA), which are known to induce SMC differentiation, on VSMC phenotypic switching were compared with each other. I observed that BMP9 induced a stark re-expression of ACTA2 with a concentration of 100 pM, the effect of such concentration was comparable to 500 pM and 2.5 nM of BMP9 treatment. Stimulation with 100 pM of BMP10, TGF-β1, Activin A and RA had negligible effects on differentiation of cultured PASMCs. 500 pM of BMP10 and TGF-β1 induced ACTA2 re-expression and the effect was comparable to 100 pM of BMP9 treatment (Figure 19A-C). In comparison, the potency of Activin A and RA to induce contractile markers in PASMCs was much lower, requiring 2.5 nM and 10 nM, respectively (Figure 19D, E).

Direct comparison of BMP9, BMP10 and TGF-β1 to other molecules inducing VSMC differentiation revealed that these three molecules own a remarkable potential to switch VSMCs from a synthetic to a contractile state. Thus, a combined treatment with BMP9, BMP10 and TGF-β1 of 100 pM was performed and importantly, the combined treatment resulted in a similar effect compared to BMP9 single treatment alone (data not shown). Taken together, BMP9 shows the highest potential to promote VSMC differentiation among the factors that were already known to induce SMCs differentiation.

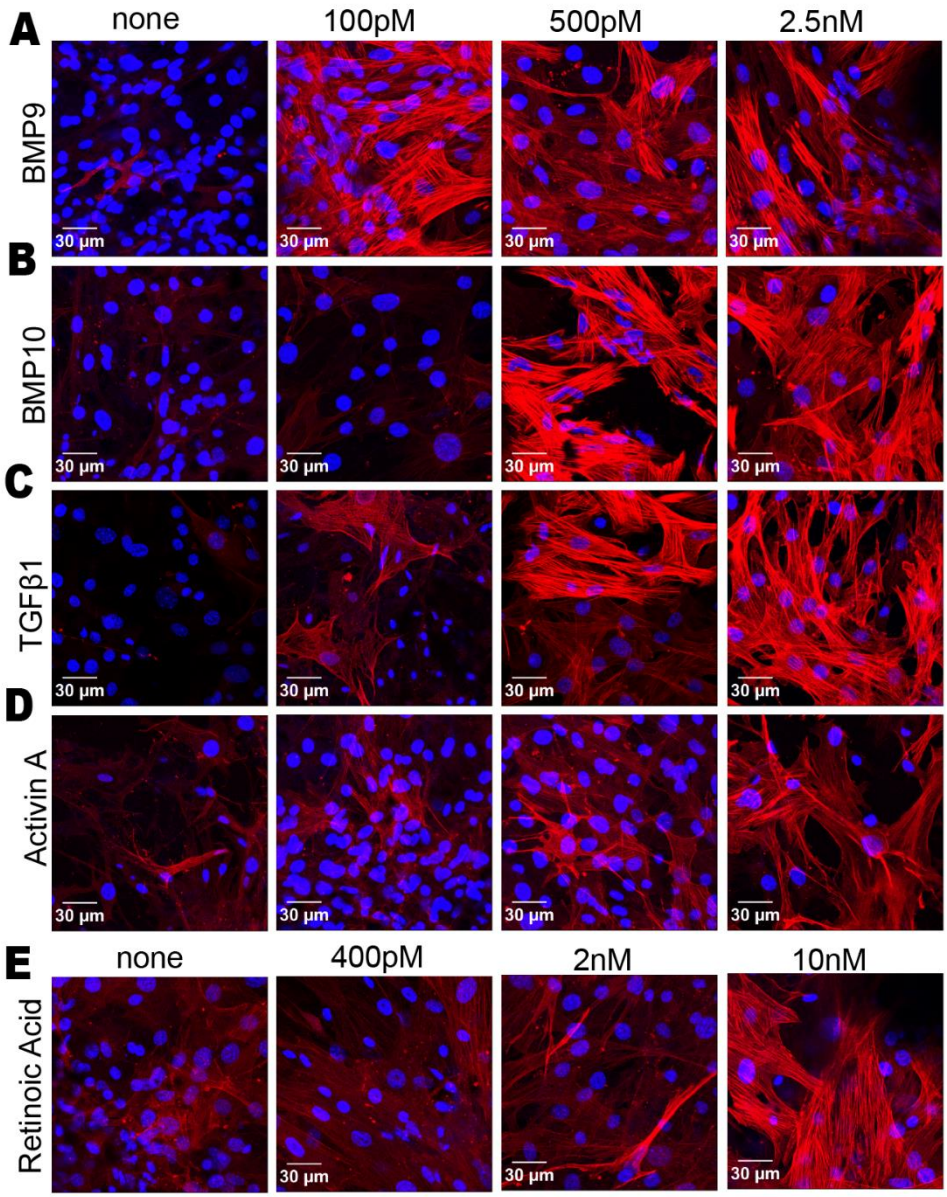

Figure 19. BMP9 and BMP10 are strong inducers of the contractile phenotype in VSMCs. **A-F.** Immunofluorescence staining for ACTA2 of PASMCs cultures treated with different concentrations of BMP9 (A), BMP10 (B), TGFβ1 (C), Activin A (D) and Retinoic acid (E). BMP9 strongly induces the contractile phenotype in cultured PASMCs at low concentrations.

3.15 Deletion of ALK1 in SMCs recapitulates the *Bmp9/10^{dko}* vascular phenotype in pulmonary but not in aortic or coronary arteries.

In vitro results suggested that ALK1 is critical to mediate BMP9/BMP10 effects in PASMCs. In order to determine whether this paradigm also holds true *in vivo* in mice, *Alk1* was specifically inactivated in SMCs using the *Sm22-Cre* mouse strain and the consequences of ALK1 inactivation were investigated. *Sm22-Cre/Alk1$^{\Delta loxP/\Delta loxP}$* mutants displayed reduced numbers of VSMCs and attenuated contractility only in pulmonary (Figure 20A) but not in aortae (Figure

20C) and coronary arteries (data not shown). Similarly, RT-qPCR analysis revealed a strong reduction of *Acta2, Tagln, Myh11* and *Smtn* expression in lung samples, but only a moderate decrease of *Acta2* and no changes of *Tagln, Myh11* and *Smtn* in aortae (Figure 20B, 20D). Furthermore, consistent with the reduction of contractile VSMCs, specific deletion of ALK1 in SMCs prevented phosphorylation of Smad1/5/8 exclusively in pulmonary but not in aortic arteries or cardiac arteries as revealed by immunostaining and western blot analysis (Figure 20E-H). I concluded that inactivation of *Alk1* in SMCs essentially recapitulated the vascular phenotype in *Bmp9/10*^{dko} mutants but only in a restricted set of vessels, specifically in pulmonary arteries. This finding differed strongly from observations in *Bmp9/10*^{dko}, where all arteries lost contractile VSMCs and phosphorylation of Smad1/5/8 was prevented in all vessel beds. To exclude any potential artifacts that might arise from differential activity of *Sm22-Cre* in different vessel beds, *Sm22-Cre/ROSA26-FloxStop-GFP* mice were generated. In line with previous reports[202], comparable activation of the GFP-reporter was found in all vessels analyzed, such as pulmonary and coronary arteries (Figure 20I, 20J). Taken together, these data indicated that BMP9/BMP10 exclusively signal via the ALK1 receptor in pulmonary arteries to induce and maintain the contractile phenotype of PASMCs. Importantly, my data show a previously unrecognized heterogeneity of VSMCs in distinct arteries and suggest that other BMP9/BMP10 receptors compensate for absence of ALK1 in non-pulmonary arteries.

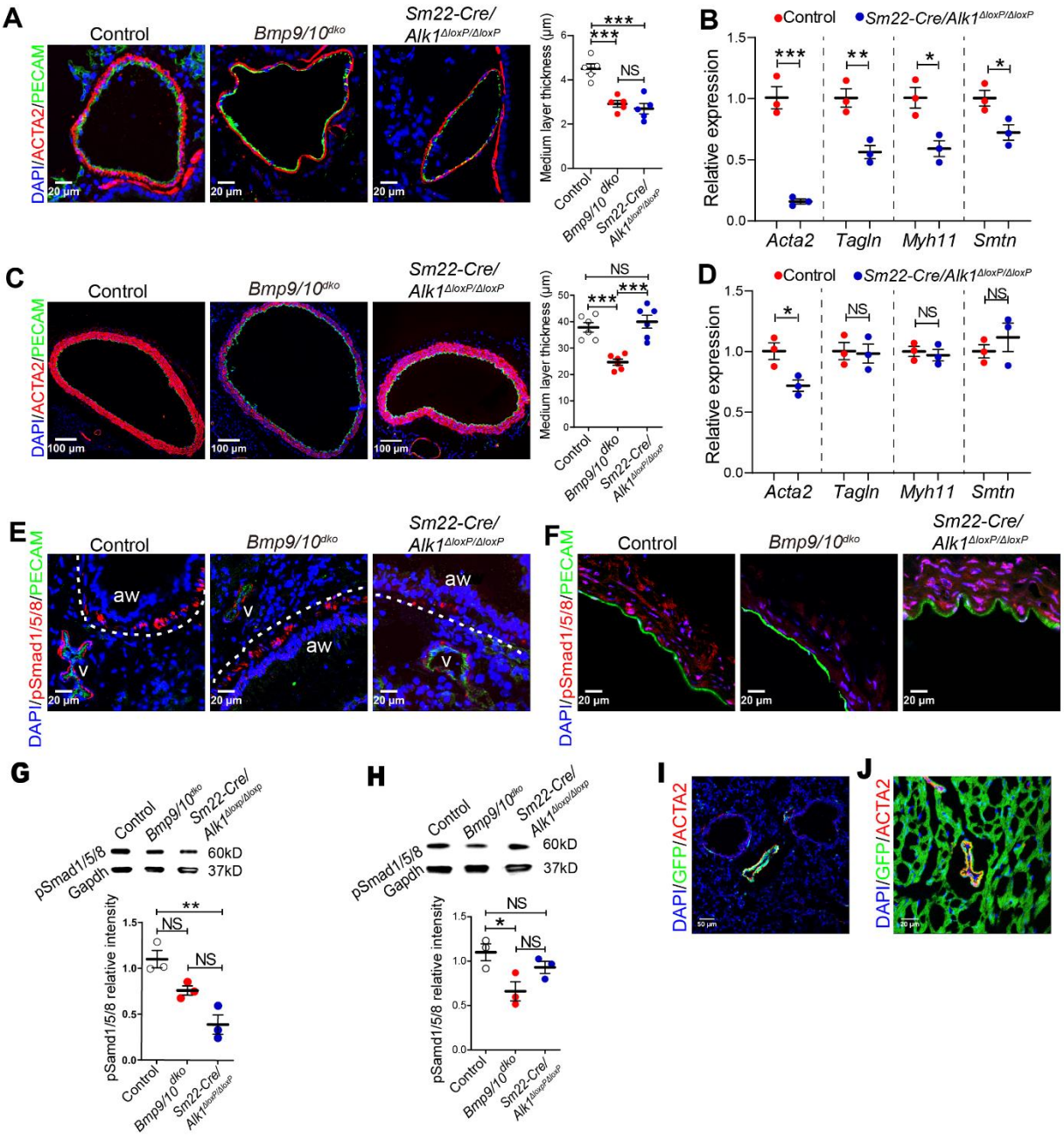

Figure 20. Deletion of ALK1 in SMCs recapitulates the *Bmp9/10^{dko}* vascular phenotype in pulmonary but not in aortic or coronary arteries.

A. Immunofluorescence staining for ACTA2 and PECAM in lungs of 8 weeks old control, *Bmp9/10^{dko}* and *Sm22-Cre/Alk1$^{\Delta loxP/\Delta loxP}$* mice (n=5). Quantification of medial layer thickness of pulmonary arteries (data represent mean±SEM; one-way ANOVA: ***P<0.001, NS P>0.05, n=5). **B.** RT-qPCR analysis of VSMC gene expression in lungs of 8 weeks old control and *Sm22-Cre/Alk1$^{\Delta loxP/\Delta loxP}$* mice (data represent mean±SEM; two tailed t-test: *P< 0.05; **P <0.01, ***P<0.001, NS P>0.05, n=3). **C.** Immunofluorescence staining of aortae from 8 weeks old control, *Bmp9/10^{dko}* and *Sm22-Cre/Alk1$^{\Delta loxP/\Delta loxP}$* mice for ACTA2 and PECAM (n=6). Quantification of aorta medial layer thickness (data represent mean±SEM; one-way ANOVA:

***P<0.001, NS P>0.05, n=6). **D.** RT-qPCR analysis of SMC gene expression in aortae of 8 weeks old control and *Sm22-Cre/Alk1*$^{\Delta loxP/\Delta loxP}$ mice (data represent mean±SEM; two tailed t-test: *P<0.05; NS P>0.05, n=3). **E, F**. Immunofluorescence staining of lungs (E) and aortae (F) from 8 weeks old control, *Bmp9/10*^{dko} and *Sm22-Cre/Alk1*$^{\Delta loxP/\Delta loxP}$ mice for phosphorylated Smad1/5/8 and PECAM (n=3).**G, H.** Western blot analysis of phosphorylated Smad1/5/8 with lung (G) and heart (H) samples of 8 weeks old control, *Bmp9/10*^{dko} and *Sm22-Cre/Alk1*$^{\Delta loxP/\Delta loxP}$ mice (data represent mean±SEM; one-way ANOVA: *P< 0.05; **P<0.01, NS P>0.05 n=3). **I, J.** Immunofluorescence staining for GFP and ACTA2 of lungs (I) and hearts (J) in 8 weeks old *Sm22-Cre/ ROSA26-FloxStop-GFP* mice (n=3).

3.16 Deletion of ALK1 in SMCs leads to excessive immunity response in the lung.

Surprisingly, the deletion of ALK1 in SMCs led to severe inflammatory reactions and fibrosis in the lung as indicated by trichrome staining. Increased collagen deposition in the lung was observed both in regions containing vascular and bronchia-tracheal SMCs (Figure 21A). In contrast no fibrosis was apparent in hearts of *Sm22-Cre/Alk1*$^{\Delta loxP/\Delta loxP}$ mice and in lungs of *Bmp9/10*^{dko} mutants (Figure 21B). Immunofluorescence staining against CD45, a marker for common lymphocyte antigen suggested that immune cells accumulate in the lung of *Sm22-Cre/Alk1*$^{\Delta loxP/\Delta loxP}$ mutants (Figure 21C). This finding was further supported by CD68 staining, showing a strong increase in the number of macrophages in lungs of *Sm22-Cre/Alk1*$^{\Delta loxP/\Delta loxP}$ animals (Figure 21D). The observation is consistent with previous reports that BMP signalling acts as a suppressor of innate immune responses[203-206]. Importantly, collagen deposits were not observed in other organs, such as heart (Figure 21B), liver and aorta (data not shown) of *Sm22-Cre/Alk1*$^{\Delta loxP/\Delta loxP}$ mice, which further supports the hypothesis of heterogenic expression of ALK receptors in distinct vessel beds.

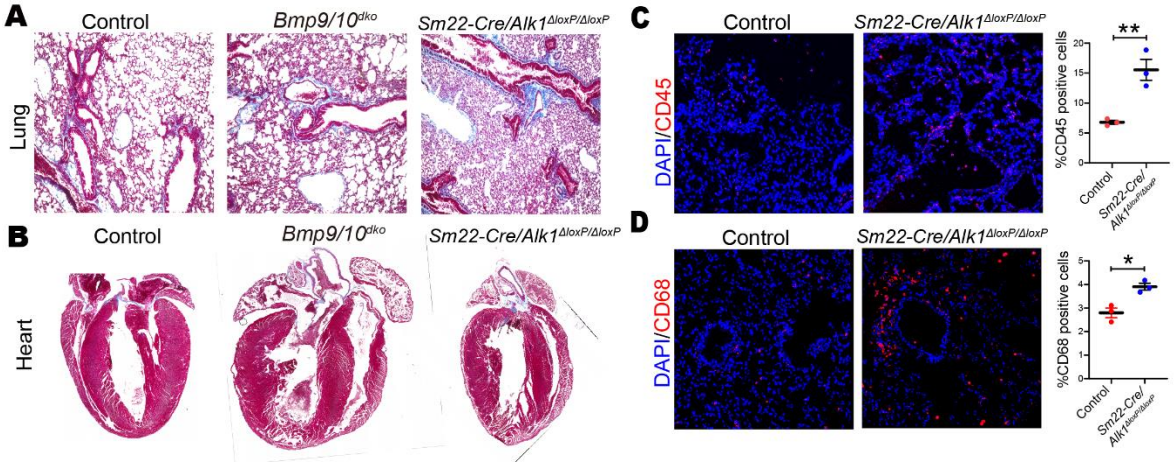

Figure 21. Loss of ALK1 in SMCs leads to excessive inflammatory response in the lung. **A.** Trichrome staining of lung samples from 8 weeks old control, *Bmp9/10*^{dko} and *Sm22-Cre/Alk1*$^{\Delta loxP/\Delta loxP}$ (n=3). **B.** Trichrome staining of heart samples from 8 weeks old control,

Bmp9/10^{dko} and *Sm22-Cre/Alk1$^{\Delta loxP/\Delta loxP}$* (n=3). **C.** Immunofluorescence staining against CD45 in lung samples from 8 weeks old control and *Sm22-Cre/Alk1$^{\Delta loxP/\Delta loxP}$* mice. Quantification of the CD45-positive cells in the lung (data presented as mean±SEM; two tailed t-test: **P< 0.01, n=3). **D.** Immunofluorescence staining against CD68 in lung samples from 8 weeks old control and *Sm22-Cre/Alk1$^{\Delta loxP/\Delta loxP}$* mice. Quantification of the CD68-positive cells in the lung (data presented as mean±SEM; two tailed t-test: *P< 0.05, n=3).

3.17. Differential expression of BMP type one receptors reveals heterogeneity among VSMCs in distinct vessel beds.

The differential effects of ALK1 inactivation on VSMCs in different arteries suggests a strong heterogeneity of VSMCs, which might correspond to differential physiological requirements and different signaling needs[79]. VSMCs might exhibit diverse molecular and functional properties depending on the organ and vessel where they reside, thereby increasing the intrinsic heterogeneity of the vascular network, which so far has been mostly attributed to ECs. Signaling through the TGF-β/BMP receptor family occurs via ligand binding to heterodimeric complexes of type I and type II serine/threonine kinase receptors, where the type I receptors determine signal specificity[87]. I hypothesized that additional type I receptors in VSMCs of the aortic and coronary VSMCs might compensate for the loss of ALK1 to transmit signaling and phosphorylate Smad1/5/8 in *Sm22-Cre/Alk1$^{\Delta loxP/\Delta loxP}$* mutants, thus preventing the full phenocopy of the vascular phenotype of *BMP9/10^{dko}* mice. To corroborate this hypothesis, I studied the expression of different ALK receptors in distinct vessels by RNA-FISH at single cell resolution. Spatial expression analysis of type one receptors by RNA-FISH clearly demonstrated that virtually all BMP type I receptors were expressed in aortic SMCs, although expression of *Alk6* was relatively low compared to *Alk1, Alk2* and *Alk3* (Figure 22A). A similar pattern was observed in coronary arteries, in which *Alk1, Alk2* and *Alk3* showed comparable expression levels while *Alk6* was much lower (Figure 22B). In stark contrast, VSMCs in pulmonary arteries only expressed *Alk1* at high levels but not *Alk2, Alk3* and *Alk6* (Figure 22C), explaining why SMC-specific *Alk1* inactivation was sufficient to prevent Smad1/5/8 phosphorylation in pulmonary arteries and recapitulate the loss of contractile VSMCs phenotype observed in of *Bmp9/10^{dko}* mice.

To further validate these results, the *Sm22a-Cre* line was crossed with a GFP reporter mice (*Rosa26-FloxStop-GFP*) to specifically label SMCs. SMCs from lungs of *Sm22-Rosa26-FloxStop-GFP* mice were isolated by cell sorting for subsequent RNA-seq. In addition, using published RNA-seq data obtained from Lina and coworkers (available in the Gene Expression Omnibus under accession number GSE117963), expression of type I receptors in VSMCs from the medial layer of the descending thoracic aorta was analyzed[79]. Calculation of relative expression levels of BMP type I receptors revealed that in descending thoracic aortae, *Alk1,*

Alk2 and *Alk3* were highly expressed but *Alk3* was more dominant compared to *Alk1 and Alk2* (Figure 22D). In contrast, *Alk1* was clearly the dominant receptor in SMCs of the lung and *Alk2*, *Alk3* and *Alk6* expression was much lower compared to *Alk1* (Figure 22E). However, RNA-seq data from pulmonary SMCs need to be viewed with caution, since isolated cells from the lung will contain a certain fraction of bronchio-tracheal SMCs that might express a different profile of *Alk* receptors. My result showed that inactivation of *Alk1* in SMCs prevented phosphorylation of Smad1/5/8 not only in pulmonary VSMCs but also bronchio-tracheal SMCs, indicating that vascular and tracheal SMCs share same receptor system and *Alk1* is the dominant type I receptor in both SMC populations in the lung. These findings were further supported by antibody staining, which further confirmed that ALK2 and ALK3 are only present in aortic but not in pulmonary arteries (Figure 22F, 22G). Taken together, the unexpected heterogeneity of ALK receptor expression explains why only pulmonary but not aortic and coronary arteries in *Sm22-Cre/Alk1*$^{\Delta loxP/\Delta loxP}$ mutant mice recapitulate the defects observed in *Bmp9/10*^{dko}.

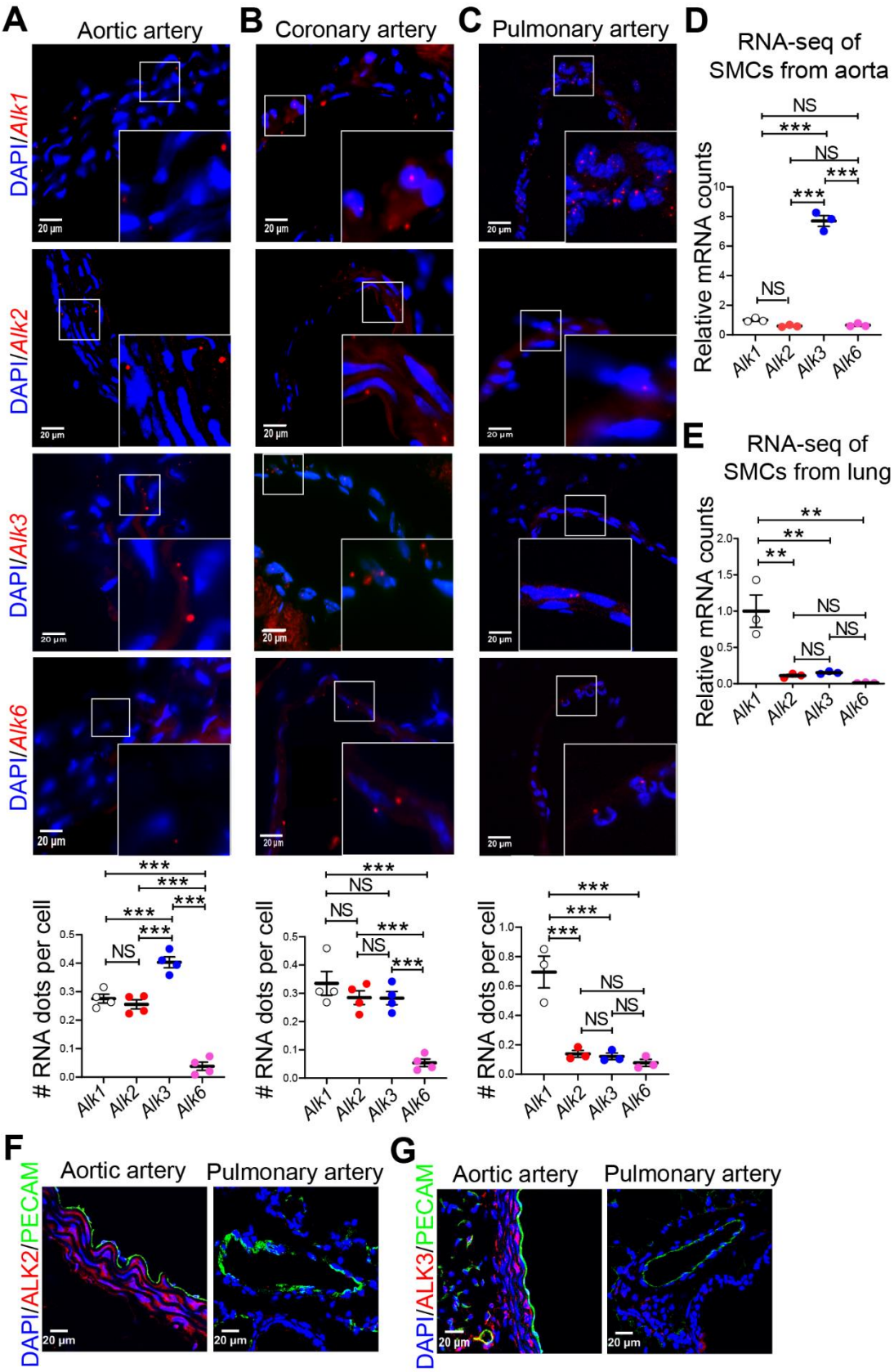

Figure 22. Differential expression of BMP type one receptors in VSMCs of distinct vessels.

A, B. RNA-FISH of *Alk1, Alk2, Alk3* and *Alk6* expression in aortic arteries (A) and cardiac

arteries (B). Quantification of type I receptor expression in aortae (A) and coronary arteries (B.) (data represent mean ±SEM; one-way ANOVA: ***P< 0.001, NS P>0.05, n=4). **C.** RNA-FISH and quantification of *Alk1, Alk2, Alk3* and *Alk6* expression in pulmonary arteries (data represent mean ±SEM; one-way ANOVA: ***P< 0.001, NS P>0.05, n=3). **D, E.** RNA-seq analysis of *Alk1, Alk2, Alk3* and *Alk6* expression in VSMCs from aortae (D) and pulmonary arteries (E) (data represent mean ±SEM; one-way ANOVA: **P< 0.01; ***P< 0.001, NS P>0.05, n=3). **F, G.** Immunofluorescence staining for ALK2 (F) and ALK3 (G) in aorta and pulmonary arteries of 8 weeks old wild type mice (n=3).

3.18 Co-accessibility of Smad4 and TEADs binding sites in BMP9/BMP10 stimulated PASMCs.

To understand precisely how BMP9/BMP10 regulate differentiation of VSMCs and acquisition of the contractile state, I performed ATAC-seq of cultured PASMCs treated with BMP9/10. ATAC-seq footprinting in combination with RNA-seq and bioinformatics analysis identified numerous potential target genes defined by BMP9/BMP10 upregulation, increase of chromatin accessibility, and presence of canonical Smad binding sites. Volcano plot analysis revealed that the accessibility of binding sites for SMAD4, JUN/FOS, TEADs and other transcription factors (in blue) was increased after BMP9/BMP10 treatment of PASMCs. On the other hand, stimulation with BMP9/BMP10 resulted in decreased accessibility of binding sites for NRF1, E2F4, TFDP1 and other transcription factors (in red) (Figure 23A). Motif Enrichment Analysis (MEA) suggested that TEADs might control the transcription of VSMC genes by binding typical TEAD binding motifs in gene regulatory regions (Figure 23B). Moreover, the ATAC-seq analysis revealed a striking correlation of Smad4 and TEAD transcription factor binding sites in promoter regions of BMP9/BMP10 target genes. Integrative Genomic Viewer (IGV) track analysis suggested that numerous promoters of SMCs specific genes, such as ACTA2, carry Smad4 and TEAD binding sites in close vicinity (Figure 23C). TEAD transcription factors are the endpoint of Hippo-signalling and according to previous reports that Hippo-signalling promotes proliferation and migration of VSMCs at the expanse of differentiation[207-209]. Thus it is tempting to speculate that BMP-and Hippo-signalling converge at the chromatin level, probably antagonizing each other.

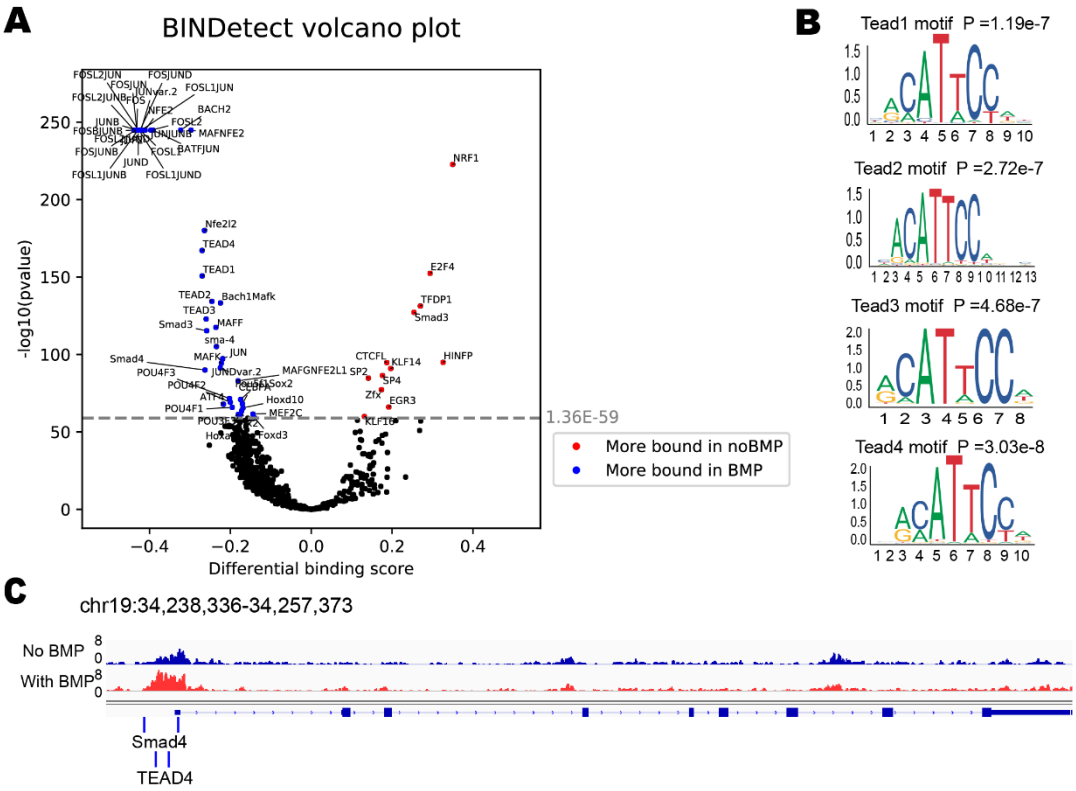

Figure 23. ATAC-seq analysis of cultured PAMSCs treated with BMP9/BMP10.
A. Volcano plot showing increased accessibility of binding sites for SMAD4, JUN/FOS, TEADs and decreased accessibility of binding sites for NRF1, E2F4 and other transcription factors. **B.** Enriched transcription factor-binding motifs for TEADs family in BMP9/BMP10 treated cultured PASMCs. The height of the letters indicates the frequency of each base in the motif. **C.** Integrative Genomic Viewer track analysis showed that the binding sites of Smad4 and TEAD4 were in close proximity to each other.

3.19 YAP/TAZ/TEAD axis antagonizes BMP9/BMP10 signalling-dependent VSMC differentiation.

Previous studies suggest that TEAD1 suppresses expression of VSMC genes by abolishing the pro-myogenic function of Myocardin, the master regulator of VSMC differentiation. TEAD transcription factors were shown to compete with Myocardin for binding of SRF, thereby disrupting Myocardin/SRF interactions, causing suppression of VSMC specific genes and attenuation of the contractile VSMC phenotype[207, 208]. Similarly, repression of the Hippo pathway, which leads to activation of TEAD cofactors YAP/TAZ, promotes proliferation and migration of SMCs. In contrast, inactivation of YAP following arterial injury reduces neointima formation *in vivo* by preventing injury-induced dedifferentiation of VSMCs[209-211]. Since the ATAC-seq analysis revealed a correction of Smad4 and TEADs binding sites in promoter regions of VSMC genes, it was interesting to study whether the balance between Hippo/YAP-TEAD and BMP9/BMP10/Smad-signalling at the chromatin level is decisive for the fate of

VSMCs. Increased Smad binding to VSMC promoters might alter binding or composition of the YAP/TEAD complex or *vice versa* increased YAP/TEAD activity might restrict binding or activity of Smad-dependent transcriptional complexes.

To manipulate the YAP-TEAD signaling, mouse strains carrying conditional alleles for TEAD1, 3 and 4 as well as a constitutive allele for TEAD2 (TEAD1-4 quadruple knockout) transcription factors were analyzed. PASMCs were isolated from this strain and infected with the adenovirus expressing Cre recombinase to delete all TEADs or infected with adenovirus Null as a control treatment. Intriguingly, BMP9/BMP10 stimulation increased expression of smooth muscle specific genes including *Acta2, Tagln, Myh11* and *Smtn* in PASMCs much stronger after deletion of *Tead1-4* compared to WT controls (Figure 24A). In addition, I also analyzed conditional alleles for the co-activators YAP/TAZ (double knockout strain). Inactivation of YAP and TAZ in PASMCs by infection with adenovirus Cre strongly increased the expression of SMC specific genes when cells were subjected to BMP9/BMP10 stimulation compared to the cells infected with control adenovirus (Figure 24B).

Since loss-of-function studies reveals that loss of YAP/TAZ/TEAD enhanced BMP9/BMP10-dependent induction of the contractile state, I investigated whether increased YAP/TAZ/TEAD signaling has opposite effects. To perform such gain-of-function studies, I used a mouse strain carrying a conditional, constitutively active TEAD1-VP16 allele, in which the activation domain of VP16 (TEAD1-VP16) is fused to YAP. Over-expression of *Tead1-VP16* by adenovirus Cre mediated recombination strikingly suppressed BMP9/BMP10 induced PASMCs differentiation assessed by expression of typical VSMC genes (Figure 24C). Likewise, SMCs with a constitutively active conditional *Yap5SA* allele were analyzed, which contains a mutation of all 5 Lats kinase phosphorylation motifs (5SA) and thereby prevents the negative regulation by Hippo pathway. As in the case of *Tead1-VP16* overexpressing PASMCs, expression of *Yap5SA* suppressed BMP9/BMP10 induced re-expression of VSMC genes (Figure 24D). Furthermore, I analyzed a transgenic mouse strain carrying a conditional knock-out allele for *Vgll4*, a previously identified YAP antagonist[212, 213]. Similar to PASMCs overexpressing *Tead1-VP16* or *Yap5SA*, inactivation of *Vgll4* in PASMCs induced a lower expression of typical VSMC genes upon BMP9/BMP10 stimulation (Figure 24E). Taken together, the gain- and loss-of-function studies demonstrated that the YAP/TAZ/TEADs signalling axis antagonizes BMP9/BMP10-dependent VSMC differentiation.

In order to study whether components of Hippo and BMP signaling interact with each other, co-immunoprecipitation (Co-IP) experiments were perfomed using cultured PASMCs stimulated with BMP9/BMP10. Using a Smad4 antibody, I detected a stronger interaction between Smad4 and TEAD1 after BMP stimulation. I did not detect an interaction of Smad4 with TEAD2-4, which is consistent with reports that TEAD1 is the only abundant TEAD family

member in SMCs[207, 214]. Similarly, I also found that TEAD1 (using a pan-TEAD antibody) binds robustly to Smad4 after BMP9/10 stimulation (Figure 24F). From these results, I concluded that TEAD1 competes with Smad4 for the binding of SMC specific genes to restrict excessive BMP signalling, thereby attenuating BMP9/BMP10 induced expression of typical VSMC genes.

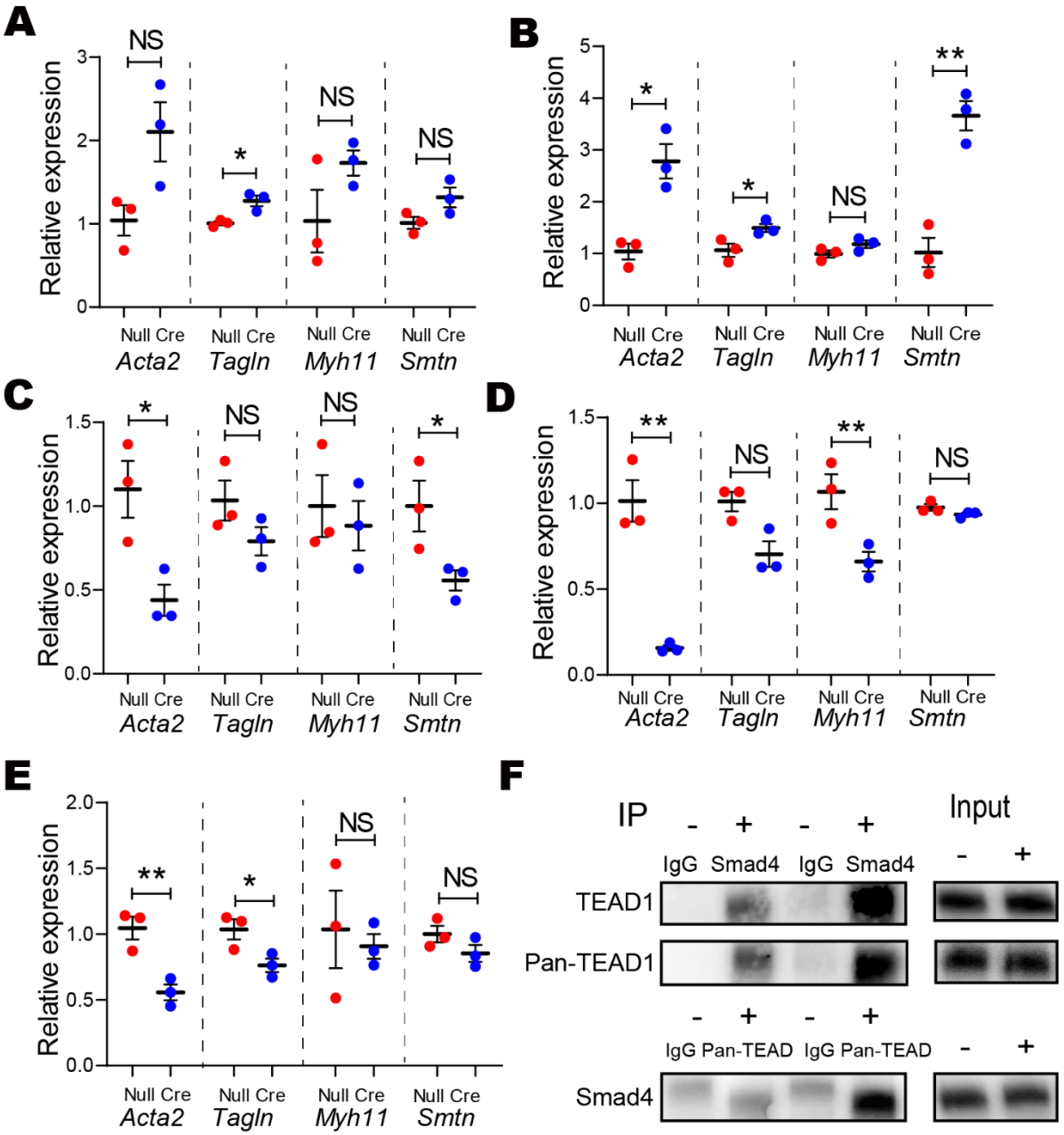

Figure 24. YAP/TAZ/TEADs signalling axis antagonizes BMP9 and BMP10-dependent VSMC differentiation.

A. RT-qPCR analysis of SMC gene expression in PASMCs isolated from *Tead1-4* quadruple knockout mice after adenoviral transduction of Cre recombinase and BMP9/BMP10 treatment (data presented as mean±SEM; two tailed t-test: *P<0.05, NS P>0.05, n=3 biological replicates). **B.** RT-qPCR analysis of SMC gene expression in PASMCs isolated from

Yap$^{loxP/loxP}$/*Taz*$^{loxP/loxP}$ mice after adenoviral transduction of Cre recombinase and BMP9/BMP10 treatment (data presented as mean±SEM; two tailed t-test: *P<0.05, **P<0.01, NS P>0.05, n=3 biological replicates). **C-E.** RT-qPCR analysis of SMC gene expression in PASMCs isolated from *Rosa26*$^{iTead1\text{-}VP16}$ (C), *Rosa26*^{iYap5SA} (D), and *Vgll4*$^{loxP/loxP}$ (E) mice after adenoviral transduction of Cre recombinase and treated by BMP9/BMP10 (data presented as mean±SEM; two tailed t-test: *P<0.05, **P<0.01, NS P>0.05, n=3 biological replicates). **F.** Co-immunoprecipitation analysis of Smad4 and TEAD1 in PASMCs treated by BMP9/BMP10.

4 Discussion

4.1 The role of BMP-ALK1-SMAD signalling in SMCs differentiation and maintenance of contractile state.

The cardiovascular system is the first organ to develop and function during embryogenesis. Differentiation, recruitment and attachment of VSMCs to newly forming vessels is crucial for this process. The principal function of VSMCs is to mediate vascular contraction, blood vessel tone, and establish constant blood pressure. In mature arteries, the majority of VSMCs are differentiated and contractile, which corresponds to expression of contractile proteins, including ACTA2, TAGLN, MYH11 and SMTN. Members of TGFβ/BMPs and their downstream signalling molecules are irreplaceable for VSMC differentiation and formation of contractile VSMCs. One prominent example is the constitutive ALK1 knockout mice which forms few/no VSMCs during embryogenesis[6-8], suggesting that ALK1 and probable the corresponding ligands BMP9 and BMP10 are pivotal for VSMC differentiation. The TGFβ superfamily also plays essential roles in pathological changes during disease conditions, including atherosclerosis, aortic aneurysms and hypertension[215]. However, the specific roles of BMP9/BMP10 in vascular development and homeostasis maintenance are still under debate.

It had been assumed that BMP9 and BMP10 are EC quiescence factors and act selectively on vascular ECs to maintain vascular homeostasis and to inhibit EC apoptosis, migration, proliferation and angiogenesis[100,166,216]. BMP9 mutant mice develop normal vasculature but were reported to show defects in lymphatic vessel maturation and valve formation while the function of BMP10 in adult mice was unknown due to the embryonic lethality[14-16]. To determine the endogenous expression pattern of *Bmp10*, we generated a *Bmp10*-LacZ reporter strain, which revealed *Bmp10* expression at E9.5 both in the developing atria and ventricles, consistent with a previous study[15]. However, during later fetal stages, the expression of *Bmp10* becomes restricted to right atria. Since the germ line knockout of BMP10 results in embryonic lethality at E10.5, a mouse line in which exon2 of BMP10 are flanked by loxP sites (*Bmp10*$^{loxP/loxP}$) was generated and BMP10 was specifically inactivated in the atria by using an *Anf-Cre* strain, in which the Cre recombinase is expressed in the atria from at least E10.5 onwards. Unlike the constitutive knockout of BMP10, inactivation of BMP10 in the atrium did not cause embryonic lethality. BMP9 or BMP10 single mutants did not show obvious vascular defects and the vessel morphology in adult animals appeared normal. Due to the fact that BMP9 and BMP10 both bind with high affinity to ALK1 and endoglin, it was hypothesised that these proteins functionally overlap and form BMP9-BMP10 heterodimers to exhibit full biological BMP activity. Thus, a *Bmp9/Bmp10* double knockout strain (*Bmp9/10*^{dko}) was developed to systematically characterize potential overlapping roles of BMP9 and BMP10 for

vascular development and maintenance. The foremost effect of concomitant BMP9 and BMP10 inactivation was the profound loss of contractile VSMCs, leading to dilation of major vessels and reduced blood pressure.

The strong difference between the *Bmp9/10*^{dko} and the single mutants clearly indicates that these two BMP proteins exert redundant roles. Importantly, the results also indicated that heterodimers possess potency comparable to BMP9-BMP10 homomers. This finding is consistent with the several previous reports describing that inactivation of essential components of the BMP signalling pathways leads to vessel dilation and attenuated VSMC differentiation. Furthermore, acute deletion of BMP10 in adult mice (*Bmp9*$^{-/-}$*/Bmp10*^{iMhc}) recapitulated the defects observed in *Bmp9/10*^{dko} mice, which suggested that the loss of contractile VSMCs observed in adult *Bmp9/10*^{dko} was not caused by a developmental phenotype. In contrast, overexpression of *Bmp10* in ECs (*Rosa26*^{iBMP10}) of adult mice dramatically increased VSMC contractility, blood pressure and resulted in right ventricle dilation, demonstrating that enhanced BMP signalling is sufficient to increase the contractility and reduce the diameter of vessels.

So far, it was assumed that ALK1 is primarily an endothelial receptor of the TGFβ/BMP receptor family, ruling out the possibility that BMP9/BMP10 act directly on VSMCs. The resulting model suggested that circulating BMP9/BMP10 modulate the cellular state of ECs, which release signalling cues, such as NO and apelin, to modulate VSMCs. In this thesis, strong evidence was provided that ALK1 is highly expressed in VSMCs. RT-qPCR, antibody staining and RNA-FISH revealed that VSMCs of distinct vessel beds both in mouse and human express *Alk1* as well as *Bmpr2*. The finding led to the question whether BMP9/BMP10 directly control formation of contractile VSMCs. To address this question, SMCs were isolated from pulmonary arteries and subjected to BMP9/BMP10 stimulation. Treatment of cultured PASMCs, which acquired a synthetic state soon after culturing, induced re-expression of contractile markers after exposure to BMP9/BMP10. RNA-seq analysis of BMP9/BMP10 treated PASMCs corroborated the increased expression of VSMC genes. Furthermore, GSEA of ATAC-seq in PASMCs treated by BMP9/BMP10 revealed enrichment of terms for elastic fiber formation, Wnt ligand biogenesis, ECM organization and gap junction formation. In contrast, terms related to PDGF, EGF and VEGF signalling were reduced, suggesting that cellular processes related to maturation of VSMCs depend on BMP9 and BMP10. Thus, I hypothesize that circulating BMP9/BMP10 is able to bypass the endothelial barrier to directly modulate the VSMC phenotype and control phenotype switching.

To validate this hypothesis, *Rosa26*$^{Sm22\text{-}iSmad7}$ and *Rosa26*$^{Smmhc\text{-}iSmad7}$ strains were generated, allowing overexpression of inhibitory Smad7 in SMCs. The increased expression of Smad7

during embryogenesis essentially abrogated formation of VSMCs. Conditional expression of Smad7 in SMCs of adult mice strongly decreased the number of contractile VSMCs and reduced the thickness of the muscular layer. In cultured PASMCs, overexpression of Smad7 inhibited phosphorylation of Smad1/5/8 more efficiently than Smad2/3, leading to a strong reduction of cell type-specific gene expression in VSMCs. The results demonstrated direct effects of BMP signalling on VSMC differentiation and contractile state maintenance. Furthermore, *in vitro* experiments revealed that BMP9 is the strongest inducer of the contractile VSMC phenotype, when compared to TGF-β, Activin A and retinoic acid. Further support for this conclusion came from studies using the *Sm22-Cre/Alk1*$^{\Delta loxP/\Delta loxP}$ strain, where only pulmonary arteries were dilated and showed attenuated contractility, whereas aortae or coronary arteries were not affected. This result was consistent with decreased Smad1/5/8 phosphorylation levels in distinct vessels in *Sm22-Cre/Alk1*$^{\Delta loxP/\Delta loxP}$ mice: Smad1/5/8 phosphorylation was only prevented in pulmonary arteries but not in the aorta and heart. Deletion of *Alk1* in SMCs also led to severe autoimmune reactions only in the lung but not in other tissues. The thesis describes that VSMCs are intrinsically heterogeneous and react differentially to *BMPR2* mutants in humans showing increased muscularization of small arteries with elevated right ventricle systolic pressure[217], while SMC-specific deletion of Smad4 in mice reduced proliferation, differentiation and contractility of VSMCs[47]. Taken together, the data indicated that BMP9/BMP10 directly exert their effects on VSMCs and uncovered a previously unrecognized heterogeneity between VSMCs of different arteries regarding the BMP receptor family, which was so far only described for the endothelium.

BMP9/BMP10 may reach VSMCs either via fenestrated *vasa vasorum*, by transendothelial transport mechanisms, or by transient opening of adherens junctions. To study how BMP9/BMP10 reach VSMCs, mesenteric arteries were isolated from wild type mice and mounted in a pressure myograph system, which mimics blood circulation *in vivo*. Perfusion with BMP9/BMP10 induced Smad1/5/8 phosphorylation in the VSMC layer, indicating that circulating BMP9/BMP10 reach VSMCs by passing the endothelial barrier. Unlike many microvessels in the liver or bone marrow, the endothelium of muscularized vessels is continuous, which is characteristic for endothelia in exocrine and endocrine glands, renal glomeruli, or intestinal mucosa[218]. Thus, BMP9 and BMP10 have to take advantage of transendothelial transport mechanisms via paracellular or transcellular routes. At the first glance the localized control of BMP9/BMP10 uptake does not seem to make much sense for circulating hormone-like molecules required for formation and contractility of VSMCs in all muscularized vessels. However, a locally controlled “permission” for BMP9 and BMP10 to pass the endothelial barrier will establish an additional layer of regulation that builds on a basic signalling framework favoring differentiation and the contractile state of VSMCs to allow local regulation of the vascular tone where necessary.

The result presented in this thesis indicate that BMP9/BMP10 reaches VSMCs by passing the endothelial barrier. To further address the mechanisms, isolated mesenteric arteries from wild type and also *Sm22-Cre/Alk1*$^{\Delta loxP/\Delta loxP}$ mutants should be subjected to analysis in a pressure myograph, which allows many different manipulations. For example, staining for pSmad1/5/8 in nuclei of VSMCs or BMP downstream genes, such as ATOH8, may be used to monitor BMP9/BMP10-dependent activation of Smad-signalling. Different inhibitors should be used to specifically block different transport processes in the endothelium, such as endocytosis and vesicle trafficking (dynasore, brefeldin A, nystatin and N-ethylmaleimide) and score for phosphorylated Smad1/5/8 and expression of contractile VSMC markers. In addition, perfusion of isolated vessels with fluorochrome-labelled molecules of different sizes should be done to rule out non-physiological and unspecific leakage of the endothelium.

The concurrent inactivation of BMP9 and BMP10 foremost affected VSMCs but not ECs. Of course, this does not mean that BMP9 and BMP10 have no effects on ECs. Previous studies suggested indirect signals from ECs in response to BMP9 and BMP10 stimulation via release of apelin and NO, causing vessel dilation and thus protecting animals from PAH[12, 169, 219]. In our hands, BMP9/BMP10 strongly down-regulated apelin in HUVECs and loss of BMP9/10 resulted in increased expression of apelin, which initially suggested that apelin might be a promising candidate to explain the defects observed in *Bmp9/10*^{dko} mice. However, the regulation of apelin in ECs does not seem to be relevant for the loss of contractile VSMC phenotype, since constitutive loss of apelin on a BMP9/BMP10 double knockout background (*Bmp9/Bmp10/Apelin* triple knockout mutation) did not restore VSMC numbers and the attenuated contractility. In addition, overexpression of apela, which is a novel ligand for the apelin receptor APJ[214, 220], has no obvious effects on VSMC integrity. The work presented here clearly indicates that apelin does not play a major role in mediating BMP9 and BMP10 effects. Furthermore, *Atoh8*, a direct upstream transcription factor of eNOS, which binds to the regulatory E-box in the eNOS promoter[194], was remarkably increased after BMP9/BMP10 stimulation both in ECs and PASMCs. However, overexpression of *Atoh8* in ECs or SMCs did not cause any obvious defects in vessel beds. Although the genetic analysis suggests a direct action of BMP9/BMP10 on VSMCs, one cannot exclude that signalling cues from the endothelium regulates the contractile state of VSMCs. Interestingly, overexpression of inhibitory Smad7 in endothelium with *iCdh5-Cre* driver also resulted in vessel dilation due to the loss of contractile VSMCs, which reiterates the essential role of ECs in VSMC differentiation and contractility. The role of BMP9/BMP10 for regulation of VSMC physiology is more complicated than previous anticipated, requiring further research and a better understanding of the signals reaching VSMCs, either directly or indirectly from ECs.

4.2 Heterogeneity of BMP type one receptors

Regional heterogeneity exists in the whole vascular tree and might lead to different responses to pathogenic stimuli[82]. Vascular differences might reflect differential physiological requirements and different signalling needs of vessels in distinct organs. It is increasing recognized that both in normal and disease conditions there is a molecular, morphological and functional heterogeneity within the endothelium. So far, vessel heterogeneity has been mostly attributed to ECs[79, 82] but a contribution of VSMCs to heterogeneity of vessels makes sense, further enabling them to mount divergent responses to exogenous stimuli.

The finding that inactivation of *Alk1* in SMCs only recapitulated the *Bmp9/10*^{dko} phenotype in pulmonary arteries but not in aortae or coronary vessels clearly indicates a substantial heterogeneity of VSMCs in distinct vessels. RNA-FISH and bulk RNA-seq revealed that VSMCs in distinct vessel beds expressed different combinations of *Alk* receptors. *Alk1* is the dominant receptor in pulmonary VSMCs while *Alk2* and *Alk3* are also highly expressed in aortae and coronary arteries, which seem to compensate for the absence of ALK1. Therefore, contractile VSMCs are only lost and phosphorylation of Smad1/5/8 is only prevented in pulmonary arteries of *Sm22-Cre/Alk1*$^{\Delta loxP/\Delta loxP}$ mutants. Since inactivation of BMP9 and BMP10 caused a profound reduction of contractile VSMCs in all vessel beds, it is reasonable to hypothesize that BMP9/BMP10 also employ ALK2 and ALK3 for signaling transmission in aortae and coronary arteries. In other words, *Alk2* and *Alk3* in VSMCs of aortae and coronary arteries may compensate for the absence of *Alk1* and thus contractile VSMCs are maintained. However, it remains possible that ALK2 and ALK3 preferentially employ different ligands and are only relevant for BMP9/BMP10 signalling in the absence of ALK1. Generation of *Alk1/Alk2/Alk3* or *Alk1/Bmp9/Bmp10* triple knockout mice might address this hypothesis.

VSMCs originate from at least eight different sources of progenitor cells, showing sharp boundaries without intermixing of cells from other lineages, which might contribute to their heterogeneity[76, 78]. For example, only mesenteric vasculature originates from serosal mesothelium[221]. The observed variation of combinatorial *Alk* receptor expression in distinct vessel beds might result from different developmental origins of VSMCs, as well as from specific structural and physiological requirements of VSMCs in their vascular context. The understanding of VSMC heterogeneity is in its infancy and the phenotypic and organotypic heterogeneity as well as their origins and specific markers are still largely unknown. A better understanding of this heterogeneity will provide a new perspective for the identification of potential therapeutic targets that specifically take advantage of vascular heterogeneity to combat diseases. For example, specific inhibition of ALK1 signalling processes in VSMCs might reduce hypermuscularization of pulmonary arteries in PH without affecting aortic and coronary arteries.

To further explore this heterogeneity, transcriptionally and proteomically profiling VSMCs from distinct arteries should be performed to identify unique and distinguishable signatures. The presence of bronchial smooth muscle cells (BSMCs) in the lung makes it difficult to selectively label and isolate VSMCs without contaminations from BSMCs. Using a similar method described by Liu[222], generation of a dual-recombinasebased lineage-tracing system capitalizing on intersectional genetics, using co-expression of two marker genes in pulmonary VSMCs provides an interesting opportunity. NG2 (Chondroitin Sulfate Proteoglycan 4) is expressed in pericytes and VSMCs but not in BSMCs whereas *Acta2* is expressed both in VSMCs and BSMCs. Insertion of a Dre recombinase into the NG2 locus and a CFP-Stop-RSR-cassette into the *Acta2* locus offers such an opportunity. Such an experimental set-up can be combined with different Cre-dependent effector alleles to specifically label nascent RNAs (UPRT allele), purify translated RNAs (Ribo-Tag allele) or label newly synthesized proteins for mass spectrometry exclusively in VSMCs.

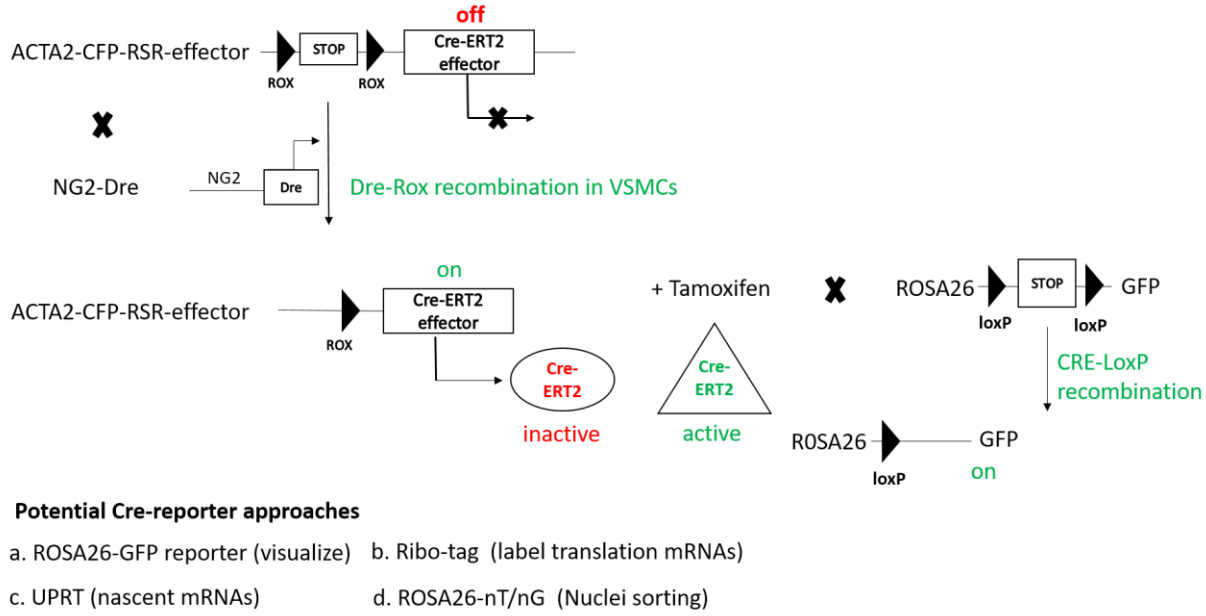

Figure 25. NG2-Dre and ACTA2-Rox-Stop-Rox based binary recombination system to label PASMCs.

Acta2 is both expressed in PASMCs and BSMCs, while *Ng2* expression is restricted to PASMCs and pericytes. Only PASMCs in which both alleles are active ($Dre^{+}Cre\text{-}ERT2^{+}$ cells) will allow Cre-recombinase mediated recombination, thus leading activation of reporter gene expression after administration of tamoxifen.

Furthermore, the use of Cre-inducible CRISPR-Cas9-activator strain as described by Zhou[223], is a potential tool to simultaneously overexpress *Alk*2 and *Alk3* in PASMCs of *Sm22-Cre/Alk1*$^{\Delta loxP/\Delta loxP}$ mutants to investigate whether such overexpression will restore the loss of contractile VSMCs. Likewise, a Cre-inducible CRISPR-Cas9-repressor strain might be implemented to simultaneously repress *Alk2* and *Alk3* expression in aortae and coronary

arteries to study whether absence of *Alk2* and *Alk3* expression in these arteries will result in loss of contractile VSMCs. To study the consequences of altered ALK receptor expression, a battery of experiments including measuring blood pressure, vessel contractility and immunofluorescence staining for pSmad1/5/8 will shed light into the functional heterogeneity of BMP type I receptors in VSMCs.

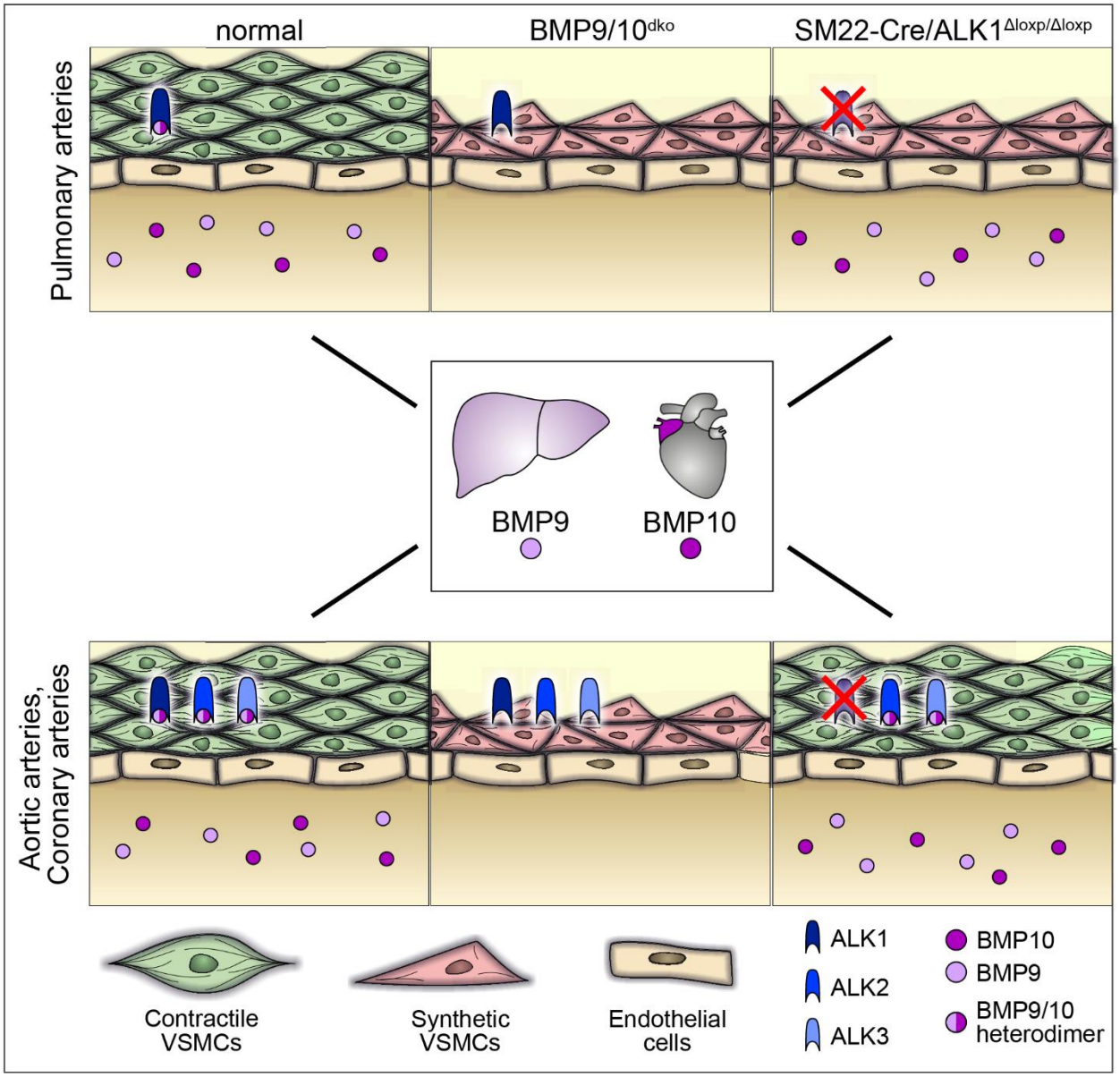

Figure 26. Model of the role of BMP9/BMP10 for formation of contractile VSMCs in distinct vessels.

BMP9 and BMP10 are released into the blood stream by the liver and the right atrium, respectively. BMP9 and BMP10 pass the endothelium to directly stimulate formation of contractile VSMCs via different ALK receptors. Concurrent loss of BMP9 and BMP10 leads to a massive loss of contractile VSMCs in all muscularized vessels. Since pulmonary arteries

only express *Alk1* at high levels, inactivation of *Alk1* in SMCs recapitulates the *Bmp9/10*^{dko} phenotype only in pulmonary arteries but not in aortae and coronary arteries, which also contain ALK2 and ALK3, potentially compensating for the absence of ALK1 and transmit the BMP signalling.

4.3 Cross-talk of BMP/Smad4 signalling with Hippo-signalling in VSMCs

Hippo signalling was originally identified in *Drosophila* as an organ size control pathway and now emerged as a critical conserved pathway mediating development and homeostasis in various processes[224-226]. In the mammalian Hippo pathway, Mst1/2 and Lats1/2, which are the core kinase cascade, phosphorylate, retain and degrade the transcriptional co-activators YAP and TAZ. Upon Hippo inactivation, YAP/TAZ translocate into nucleus and form a complex with TEAD family of transcriptional factors to regulate downstream gene expression. Previous studies suggested that TEAD1 suppresses expression of VSMC typical genes by abolishing the pro-myogenic function of Myocd, the master regulator of VSMC differentiation. Myocd is a co-activator of the transcription factor SRF and the Myocd/SRF complex activates transcription of several SMC differentiation genes, including *Acta2, Tagln* and *Myh11*[227]. TEAD transcription factors compete with Myocd for binding of SRF, thereby disrupting Myocd/SRF interactions, causing downregulation of SMC specific genes and attenuation of the contractile VSMC phenotype[201, 203]. Likewise, repression of the Hippo pathway, which leads to activation of the TEAD cofactors YAP/TAZ, promotes proliferation and migration of SMCs at the expense of differentiation[205]. TEAD transcriptional factors bind to a conserved DNA sequence motif, which is called MCAT (Muscle Specific Cytidine-Adenosine-Thymidine-Sequence (5´-CATTCCT-3`)) elements. Such MCAT elements are located in promoter regions of numerous skeletal, cardiac and smooth muscle genes, such as *Acta2, Acta1* and *Myh7*[228, 229]. TEADs have been found to form a complex with several transcriptional factors of the TGFβ pathway. For example, in malignant mesothelioma cells, TEAD4 has been discovered to form a complex of YAP1-Smad2/3-P300 on some positions of the *Ctgf* promoter, indicating a synergistic action of TEAD and Smad2/Smad3[230].

To understand how precisely BMP9/BMP10 regulate differentiation of VSMCs and acquisition of the contractile state, ATAC-seq and RNA-seq analysis of BMP9/BMP10 stimulated PASMCs were performed. ATAC-seq footprinting in combination with RNA-seq and bioinformatics analysis identified numerous potential target genes defined by BMP9 and BMP10 upregulation, increase of chromatin accessibility, and presence of canonical Smad binding sites. Further analysis revealed co-accessibility of Smad4 and TEADs transcription factor binding sites at several VSMC genes, such as *Acta2* and *Tagln*, suggesting that BMP-SMAD-signalling and Hippo-signalling closely cooperated to control VSMC differentiation and contractility. Co-IP experiments revealed a directly physical interaction between Smad4 and TEAD1 upon

BMP9/BMP10 treatment. It seems reasonable to hypothesize that the balance between YAP/TAZ/TEAD and BMP9/BMP10/Smad-signalling at the chromatin level is crucial for the fate of VSMCs. Hippo-signalling is suggested to promote proliferation and migration of VSMCs, while Smad-dependent BMP9/BMP10 signalling strongly induces differentiation. Hence, these two pathways may mutually antagonize each other at the chromatin level. Loss- and Gain-of-function studies presented in this study showed that the YAP/TAZ/TEAD signalling strongly attenuated BMP9/BMP10 induced re-expression of typical VSMC genes in differentiated PASMCs. However, direct evidence for concomitant or mutually exclusive binding of TEADs and Smads to the same regulatory region of VSMC genes is still missing. Yet, a previous study demonstrated that the Smad2/Smad3/TEADs complex directly bind to the promoter region of several typical VSMC genes[205]. Thus, it is reasonable to assume that the activity of the Smad1/5/8/Smad4 complex depends on the extent of YAP/TAZ/TEAD complex formation and vice versa. Performing YAP/TEAD as well as Smad4/Smad1/5/8 genome wide chromatin binding studies (ChIP-seq analysis) in cultured PASMCs stimulated by BMP9/BMP10 will help to address this hypothesis and answer the question whether target promoters are differentially occupied by the YAP/TAZ/TEADs and the Smad4/Smad1/5/8 complex in the presence of BMP signaling.

4.4 BMP9/BMP10 as potential therapeutic targets for vascular diseases

In the past decades, a better understanding of the functions of BMP signalling has expanded dramatically beyond the initially discovered role in the bone formation. Recent studies have uncovered the non-redundant but multifaceted roles of this family in regulation of vascular development, maintenance as well as related disease states. Defining the multifaceted roles of BMP signalling in vascular diseases will provide broader and deeper insight into the molecular mechanisms that drive diseases.

4.4.1 The role of BMP9 and BMP10 in pulmonary arterial hypertension

PAH is a severe life-threatening disease characterized by progressive increase of pulmonary vascular resistance, leading to maladaptive right ventricular hypertrophy (RVH) and ultimately right ventricular failure. Patients with heritable forms of PAH often have mutations in genes encoding receptors of the TGF-β receptor superfamily, in particular in BMPRII, ALK1 and ENG. Conflicting results make it difficult to judge whether ALK1 and its ligands BMP9 and BMP10 protect or promote adverse vascular remodeling during onset and progression of PAH. In our hands, genetic inactivation of *Bmp9/Bmp10* results in a massive loss of contractile VSMCs and diminution of smooth muscle layer, which leads to reduced systemic blood pressure. Additional experiments revealed that administration of L-NAME, a nitric oxide synthase inhibitor, did not increase blood pressure in *Bmp9/10*^{dko} mice, further suggesting attenuated vasoconstriction. Gene expression profiling analysis revealed that loss of these two BMPs affected several

signaling pathways regulating angiogenesis as well as VSMC proliferation and maturation, all of which are known to be crucial for the pathology of PAH. Furthermore, overexpression of the inhibitory *Smad7* or deletion of *Alk1* in SMCs resulted in vascular dilation and impaired contractility. One might hypothesize that genetic deletion of BMP9/BMP10 might provide protection against hypoxia-induced PH and indeed, this study suggests that this hypothesis is correct. This finding is intriguing because the current approaches to treat PH mainly target drugs for vasodilation while the current study suggests that vessel bed specific inhibition of BMP9/BMP10/ALK1 signalling may protect patients from PH.

Mutations in BMPR2 are the most common genetic cause favoring PH[145, 152]. Surprisingly, administration of BMP9 into two rat models of PH as well as into a mouse model bearing a knock-in allele of a human *BMPR2* mutation (RX99X), prevent and reverse established PH[11]. These finding are difficult to reconcile with the results of this study, which disclosed that inactivation of BMP signalling leads to loss of contractile VSMCs with dilated vessel diameters, while enhanced BMP signalling had opposite effects. How to explain that PH is associated with reduced plasma levels of BMP9/BMP10 and administration of BMP9 to animal models reverse established PH when BMP9/BMP10 strongly promote formation of contractile VSMCs? BMP signalling occurs through the type I and type II receptors, dependent on various co-receptors and endogenous ligand traps, which leads to highly context dependent effects. The reduced plasma levels of BMP9/ BMP10 in PH patients may be due to a negative feed-back loop restraining formation of excessive contractile VSMCs. Exogenous administration of BMP9 might partially restore physiological conditions and reduce the impact of pathological signals[231]. This hypothesis is further supported by a study, which describes that inhibition of BMP9 or ALK1 partially protects against chronic hypoxia induced PH in mice models[12]. Another potential explanation might rely on an imbalance between the synthetic and contractile states of VSMCs. BMP signaling strongly stimulates formation of contractile VSMCs whereas suppression of BMP signaling causes acquisition of a synthetic phenotype, characterized by high proliferative index. It is possible that loss of BMPR2 increases the number of synthetic VSMCs and leads to higher number of proliferating VSMCs, which will increase medium layer thickness and reduce vessel lumen diameter.

To further explore whether manipulation of different components of the BMP9/BMP10/ALK1-Smad1/5/8 axis alters susceptibility to PH and right ventricle hypertension, it will be helpful to subject the following selected mouse strains, including *Sm22-Cre/Alk1*$^{\Delta loxP/\Delta loxP}$, overexpression of inhibitory *Smad6* or *Smad7* in VSMCs or ECs and *Bmp9*$^{-/-}$*/Bmp10*^{iMhc} mutants to the well-established hypoxia induced PH and Sugen 5416/hypoxia regimens. Furthermore, it will be interesting to study whether termination of *Bmp10* overexpression is sufficient to revert hyper-contractile pulmonary arteries back to normal. Generation of a Tet-responsive *Bmp10* overexpression strain will offer the opportunity to reversibly express *Bmp10*

by timed doxycycline treatment and to study phenotypic switching of VSMCs from normal to hyper-contractile and *vice versa*. Compound alleles combining *Alk1* mutant alleles and overexpression of *Bmp10* will reveal whether effects of increased circulating BMP10 are blunted by *Alk1* inactivation in PASMCs compared to VSMCs expressing *Alk2* and *Alk3* (aortic and coronary arteries). These approaches will provide a better functional insight into BMP9/BMP10/ALK1/Smad signaling in PH and right ventricle hypertrophy and will open up new opportunities to selectively manipulate VSMCs in the context of PH.

4.4.2 BMP9 and BMP10 are potential therapeutic targets for the treatment of fibrotic diseases

Fibrotic diseases include a group of disorders, characterized by progressive and irreversible destruction of structures with formation of a fibrotic scar[232]. Increased deposition of ECM proteins compromises tissue architecture and impairs normal organ function. The formation of fibrotic lesions is primarily caused by the release of inflammatory cytokines, which eventually lead to activation of fibroblasts, myofibroblast differentiation and enhanced collagen synthesis[233]. A large body of evidence indicates that several members of TGFβ superfamily, including TGFβ1, Activin A and Activin B, enhance cytokine production[234-236] and increase transcription of genes involved in ECM production, such as *Ctgf* and *fibronectin*[237]. Furthermore, TGFβ signalling reduces degradation of matrix proteins by down-regulation of the expression of matrix metalloproteinases[234, 235].

Suppression of TGF-β signalling represents a potential approach to prevent adverse organ remodelling. In contrast, numerous experiments suggest that activation of BMP signalling attenuates the onset and formation of fibrosis. For example, exogenous administration or overexpression of BMP7 causes anti-fibrotic effects in chronic kidney disease models[107], liver fibrosis[238] as well as pulmonary fibrosis[239, 240]. It has been shown that activation of BMP signalling via Smad1/5/8 suppresses TGFβ induced fibrotic gene expression[241,242]. Specifically, in bleomycin induced pulmonary fibrosis, activation of TGFβ signalling and suppression of BMP signalling was observed[243]. BMP2 was shown to neutralize TGFβ1 activity by promoting formation of the Smad6/Smurf1 complex, which reverses pro-fibrotic effects of TGFβ1 in the lung[244]. The antagonistic effect of BMP-signaling on fibrosis is further supported by the observation that anti-fibrotic agent pirfenidone, which is used to treat idiopathic pulmonary fibrosis, enhances BMP signalling while inhibiting non-canonical AKT and ERK dependent TGF-β signalling[245]. Taken together, previous studies revealed that these two pathways mutually antagonize each other in regulating fibrotic responses.

Despite intensive research, the role for BMP9/BMP10/ALK1 signalling in fibrotic diseases remains enigmatic. Several previous reports suggest a pro-fibrotic role of BMP9 in liver fibrosis

by increasing the levels of hepcidin, which inhibited hepatic iron absorption, resulting in iron accumulation and subsequent fibrosis[246-248]. Other studies demonstrate that BMP9 signalling enhances vascular inflammation and induce the development of atherosclerosis[249, 250], a chronic vascular disease characterized by the formation of plaques in the inner lining of arteries[251]. In contrast, suppression of BMP9 signalling prevents vascular inflammation and reduces recruitment of leukocytes[252,255], thus ameliorating adverse effects caused by atherosclerotic diseases[252, 253]. In heart failure, BMP9 was recently found to act as an endogenous inhibitor of cardiac fibrosis by increasing pSmad1 levels and reducing pSmad3 levels[242]. Two other studies also show that ALK1 heterozygous mutant mice exhibit impaired cardiac function with progressive fibrosis in pressure overload-induced heart failure models[242, 254]. In this study it was found that *Sm22-Cre/Alk1*$^{\Delta loxP/\Delta loxP}$ mutants develop a severe auto-inflammation reaction due to excessive recruitment of lymphocytes and macrophages to the lung, which leads to massive fibrosis and lethality of mice around 6-8 weeks. The detailed mechanisms behind this phenotype still needs to be explored but the findings reiterate the conclusion that BMP/ALK1 signalling is a main repressor of immune inflammation. Further support for this idea comes from *in vitro* experiments, demonstrating that BMP9 and BMP10 down-regulate several pro-fibrotic genes including *vimentin* and *Col1a1* in cultured PASMCs and are capable to suppress pro-fibrotic TGFβ1 signalling. Furthermore, GSEA showed that the genes involved in ECM formation and atherosclerosis development are also suppressed upon BMP9/BMP10 treatment.

These findings raise the possibility that administration of BMP9/BMP10 may ameliorate inflammation and chronic fibrotic disorders. However, the use fullness of BMP9 as a therapeutic agent is limited by need of frequent parental injections and risks of altering angiogenesis at injection sites. Furthermore, the complicated cross-talk between TGFβ and BMP signalling might lead to unwanted side effects that either reciprocally enhance or antagonize effects in context dependent manners. The design of more specific and promising pharmacological strategies to modulate TGFβ/BMP signalling in the context of fibrotic disease treatment is challenging, requiring further studies involving combinatorial targeting of different components of the TGFβ/BMP signalling pathway.

4.4.3 The role of BMP9 and BMP10 in myocardial infarction

Occlusion of coronary vessels is a life-threatening and devastating event leading to myocardial infarction (MI) or stroke. Such occlusions may be the result of atherosclerosis, inflammation, embolism or thrombus formation, causing either acute or chronic ischemia. During MI, numerous cardiomyocytes (CMs) become necrotic, followed by replacement of dead cells by collagen-containing scars. The cellular events involved in infarct healing can be separated into three overlapping phased: the inflammatory phase, the proliferative phase, and the maturation

phase. During the inflammatory phase, cytokine and chemokine cascades are activated and leukocytes are recruited into the infarcted myocardium. These leukocytes clear dead cells and matrix debris enabling the formation of granulation tissue. During the proliferative phase, activated myofibroblasts deposit extracellular matrix proteins, followed by the maturation phase in which the scar contracts and becomes fully organized. Anti-fibrotic pathways limit the fibrogenic response while the collagen-based scar is formed[255]. Cardiac fibrosis compromises heart function and reduces survival[256].

Previous studies reported beneficial roles of BMP signalling in myocardial injury. BMP2 was found to reduce the size of infarcts and the number of apoptotic cells and increase the contractility and beating frequency of isolated CMs[257]. Furthermore, it was shown that BMP4 protects CMs from apoptosis after hypoxia-reoxygenation injury[258]. Work by Morine et al revealed that BMP9 limits adverse cardiac remodeling by activating Smad1 and attenuating Smad3, thus neutralizing TGFβ induced pro-fibrosis effects[242]. Recently, it was shown that BMP10 has cardioprotective effects by promoting survival of CM and suppressing CM apoptosis and myocardial fibrosis[259]. Preliminary data obtained in this study using RNA-FISH analysis revealed that *Bmp10* and *Alk1* transcripts were significantly increased in the infarct zone of mice subjected to ligation of the left anterior descending artery (LAD). In addition, immunofluorescence staining and western blot analysis revealed that Smad1/5/8 becomes phosphorylated in the infarct and border zones but not in the remote zone of the ischemic hearts. These results provide evidence for a potential roles of BMP signalling in cardiac remodelling during MI. It is reasonable to assume that BMP9/BMP10 might exert similar protective function as BMP2 and BMP7, which also activate Smad1/5/8 via ALK receptors. Specifically, inactivation or overexpression of components of *Bmp/Alk* signaling in CMs by using a CM specific driver, such as *aMhc-Cre* mice, will provide the opportunity to study the roles of BMP9/BMP10/ALK1 during MI. In addition, manipulation of BMP signaling specifically in de-differentiated CMs by using AAV-mediated expression of Cre recombinase[260, 261] creates new opportunities. Based on such methods, it is feasible to decipher more precisely the role of BMP signalling during different phases of myocardial injury.

It is imperative to closely monitor secondary effects when manipulating BMP9 and BMP10 activity in cardiac remodelling. During heart failure or myocardial infarction, CMs undergo cell death due to lack of blood flow, which causes acute imbalance between oxygen supply and demand. Ischemia leads to activation of angiogenesis to re-establish blood flow for provision of oxygen and nutrients. Angiogenesis, i.e. the sprouting of pre-existing vessels, is beneficial when activated in conditions like wound healing or tissue regeneration[262]. Thus, therapeutic strategies to activate or improve angiogenesis are promising approaches to treat vascular occlusive diseases[263]. Soon after infarction there is a robust increase in EC numbers but newly formed vessels are highly permeable due to the lack of SMC coverage[264, 265]. This study and

others[10, 166] have demonstrated that BMP9 and BMP10 are instrumental for the recruitment and differentiation of VSMCs, which is a prerequisite for vessel maturation. From this point of view, reduction of BMP9/BMP10 in the circulation may compromise adult hearts after infarction. However, the situation might be different in neonatal hearts, in which CM retain some proliferative capacity, allowing to restore contractile function[266-268]. Recent studies uncovered that the transition from the relatively hypoxic condition *in utero* to the oxygen-rich postnatal environment causes accumulation of reactive oxygen species, triggering DNA damage response, which leads to the arrest of CM proliferation and the loss of endogenous regenerative capacity[269-271]. Results obtained in this study suggest that reduced formation of mature VSMCs during postnatal angiogenesis by inactivation of BMP9/BMP10 extended the prenatal hypoxic condition in hearts of neonatal mice, which decreases the accumulation of reactive oxygen species and DNA damage. As a consequence, the proliferative window of CMs is prolonged, allowing regenerative response at later developmental stages.

4.5 Perspective

This study reveals that circulating BMP9 and BMP10 directly target VSMCs and maintain the contractile state through ALK receptors. Inactivation of BMP9/BMP10 leads to dedifferentiation of VSMCs, diminution of the medial arterial layer, arterial dilatation and lowered blood pressure, while BMP10 overexpression has opposite effects. I showed that BMP9/10 act through ALK receptor in VSMCs and uncovered the surprising heterogeneity of VSMCs between pulmonary and other arteries, which in principle allows to specifically modulate BMP signal transduction in PASMCs. The new concept of regionalization of VSMC based on compartmentalization of key VSMC receptors has broad implications for physiology and pathology, especially in the field of PAH.

However, it is still necessary to obtain a more comprehensive understanding of BMP signaling in VSMCs and associated diseases. Specifically, alteration of cellular properties of VSMCs by manipulation of the BMP9/BMP10-ALK1-Smad1/5/8 axis under normal and hypoxic conditions holds great promise. The newly generated conditional BMP10 overexpression strain allows to explore effects of BMP10 on pulmonary arteries. *Sm22-Cre/Alk1*$^{\Delta loxP/\Delta loxP}$ and *Bmp9*$^{-/-}$*/Bmp10*^{iMhc} mutants should be subjected to hypoxia treatment for analyzing effects on the pulmonary circulation and right ventricle hypertrophy. In addition, profiling of the transcriptome and proteome of VSMCs will allow identification of unique signatures in different vessel beds, which will be helpful to further address the heterogeneity of VSMCs. In this regard, the differential expression of ALK receptors in VSMCs in different vessels is an exciting starting point. Furthermore, deeper insights into the potential cross-talk of BMP9/BMP10 with other signaling cascades, such as the Hippo signalling pathway should be obtained to understand how the interplay between pro-proliferative and pro-differentiation works for the regulation of

the contractile/synthetic states. Furthermore, it is an exciting perspective to unravel the mechanisms by which circulating BMP9/BMP10 ligands pass the endothelial barrier to regulate VSMCs. Clearly, the better comprehensive understanding of BMP signalling in the vasculature will contribute to the understanding of vascular diseases and the development of novel therapeutic strategies.

5 Supplemental figures

5.1 Top 50 enriched gene sets or pathways in RNA-seq analysis

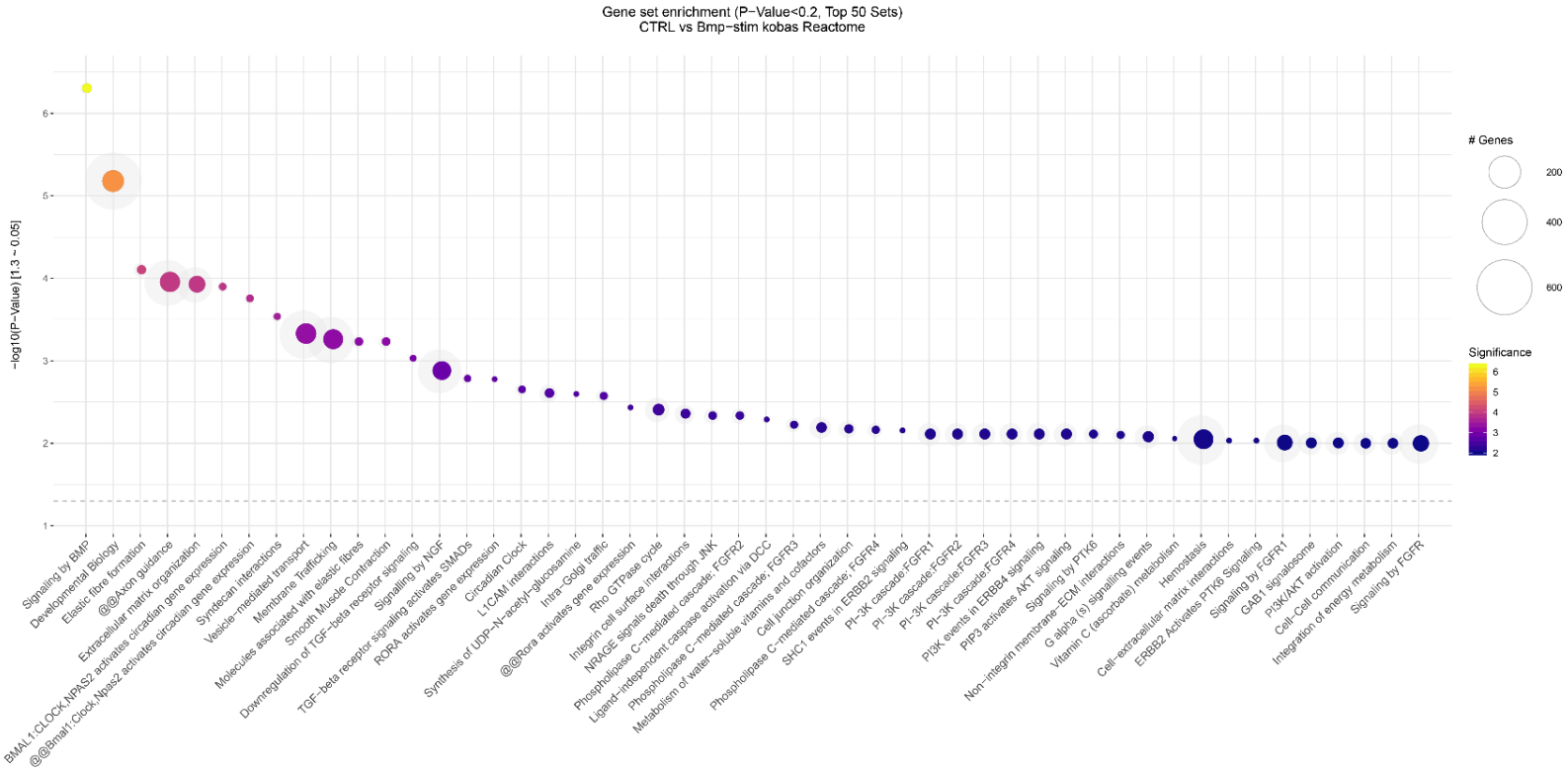

Gene set enrichment analysis of genes up-regulated in PASMCs stimulated with BMP9/BMP10 for 6 hours. Top50 pathways are displayed based on p value using Kobas database. Significant gene set enrichment is defined by p value and the dashed line represents p value=0.05. Circle sizes represent the scale and colored circles represent the number of genes that up-regulated in pathways.

5.2 Top 50 enriched gene sets or pathways in ATAC-seq analysis

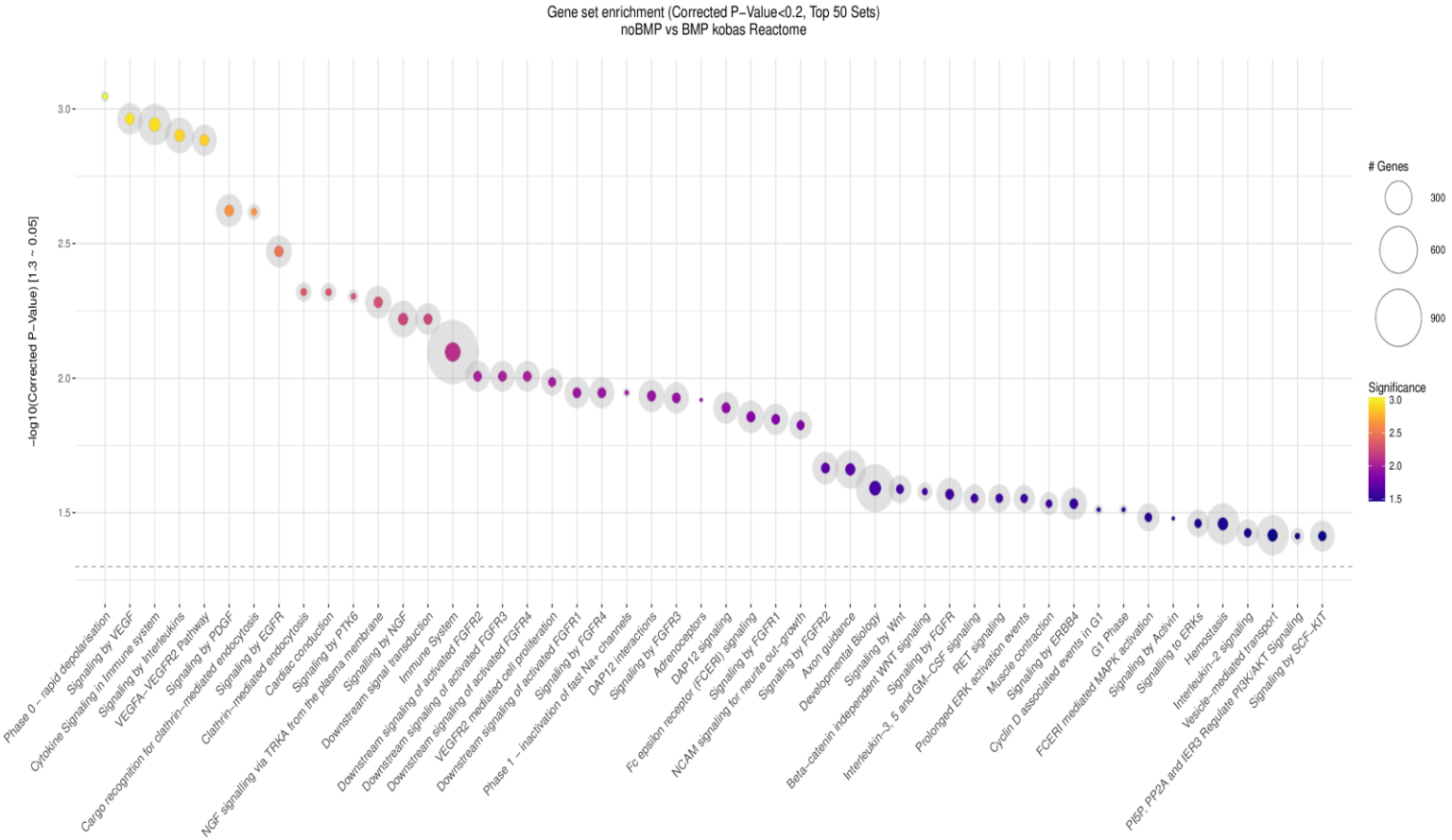

Gene set enrichment analysis showing open chromatin configuration in PASMCs stimulated with BMP9/BMP10 for 6 hours. Top50 pathways are displayed based on p value using Kobas database. Significant gene set enrichment is defined by p value and the dashed line represents p value=0.05. Circle sizes represent the scale and colored circles represent the number of genes that up-regulated in pathways.

Ⅳ. List of figures

V. List of tables

Ⅵ. List of abbreviation

Abbreviation	Meaning
%	Percent
ACTA2	mooth muscle a-actin
ALK	Activin receptor-like kinase
ANF	Atrial natriuretic peptide
APJ	Apelin receptor
APLN	Apelin
APS	Ammoniumperoxodisulfat
ATAC	Assay for Transposase-Accessible Chromatin
ATOH8	Atonal BHLH transcription factor 8
AVMs	Arteriovenous malformation
BMP	Bone morphogenetic proteins
BMPR	Bone morphogenetic protein receptor
BSA	Bovine serum albumin
BSMCs	Bronchial smooth muscle cells
℃	Degrees celcius
CCPs	Cardiopulmonary progenitor cells
cDNA	Complementary DNA
ChIP	Chromatin immunoprecipitation
cm	Cenetimetre
CMs	Cardiomyocytes
CNN1	Calponin
Co-IP	Co-immunoprecipitation
Co-Smad	Co-mediated Smad
CREB	cAMP response element-binding protein
Ctgf	Connective tissue growth factor
DAPI	4',6-diamidino-2-phenylindole
DEPC	Diethylpyrocarbonate
DMEM	Dulbecco’s Modified Eagle Medium
DNA	Deoxyribonucleic acid
dNTP	DeoxyriboNucleotide TriPhosphate
E	Embryonic day
EC	Endothelial cell
ECM	Extracellular matrix
EDTA	Ethylenediaminetetraacetic acid

EEL	External elastic layer
End-1	Endothelin-1
ENG	Endoglin
eNOS	Endothelial nitric oxide synthase
ERK	Extracellular signal regulated kinase
EVs	Extracellular vesicles
FAL	Formal artery ligation
FBS	Fetal bovine serum
FGFR1	Fibroblast growth factor receptor 1
FISH	Fluorescence In Situ Hybridization
g	Gram
GAPDH	Glyceraldehyde-3-phosphate dehydrogenase
GFP	Green Fluorescent Protein
GOF	Gain-Of-Function
GSEA	Gene set enrichment analysis
H&E	Hematoxylin and eosin staining
HHT	Hereditary haemorrhagic telangiectasia
HMVEC	Human dermal microvascular endothelial cell
HUVEC	Human umbilical vein endothelial cell
i.p	Intraperitoneal
ID	Inhibitor Of DNA Binding
IF	Immunofluorescence
IGV	Integrative genomic viewer
In Situ	In place(Lain)
in vitro	in the glass (Latin)
in vivo	within the living (Latin)
KLF	Kruppel-like factor
KO	Knockout
L	Litre
L-NAME	NG-nitro-L-arginine methyl ester
LOF	Loss of function
LoxP	Locus of cross-over (x) of the bacteriophage P1
M	Molar
MAPKs	Mitogen activated protein kinases
MCAT	Muscle specific Cytidine-Adenosine-Thymidine-Sequence
MCT	Monocrotaline
MEA	Motif Enrichment Analysis

MEJs	Myoendothelial gap junctions
mg	Milogram
mL	Millilitre
Mm	Millimetre
mM	Millimolar
mRNA	messenger RNA
MYH11	Myosin Heavy Chain 6
Myocd	Myocardin
NES	Normalized enrichment score
ng	Nagogram
NG2	Neural glial antigen 2
nm	Manometers
NO	Nitric oxide
NOS	Nitric oxide synthase
OCT	Octamer binding transcription factor
OSM	Oncostatin M
PAH	Pulmonary arterial hypertension
PASMC	Pulmonary artery smooth muscle cell
PBS	Phosphate-buffered saline
PCR	Polymerase chain reaction
PECAM	Platelet-endothelial cell adhesion molecule
PFA	Paraformaldehyde
PH	Pulmonary hypertension
qRT-PCR	Quantitative real-time polymerase chain reaction
RNA	Ribonucleic acid
RNA-seq	RNA-sequencing
ROS	Reactive oxygen species
ROSA26	Reverse oriented splice acceptor, clone 26
RT	room temperature
SAPK/JNK	Stress-activated protein kinases /Jun amino-terminal kinases
SDS	Sodium dodecyl sulfate
SDS-PAGE	Sodium dodecyl sulfate-polyacrylamide gel electrophoresis
SMA	Smooth muscel actin
Smad	Mothers against DPP homolog
SMC	Smooth muscle cell
SMTN	Smoothelin
SMURF	Smad-mediated ubiquitin regulatory factor

SOX	Sex deternububg region Y box
SRF	Serum response factor
TAGLN	Transgelin
TAPSE	Tricuspid annular plane systolic excursion
TAZ	Tafazzin
TBST	Tris buffered saline/tween-20
TE	Tris-EDTA
TEAD	Transcription Enhancer Factor
TEM	Transmission electron microscope
TF	Transcription factor
TGF	Transforming growth factor
TPM4	Tropomyosin 4
uCT	Micro computed tomography
ug	Microgram
uL	Microliter
V	Volts
Vgll	Vestigial like family member
VIM	Vimentin
VIM	Vimentin
VSMC	Vascular smooth muscle cell
WT	Wild type
YAP	Yes-Associated Protein

Ⅶ Acknowledgements

I would like to express my sincere gratitude and appreciation to a large number of colleagues who supported me during the past years at the prestigious Max Planck Institute for Heart and Lung research in Bad Nauheim.

First of all, I would like to particularly express my deepest appreciation to my supervisor Prof. Dr. Dr. Thomas Braun, for giving me the opportunity to pursue my doctor degree and for his constructive supports, suggestions and supervisions over the years, which impressed me deeply and enabled me to acquire a good understanding and performing of this thesis. I would like to take the change to thank the rest of my thesis committee: Prof. Dr. Norbert Weissmann, Prof. Dr. Saverio Bellusci and Prof. Dr. Reinhard Dammann, for the review my thesis and comments.

I am particularly grateful for the great and meticulous supports from my directly supervisor, Dr. André Schneider. He is one of the most conscientious and patient man I have ever met. Your giving is highly appreciated.

My grateful thanks are also addressed to Dr. Stefan Günther and Dr. Mario Looso, for their cooperation in processing and analysis of RNA-seq and ATAC-Seq, to Prof. Dr. Thomas Böttger for his processing and analysis of microarray data, to Marion Wiesnet for her support in all kind of surgery, to Sonja Krüger, Susanne Kreutzer and Ann Atzberger for their technological support. I also like to thank the animal caretakers Diefenthaeler Meike and Gajda Michael for the important and unerring work. My colleagues here always show great professionalism, which impressed me greatly. My special thanks are extended to all members of AG Schneider group, to all lab members who supported me greatly and are always willing to help.

I also would like to thank the China Scholarship Council (CSC) for the financial support of top four years during my research in Germany.

I wish to thank my girlfriend, Dr. Wen ting Zhao for her contribution to my emotional well-being and support always.

Finally, I gratefully acknowledge the support, encouragement and loving from my parents. I can not thank you enough.

Ⅷ Curriculum vitae

IX References

1. Owens GK, Kumar MS, Wamhoff BR. Molecular regulation of vascular smooth muscle cell differentiation in development and disease. *Physiol. Rev* 2004;84(3):767-801.
2. Beamish JA, He P, Kottke-Marchant K, Marchant RE. Molecular regulation of contractile smooth muscle cell phenotype: implications for vascular tissue engineering. *Tissue Eng. Part B Rev.* 2010;16(5):467-91.
3. Paul R, Herbert JM, Maffrand JP, Lansen J, Modat G, Pereillo JM, et al. Inhibition of vascular smooth muscle cell proliferation in culture by pentosan polysulphate and related compounds. *Thromb. Res.* 1987;46(6):793-801.
4. Frismantiene A, Philippova M, Erne P, Resink TJ. Smooth muscle cell-driven vascular diseases and molecular mechanisms of VSMC plasticity. *Cell. Signal.* 2018;52:48-64.
5. Rosenkranz S. Pulmonary hypertension 2015: current definitions, terminology, and novel treatment options. *Clin. Res. Cardiol.* 2015;104(3):197-207.
6. Urness LD, Sorensen LK, Li DY. Arteriovenous malformations in mice lacking activin receptor-like kinase-1. *Nat. Genet.* 2000;26(3):328-31.
7. Oh SP, Seki T, Goss KA, Imamura T, Yi Y, Donahoe PK, et al. Activin receptor-like kinase 1 modulates transforming growth factor-beta 1 signaling in the regulation of angiogenesis. *PANS.* 2000;97(6):2626-31.
8. Park SO, Wankhede M, Lee YJ, Choi EJ, Fliess N, Choe SW, et al. Real-time imaging of de novo arteriovenous malformation in a mouse model of hereditary hemorrhagic telangiectasia. *J Clin Invest.* 2009;119(11):3487-96.
9. Mueller TD, Nickel J. Promiscuity and specificity in BMP receptor activation. *FEBS letters.* 2012;586(14):1846-59.
10. Wood JH, Guo J, Morrell NW, Li W. Advances in the molecular regulation of endothelial BMP9 signalling complexes and implications for cardiovascular disease. *Biochem Soc Trans.* 2019;47(3):779-791.
11. Long L, Ormiston ML, Yang X, Southwood M, Graf S, Machado RD, et al. Selective enhancement of endothelial BMPR-II with BMP9 reverses pulmonary arterial hypertension. *Nat. Med.* 2015;21(7):777-85.
12. Tu L, Desroches-Castan A, Mallet C, Guyon L, Cumont A, Phan C, et al. Selective BMP-9 Inhibition Partially Protects Against Experimental Pulmonary Hypertension. *Circ. Res.* 2019;124(6):846-855.
13. Budhiraja R, Tuder RM, Hassoun PM. Endothelial dysfunction in pulmonary hypertension. *Circulation*. 2004;109(2):159-65.
14. Levet S, Ciais D, Merdzhanova G, Mallet C, Zimmers TA, Lee SJ, et al. Bone morphogenetic protein 9 (BMP9) controls lymphatic vessel maturation and valve formation. *Blood.* 2013;122(4):598-607.
15. Chen H, Shi S, Acosta L, Li W, Lu J, Bao S, et al. BMP10 is essential for maintaining cardiac growth during murine cardiogenesis. *Development.* 2004;131(9):2219-31.
16. Chen H, Brady Ridgway J, Sai T, Lai J, Warming S, Chen H, et al. Context-dependent signaling defines roles of BMP9 and BMP10 in embryonic and postnatal development. *PNAS.* 2013;110(29):11887-92.
17. Levet S, Ouarne M, Ciais D, Coutton C, Subileau M, Mallet C, et al. BMP9 and BMP10 are necessary for proper closure of the ductus arteriosus. *PNAS.* 2015;112(25):E3207-15.
18. McEniery CM, Wilkinson IB, Avolio AP. Age, hypertension and arterial function. *Clin Exp Pharmacol Physiol.* 2007;34(7):665-71.
19. Rensen SS, Doevendans PA, van Eys GJ. Regulation and characteristics of vascular smooth muscle cell phenotypic diversity. *Neth Heart J.* 2007;15(3):100-8.

20. Pugsley MK, Tabrizchi R. The vascular system - An overview of structure and function. *J Pharmacol Toxicol.* 2000;44(2):333-340.
21. Majesky MW, Dong XR, Hoglund V, Daum G, Mahoney WM, Jr. The adventitia: a progenitor cell niche for the vessel wall. *Cells, tissues, organs*. 2012;195(1-2):73-81.
22. Passman JN, Dong XR, Wu SP, Maguire CT, Hogan KA, Bautch VL, et al. A sonic hedgehog signaling domain in the arterial adventitia supports resident Sca1+ smooth muscle progenitor cells. *PNAS.* 2008;105(27):9349-54.
23. Kawabe J, Hasebe N. Role of the vasa vasorum and vascular resident stem cells in atherosclerosis. *BioMed Res. Int.* 2014;2014:701571.
24. Mazurek R, Dave JM, Chandran RR, Misra A, Sheikh AQ, Greif DM. Vascular Cells in Blood Vessel Wall Development and Disease. *Adv Pharmacol.* 2017;78:323-350.
25. Harkness ML, Harkness RD, McDonald DA. The collagen and elastin content of the arterial wall in the dog. *roc. R. Soc. B*. 1957;146(925):541-51.
26. Greif DM, Kumar M, Lighthouse JK, Hum J, An A, Ding L, et al. Radial construction of an arterial wall. *Dev. Cell.* 2012;23(3):482-93.
27. Wagenseil JE, Mecham RP. Vascular extracellular matrix and arterial mechanics. *Physiol. Rev.* 2009;89(3):957-89.
28. Pouget C, Gautier R, Teillet MA, Jaffredo T. Somite-derived cells replace ventral aortic hemangioblasts and provide aortic smooth muscle cells of the trunk. *Development*. 2006;133(6):1013-22.
29. Risau W, Flamme I. Vasculogenesis. *Annu. Rev. Cell Dev. Biol.* 1995;11:73-91.
30. Woo KV, Qu X, Babaev VR, Linton MF, Guzman RJ, Fazio S, et al. Tie1 attenuation reduces murine atherosclerosis in a dose-dependent and shear stress-specific manner. *J. Clin.Invest.* 2011;121(4):1624-35.
31. Baldwin AL, Thurston G. Mechanics of endothelial cell architecture and vascular permeability. *Crit Rev Biomed Eng.* 2001;29(2):247-78.
32. Galley HF, Webster NR. Physiology of the endothelium. *Br. J. Anaesth.* 2004;93(1):105-13.
33. Dave JM, Bayless KJ. Vimentin as an integral regulator of cell adhesion and endothelial sprouting. *Microcirculation.* 2014;21(4):333-44.
34. Cines DB, Pollak ES, Buck CA, Loscalzo J, Zimmerman GA, McEver RP, et al. Endothelial cells in physiology and in the pathophysiology of vascular disorders. *Blood.* 1998;91(10):3527-61.
35. Hirase T, Node K. Endothelial dysfunction as a cellular mechanism for vascular failure. *Am J Physiol* Heart *Circ Physiol.* 012;302(3):H499-505.
36. Triggle CR, Samuel SM, Ravishankar S, Marei I, Arunachalam G, Ding H. The endothelium: influencing vascular smooth muscle in many ways. *Can. J. Physiol. Pharmacol.* 2012;90(6):713-38.
37. Balcells M, Martorell J, Olive C, Santacana M, Chitalia V, Cardoso AA, et al. Smooth muscle cells orchestrate the endothelial cell response to flow and injury. *Circulation.* 2010;121(20):2192-9.
38. Billaud M, Lohman AW, Johnstone SR, Biwer LA, Mutchler S, Isakson BE. Regulation of cellular communication by signaling microdomains in the blood vessel wall. *Pharmacol. Rev.* 2014;66(2):513-69.
39. Lilly B. We have contact: endothelial cell-smooth muscle cell interactions. *Physiology.* 2014;29(4):234-41.
40. Gao Y, Chen T, Raj JU. Endothelial and Smooth Muscle Cell Interactions in the Pathobiology of Pulmonary Hypertension. *Am. J. Respir. Cell Mol.* 2016;54(4):451-60.
41. Artavanis-Tsakonas S, Rand MD, Lake RJ. Notch signaling: cell fate control and signal integration in development. *Science.* 1999;284(5415):770-6.

42. Mancini ML, Terzic A, Conley BA, Oxburgh LH, Nicola T, Vary CP. Endoglin plays distinct roles in vascular smooth muscle cell recruitment and regulation of arteriovenous identity during angiogenesis. *Dev. Dyn.* 2009;238(10):2479-93.
43. Londesborough A, Vaahtomeri K, Tiainen M, Katajisto P, Ekman N, Vallenius T, et al. LKB1 in endothelial cells is required for angiogenesis and TGFbeta-mediated vascular smooth muscle cell recruitment. *Development.* 2008;135(13):2331-8.
44. Jakobsson L, van Meeteren LA. Transforming growth factor beta family members in regulation of vascular function: in the light of vascular conditional knockouts. *Exp. Cell Res.* 2013;319(9):1264-70.
45. Baker AB, Ettenson DS, Jonas M, Nugent MA, Iozzo RV, Edelman ER. Endothelial cells provide feedback control for vascular remodeling through a mechanosensitive autocrine TGF-beta signaling pathway. *Circ Res.* 2008;103(3):289-97.
46. Akhurst RJ, Hata A. Targeting the TGFbeta signalling pathway in disease. *Rev. Drug Discov.* 2012;11(10):790-811.
47. Mao X, Debenedittis P, Sun Y, Chen J, Yuan K, Jiao K, et al. Vascular smooth muscle cell Smad4 gene is important for mouse vascular development. *Arterioscler. Thromb. Vasc. Biol.* 2012;32(9):2171-7.
48. Aird WC. Endothelial cell heterogeneity. Cold Spring Harbor perspectives in medicine 2012;2(1):a006429.
49. Planas-Paz L, Strilic B, Goedecke A, Breier G, Fassler R, Lammert E. Mechanoinduction of lymph vessel expansion. *EMBO J.* 2012;31(4):788-804.
50. Wang DZ, Olson EN. Control of smooth muscle development by the myocardin family of transcriptional coactivators. *Curr Opin* Genet *Dev.* 2004;14(5):558-66.
51. Shi N, Chen SY. Smooth Muscle Cell Differentiation: Model Systems, Regulatory Mechanisms, and Vascular Diseases. *Cell. Physiol.* 2016;231(4):777-87.
52. Libby P, Ridker PM, Hansson GK. Progress and challenges in translating the biology of atherosclerosis. *Nature.* 2011;473(7347):317-25.
53. Galis ZS, Khatri JJ. Matrix metalloproteinases in vascular remodeling and atherogenesis: the good, the bad, and the ugly. *Circ. Res.* 2002;90(3):251-62.
54. Galis ZS, Sukhova GK, Lark MW, Libby P. Increased expression of matrix metalloproteinases and matrix degrading activity in vulnerable regions of human atherosclerotic plaques. *J Clin Invest.* 1994;94(6):2493-503.
55. Owens GK. Regulation of differentiation of vascular smooth muscle cells. *Physiol. Rev.* 1995;75(3):487-517.
56. Suzuki S, Narita Y, Yamawaki A, Murase Y, Satake M, Mutsuga M, et al. Effects of extracellular matrix on differentiation of human bone marrow-derived mesenchymal stem cells into smooth muscle cell lineage: utility for cardiovascular tissue engineering. *CTO.* 2010;191(4):269-80.
57. Rana TM. Illuminating the silence: understanding the structure and function of small RNAs. *Nat. Rev. Mol. Cell Biol.* 2007;8(1):23-36.
58. Chen J, Kitchen CM, Streb JW, Miano JM. Myocardin: a component of a molecular switch for smooth muscle differentiation. *J. Mol. Cell. Cardiol.* 2002;34(10):1345-56.
59. Sun Q, Chen G, Streb JW, Long X, Yang Y, Stoeckert CJ, Jr., et al. Defining the mammalian CArGome. *Genome Res.* 2006;16(2):197-207.
60. Bennett MR, Sinha S, Owens GK. Vascular Smooth Muscle Cells in Atherosclerosis. *Circ. Res.* 2016;118(4):692-702.
61. Long X, Bell RD, Gerthoffer WT, Zlokovic BV, Miano JM. Myocardin is sufficient for a smooth muscle-like contractile phenotype. *Arterioscler. Thromb. Vasc. Biol.* 2008;28(8):1505-10.

62. Landerholm TE, Dong XR, Lu J, Belaguli NS, Schwartz RJ, Majesky MW. A role for serum response factor in coronary smooth muscle differentiation from proepicardial cells. *Development.* 1999;126(10):2053-62.
63. Cordes KR, Sheehy NT, White MP, Berry EC, Morton SU, Muth AN, et al. miR-145 and miR-143 regulate smooth muscle cell fate and plasticity. *Nature.* 2009;460(7256):705-10.
64. Xin M, Small EM, Sutherland LB, Qi X, McAnally J, Plato CF, et al. MicroRNAs miR-143 and miR-145 modulate cytoskeletal dynamics and responsiveness of smooth muscle cells to injury. *Genes. Dev.* 2009;23(18):2166-78.
65. Zheng JP, Ju D, Shen J, Yang M, Li L. Disruption of actin cytoskeleton mediates loss of tensile stress induced early phenotypic modulation of vascular smooth muscle cells in organ culture. *Exp Mol Pathol.* 2010;88(1):52-7.
66. Boettger T, Beetz N, Kostin S, Schneider J, Kruger M, Hein L, et al. Acquisition of the contractile phenotype by murine arterial smooth muscle cells depends on the Mir143/145 gene cluster. *J Clin Invest.* 2009;119(9):2634-47.
67. Boucher J, Gridley T, Liaw L. Molecular pathways of notch signaling in vascular smooth muscle cells. *Front. Physiol.* 2012;3:81.
68. Davis-Dusenbery BN, Chan MC, Reno KE, Weisman AS, Layne MD, Lagna G, et al. down-regulation of Kruppel-like factor-4 (KLF4) by microRNA-143/145 is critical for modulation of vascular smooth muscle cell phenotype by transforming growth factor-beta and bone morphogenetic protein 4. *J. Biol. Chem.* 2011;286(32):28097-110.
69. Dahan D, Ekman M, Larsson-Callerfelt AK, Turczynska K, Boettger T, Braun T, et al. Induction of angiotensin-converting enzyme after miR-143/145 deletion is critical for impaired smooth muscle contractility. *Am. J. Physiol. Cell Physiol.* 2014;307(12):C1093-101.
70. Chen S, Kulik M, Lechleider RJ. Smad proteins regulate transcriptional induction of the SM22alpha gene by TGF-beta. *Nucleic Acids Res.* 2003;31(4):1302-10.
71. Hirschi KK, Rohovsky SA, D'Amore PA. PDGF, TGF-beta, and heterotypic cell-cell interactions mediate endothelial cell-induced recruitment of 10T1/2 cells and their differentiation to a smooth muscle fate. *J. Cell Biol.* 1998;141(3):805-14.
72. Sinha S, Hoofnagle MH, Kingston PA, McCanna ME, Owens GK. Transforming growth factor-beta1 signaling contributes to development of smooth muscle cells from embryonic stem cells. *Am. J. Physiol. Cell Physiol.* 2004;287(6):C1560-8.
73. Qiu P, Feng XH, Li L. Interaction of Smad3 and SRF-associated complex mediates TGF-beta1 signals to regulate SM22 transcription during myofibroblast differentiation. *J. Mol. Cell. Cardiol.* 2003;35(12):1407-20.
74. Ruiz-Ortega M, Rodriguez-Vita J, Sanchez-Lopez E, Carvajal G, Egido J. TGF-beta signaling in vascular fibrosis. *Cardiovasc. Res.* 2007;74(2):196-206.
75. Qiu P, Ritchie RP, Fu Z, Cao D, Cumming J, Miano JM, et al. Myocardin enhances Smad3-mediated transforming growth factor-beta1 signaling in a CArG box-independent manner: Smad-binding element is an important cis element for SM22alpha transcription in vivo. *Circ. Res*. 2005;97(10):983-91.
76. Majesky MW. Developmental basis of vascular smooth muscle diversity. *Arterioscl Throm Vas.* 2007;27(6):1248-1258.
77. Torsney E, Charlton R, Diamond AG, Burn J, Soames JV, Arthur HM. Mouse model for hereditary hemorrhagic telangiectasia has a generalized vascular abnormality. *Circulation.* 2003;107(12):1653-7.
78. Wasteson P, Johansson BR, Jukkola T, Breuer S, Akyurek LM, Partanen J, et al. Developmental origin of

smooth muscle cells in the descending aorta in mice. *Development*. 2008;135(10):1823-32.

79. Dobnikar L, Taylor AL, Chappell J, Oldach P, Harman JL, Oerton E, et al. Disease-relevant transcriptional signatures identified in individual smooth muscle cells from healthy mouse vessels. *Nat. Commun.* 2018;9(1):4567.
80. Ruckman JL, Luvalle PA, Hill KE, Giro MG, Davidson JM. Phenotypic stability and variation in cells of the porcine aorta: collagen and elastin production. *Matrix Biol.* 1994;14(2):135-45.
81. Nakamura T, Colbert MC, Robbins J. Neural crest cells retain multipotential characteristics in the developing valves and label the cardiac conduction system. *Circ. Res.* 2006;98(12):1547-54.
82. Pfaltzgraff ER, Bader DM. Heterogeneity in vascular smooth muscle cell embryonic origin in relation to adult structure, physiology, and disease. *Dev. Dyn.* 2015;244(3):410-6.
83. Derwall M, Malhotra R, Lai CS, Beppu Y, Aikawa E, Seehra JS, et al. Inhibition of bone morphogenetic protein signaling reduces vascular calcification and atherosclerosis. *Arterioscler. Thromb. Vasc. Biol.* 2012;32(3):613-22.
84. Leroux-Berger M, Queguiner I, Maciel TT, Ho A, Relaix F, Kempf H. Pathologic calcification of adult vascular smooth muscle cells differs on their crest or mesodermal embryonic origin. *J Bone Miner Res.* 2011;26(7):1543-53.
85. Zhang L, Issa Bhaloo S, Chen T, Zhou B, Xu Q. Role of Resident Stem Cells in Vessel Formation and Arteriosclerosis. *Circ. Res.* 2018;122(11):1608-1624.
86. Weiss A, Attisano L. The TGFbeta superfamily signaling pathway. Wiley interdisciplinary reviews Developmental biology 2013;2(1):47df Distinct and cooperative roles of mammalian Vg1 homologs GDF1 and GDF3 during early embryonic development. *Dev. Biol.* 2007;311(2):500-11.
91. Andersson O, Reissmann E, Ibanez CF. Growth differentiation factor 11 signals through the transforming growth factor-beta receptor ALK5 to regionalize the anterior-posterior axis. *EMBO Rep.* 2006;7(8):831-7.
92. Lopez-Coviella I, Berse B, Krauss R, Thies RS, Blusztajn JK. Induction and maintenance of the neuronal cholinergic phenotype in the central nervous system by BMP-9. *Science.* 2000;289(5477):313-6.
93. Bidart M, Ricard N, Levet S, Samson M, Mallet C, David L, et al. BMP9 is produced by hepatocytes and circulates mainly in an active mature form complexed to its prodomain (vol 69, pg 313, 2012). *Cell Mol Life Sci.* 2012;69(3):485-485.
94. Neuhaus H, Rosen V, Thies RS. Heart specific expression of mouse BMP-10 a novel member of the TGF-beta superfamily. *Mech. Dev.* 1999;80(2):181-4.
95. David L, Mallet C, Mazerbourg S, Feige JJ, Bailly S. Identification of BMP9 and BMP10 as functional activators of the orphan activin receptor-like kinase 1 (ALK1) in endothelial cells. *Blood.* 2007;109(5):1953-1961.
96. Hu N, Jiang D, Huang E, Liu X, Li R, Liang X, et al. BMP9-regulated angiogenic signaling plays an important role in the osteogenic differentiation of mesenchymal progenitor cells. *J. Cell Sci.* 2013;126(Pt 2):532-41.
97. Jiang H, Salmon RM, Upton PD, Wei Z, Lawera A, Davenport AP, et al. The Prodomain-bound Form of Bone Morphogenetic Protein 10 Is Biologically Active on Endothelial Cells. *J. Biol. Chem.* 2016;291(6):2954-66.
98. Ricard N, Ciais D, Levet S, Subileau M, Mallet C, Zimmers TA, et al. BMP9 and BMP10 are critical for postnatal retinal vascular remodeling. *Blood.* 2012;119(25):6162-71.
99. Mazerbourg S, Sangkuhl K, Luo CW, Sudo S, Klein C, Hsueh AJ. Identification of receptors and signaling pathways for orphan bone morphogenetic protein/growth differentiation factor ligands based on genomic analyses. *J. Biol. Chem.* 2005;280(37):32122-32.

100. Scharpfenecker M, van Dinther M, Liu Z, van Bezooijen RL, Zhao Q, Pukac L, et al. BMP-9 signals via ALK1 and inhibits bFGF-induced endothelial cell proliferation and VEGF-stimulated angiogenesis. *J. Cell Sci.* 2007;120(Pt 6):964-72.
101. Chen YG, Hata A, Lo RS, Wotton D, Shi Y, Pavletich N, et al. Determinants of specificity in TGF-beta signal transduction. *Genes. Dev.* 1998;12(14):2144-52.
102. Laux DW, Young S, Donovan JP, Mansfield CJ, Upton PD, Roman BL. Circulating Bmp10 acts through endothelial Alk1 to mediate flow-dependent arterial quiescence. *Development.* 2013;140(16):3403-12.
103. Chen H, Ridgway JB, Sai T, Lai J, Warming S, Chen HY, et al. Context-dependent signaling defines roles of BMP9 and BMP10 in embryonic and postnatal development.*PNAS.* 2013;110(29):11887-11892.
104. Cheifetz S, Like B, Massague J. Cellular distribution of type I and type II receptors for transforming growth factor-beta. *J. Biol. Chem.* 261(21):9972-8.
105. Massague J, Wotton D. Transcriptional control by the TGF-beta/Smad signaling system. *EMBO J.* 2000;19(8):1745-54.
106. Miyazono K, Maeda S, Imamura T. BMP receptor signaling: transcriptional targets, regulation of signals, and signaling cross-talk. *Cytokine Growth Factor Rev.* 2005;16(3):251-63.
107. Zeisberg M, Hanai J, Sugimoto H, Mammoto T, Charytan D, Strutz F, et al. BMP-7 counteracts TGF-beta1-induced epithelial-to-mesenchymal transition and reverses chronic renal injury. *Nat. Med.* 2003;9(7):964-8.
108. Ross S, Hill CS. How the Smads regulate transcription. *Int J Biochem Cell*. 2008;40(3):383-408.
109. Massague J. TGFbeta signalling in context. *Nat. Rev. Mol. Cell Biol.* 2012;13(10):616-30.
110. Knaus P, Sebald W. Cooperativity of binding epitopes and receptor chains in the BMP/TGFbeta superfamily. *Biol. Chem.* 2001;382(8):1189-95.
111. Derynck R, Feng XH. TGF-beta receptor signaling. Biochimica et biophysica acta 1997;1333(2):F105-50.
112. Zhu H, Kavsak P, Abdollah S, Wrana JL, Thomsen GH. A SMAD ubiquitin ligase targets the BMP pathway and affects embryonic pattern formation. *Nature.* 1999;400(6745):687-93.
113. Murakami G, Watabe T, Takaoka K, Miyazono K, Imamura T. Cooperative inhibition of bone morphogenetic protein signaling by Smurf1 and inhibitory Smads. *Mol Biol Cell.* 2003;14(7):2809-17.
114. Sieber C, Kopf J, Hiepen C, Knaus P. Recent advances in BMP receptor signaling. *Cytokine Growth Factor Rev.* 2009;20(5-6):343-55.
115. Mulder KM. Role of Ras and Mapks in TGFbeta signaling. Cytokine Growth Factor *Rev.* 2000;11(1-2):23-35.
116. Schmierer B, Hill CS. TGFbeta-SMAD signal transduction: molecular specificity and functional flexibility. *Nat. Rev. Mol. Cell Biol.* 2007;8(12):970-82.
117. Dyer LA, Pi X, Patterson C. The role of BMPs in endothelial cell function and dysfunction. *Trends Endocrinol. Metab.* 2014;25(9):472-80.
118. Oshima M, Oshima H, Taketo MM. TGF-beta receptor type II deficiency results in defects of yolk sac hematopoiesis and vasculogenesis. *Dev. Biol.* 1996;179(1):297-302.
119. Yang X, Castilla LH, Xu X, Li C, Gotay J, Weinstein M, et al. Angiogenesis defects and mesenchymal apoptosis in mice lacking SMAD5. *Development.* 1999;126(8):1571-80.
120. David L, Mallet C, Mazerbourg S, Feige JJ, Bailly S. Identification of BMP9 and BMP10 as functional activators of the orphan activin receptor-like kinase 1 (ALK1) in endothelial cells. *Blood.* 2007;109(5):1953-61.
121. Yao Y, Zebboudj AF, Torres A, Shao E, Bostrom K. Activin-like kinase receptor 1 (ALK1) in atherosclerotic lesions and vascular mesenchymal cells. *Cardiovasc. Res.* 2007;74(2):279-89.

122. Gore B, Izikki M, Mercier O, Dewachter L, Fadel E, Humbert M, et al. Key role of the endothelial TGF-beta/ALK1/endoglin signaling pathway in humans and rodents pulmonary hypertension. *PloS one.* 2014;9(6):e100310.
123. Park SO, Lee YJ, Seki T, Hong KH, Fliess N, Jiang Z, et al. ALK5- and TGFBR2-independent role of ALK1 in the pathogenesis of hereditary hemorrhagic telangiectasia type 2. *Blood*. 2008;111(2):633-42.
124. Seki T, Hong KH, Oh SP. Nonoverlapping expression patterns of ALK1 and ALK5 reveal distinct roles of each receptor in vascular development. *Lab. Invest*. 2006;86(2):116-29.
125. Lagna G, Ku MM, Nguyen PH, Neuman NA, Davis BN, Hata A. Control of phenotypic plasticity of smooth muscle cells by bone morphogenetic protein signaling through the myocardin-related transcription factors. *J. Biol. Chem.* 2007;282(51):37244-55.
126. ten Dijke P, Goumans MJ, Pardali E. Endoglin in angiogenesis and vascular diseases. *Angiogenesis.* 2008;11(1):79-89.
127. Kirkbride KC, Townsend TA, Bruinsma MW, Barnett JV, Blobe GC. Bone morphogenetic proteins signal through the transforming growth factor-beta type III receptor. *J. Biol. Chem.*2008;283(12):7628-37.
128. Lee NY, Kirkbride KC, Sheu RD, Blobe GC. The transforming growth factor-beta type III receptor mediates distinct subcellular trafficking and downstream signaling of activin-like kinase (ALK)3 and ALK6 receptors. *Mol. Biol. Cell.* 2009;20(20):4362-70.
129. Scherner O, Meurer SK, Tihaa L, Gressner AM, Weiskirchen R. Endoglin differentially modulates antagonistic transforming growth factor-beta1 and BMP-7 signaling. *J. Biol. Chem.* 2007;282(19):13934-43.
130. Cunha SI, Pietras K. ALK1 as an emerging target for antiangiogenic therapy of cancer. *Blood.* 2011;117(26):6999-7006.
131. Bourdeau A, Dumont DJ, Letarte M. A murine model of hereditary hemorrhagic telangiectasia. *J. Clin. Invest.* 1999;104(10):1343-51.
132. Mahmoud M, Allinson KR, Zhai Z, Oakenfull R, Ghandi P, Adams RH, et al. Pathogenesis of arteriovenous malformations in the absence of endoglin. *Circ. Res.* 2010;106(8):1425-33.
133. Dickson MC, Martin JS, Cousins FM, Kulkarni AB, Karlsson S, Akhurst RJ. Defective haematopoiesis and vasculogenesis in transforming growth factor-beta 1 knock out mice. *Development.* 1995;121(6):1845-54.
134. Kocher O, Gabbiani F, Gabbiani G, Reidy MA, Cokay MS, Peters H, et al. Phenotypic features of smooth muscle cells during the evolution of experimental carotid artery intimal thickening. Biochemical and morphologic studies. *Lab. Invest.* 1991;65(4):459-70.
135. Langlois D, Hneino M, Bouazza L, Parlakian A, Sasaki T, Bricca G, et al. Conditional inactivation of TGF-beta type II receptor in smooth muscle cells and epicardium causes lethal aortic and cardiac defects. *Transgenic Res.* 2010;19(6):1069-82.
136. Ruiz-Ortega M, Rodriguez-Vita J, Sanchez-Lopez E, Carvajal G, Egido J. TGF-beta signaling in vascular fibrosis. *Cardiovasc. Res.* 2007;74(2):196-206.
137. Clempus RE, Griendling KK. Reactive oxygen species signaling in vascular smooth muscle cells. *Cardiovasc. Res.* 2006;71(2):216-25.
138. Yang X, Li C, Xu X, Deng C. The tumor suppressor SMAD4/DPC4 is essential for epiblast proliferation and mesoderm induction in mice. *PNAS.* 1998;95(7):3667-72.
139. Lan Y, Liu B, Yao H, Li F, Weng T, Yang G, et al. Essential role of endothelial Smad4 in vascular remodeling and integrity. *Mol. Cell. Biol.* 2007;27(21):7683-92.
140. Chang H, Huylebroeck D, Verschueren K, Guo Q, Matzuk MM, Zwijsen A. Smad5 knockout mice die at

mid-gestation due to multiple embryonic and extraembryonic defects. *Development.* 1999;126(8):1631-42.

141. Umans L, Cox L, Tjwa M, Bito V, Vermeire L, Laperre K, et al. Inactivation of Smad5 in endothelial cells and smooth muscle cells demonstrates that Smad5 is required for cardiac homeostasis. *Am. J. Pathol.* 2007;170(5):1460-72.
142. Lechleider RJ, Ryan JL, Garrett L, Eng C, Deng C, Wynshaw-Boris A, et al. Targeted mutagenesis of Smad1 reveals an essential role in chorioallantoic fusion. *Dev. Biol.* 2001;240(1):157-67.
143. Huang Z, Wang D, Ihida-Stansbury K, Jones PL, Martin JF. Defective pulmonary vascular remodeling in Smad8 mutant mice. *Hum. Mol. Genet.* 2009;18(15):2791-801.
144. Ramirez RL, 3rd, De Jesus Perez V, Zamanian RT. Stimulants and Pulmonary Arterial Hypertension: An Update. *Adv. Pulm. Hypertens.* 2018;17(2):49-54.
145. Deng Z, Morse JH, Slager SL, Cuervo N, Moore KJ, Venetos G, et al. Familial primary pulmonary hypertension (gene PPH1) is caused by mutations in the bone morphogenetic protein receptor-II gene. *Am. J. Hum. Genet.* 2000;67(3):737-44.
146. Farber HW, Loscalzo J. Pulmonary arterial hypertension. *N. Engl. J. Med.* 2004;351(16):1655-65.
147. Sakao S, Tatsumi K, Voelkel NF. Endothelial cells and pulmonary arterial hypertension: apoptosis, proliferation, interaction and transdifferentiation. *Respir. Res*. 2009;10:95.
148. Tantini B, Manes A, Fiumana E, Pignatti C, Guarnieri C, Zannoli R, et al. Antiproliferative effect of sildenafil on human pulmonary artery smooth muscle cells. *Basic. Res. Cardiol.* 2005;100(2):131-8.
149. Baliga RS, MacAllister RJ, Hobbs AJ. New perspectives for the treatment of pulmonary hypertension. *Br. J. Pharmacol.* 2011;163(1):125-40.
150. Andersen CU, Hilberg O, Mellemkjaer S, Nielsen-Kudsk JE, Simonsen U. Apelin and pulmonary hypertension. *Pulm. Circ.* 2011;1(3):334-46.
151. Machado RD, Aldred MA, James V, Harrison RE, Patel B, Schwalbe EC, et al. Mutations of the TGF-beta type II receptor BMPR2 in pulmonary arterial hypertension. *Hum. Mutat.* 2006;27(2):121-32.
152. International PPHC, Lane KB, Machado RD, Pauciulo MW, Thomson JR, Phillips JA, 3rd, et al. Heterozygous germline mutations in BMPR2, encoding a TGF-beta receptor, cause familial primary pulmonary hypertension. *Nat. Genet.* 2000;26(1):81-4.
153. Orriols M, Gomez-Puerto MC, Ten Dijke P. BMP type II receptor as a therapeutic target in pulmonary arterial hypertension. *Cell. Mol. Life. Sci*. 2017;74(16):2979-2995.
154. Wang XJ, Lian TY, Jiang X, Liu SF, Li SQ, Jiang R, et al. Germline BMP9 mutation causes idiopathic pulmonary arterial hypertension. *Eur. Respir. J.* 2019;53(3).
155. Beppu H, Ichinose F, Kawai N, Jones RC, Yu PB, Zapol WM, et al. BMPR-II heterozygous mice have mild pulmonary hypertension and an impaired pulmonary vascular remodeling response to prolonged hypoxia. *Am* J *Physiol Lung Cell Mol Physiol.* 2004;287(6):L1241-7.
156. Song YL, Jones JE, Beppu H, Keaney JF, Loscalzo J, Zhang YY. Increased susceptibility to pulmonary hypertension in heterozygous BMPR2-mutant mice. *Circulation.* 2005;112(4):553-562.
157. Hong KH, Lee YJ, Lee E, Park SO, Han C, Beppu H, et al. Genetic ablation of the BMPR2 gene in pulmonary endothelium is sufficient to predispose to pulmonary arterial hypertension. *Circulation.* 2008;118(7):722-30.
158. West J, Harral J, Lane K, Deng Y, Ickes B, Crona D, et al. Mice expressing BMPR2R899X transgene in smooth muscle develop pulmonary vascular lesions. *Am J Physiol Lung Cell Mol Physiol.* 2008;295(5):L744-55.
159. Reynolds AM, Holmes MD, Danilov SM, Reynolds PN. Targeted gene delivery of BMPR2 attenuates

pulmonary hypertension. *Eur. Respir. J*. 2012;39(2):329-43.

160. Madonna R, Cocco N. Novel Strategies in the Treatment of Pulmonary Arterial Hypertension. *Curr Drug Targets*. 2016;17(7):817-23.
161. Sung YK, Yuan K, de Jesus Perez VA. Novel approaches to pulmonary arterial hypertension drug discovery. *Expert. Opin. Drug. Discov.* 2016;11(4):407-14.
162. Jerkic M, Kabir MG, Davies A, Yu LX, McIntyre BA, Husain NW, et al. Pulmonary hypertension in adult Alk1 heterozygous mice due to oxidative stress. *Cardiovasc. Res.* 2011;92(3):375-84.
163. Toporsian M, Jerkic M, Zhou YQ, Kabir MG, Yu LX, McIntyre BAS, et al. Spontaneous Adult-Onset Pulmonary Arterial Hypertension Attributable to Increased Endothelial Oxidative Stress in a Murine Model of Hereditary Hemorrhagic Telangiectasia. *Arterioscl. Throm. Vas*. 2010;30(3):509-517.
164. Austin ED, Loyd JE. The genetics of pulmonary arterial hypertension. *Circ. Res.* 2014;115(1):189-202.
165. Girerd B, Montani D, Coulet F, Sztrymf B, Yaici A, Jais X, et al. Clinical outcomes of pulmonary arterial hypertension in patients carrying an ACVRL1 (ALK1) mutation. *Am. J. Respir. Crit. Care Med.* 2010;181(8):851-61.
166. David L, Mallet C, Keramidas M, Lamande N, Gasc JM, Dupuis-Girod S, et al. Bone morphogenetic protein-9 is a circulating vascular quiescence factor. *Circ. Res.* 2008;102(8):914-22.
167. Park JE, Shao D, Upton PD, Desouza P, Adcock IM, Davies RJ, et al. BMP-9 induced endothelial cell tubule formation and inhibition of migration involves Smad1 driven endothelin-1 production. *PloS one.* 2012;7(1):e30075.
168. Alastalo TP, Li M, Perez Vde J, Pham D, Sawada H, Wang JK, et al. Disruption of PPARgamma/beta-catenin-mediated regulation of apelin impairs BMP-induced mouse and human pulmonary arterial EC survival. *J Clin Invest.* 2011;121(9):3735-46.
169. Kim J. Apelin-APJ signaling: a potential therapeutic target for pulmonary arterial hypertension. *Mol. Cells*. 2014;37(3):196-201.
170. Chandra SM, Razavi H, Kim J, Agrawal R, Kundu RK, Perez VD, et al. Disruption of the Apelin-APJ System Worsens Hypoxia-Induced Pulmonary Hypertension. *Arterioscl Throm Vas.* 2011;31(4):814-U212.
171. Kim J, Kang Y, Kojima Y, Lighthouse JK, Hu X, Aldred MA, et al. An endothelial apelin-FGF link mediated by miR-424 and miR-503 is disrupted in pulmonary arterial hypertension. *Nat. Med.* 2013;19(1):74-82.
172. Gupte VV, Ramasamy SK, Reddy R, Lee J, Weinreb PH, Violette SM, et al. Overexpression of fibroblast growth factor-10 during both inflammatory and fibrotic phases attenuates bleomycin-induced pulmonary fibrosis in mice. *Am. J. Respir. Crit. Care Med.* 2009;180(5):424-36.
173. Salani D, Taraboletti G, Rosano L, Di Castro V, Borsotti P, Giavazzi R, et al. Endothelin-1 induces an angiogenic phenotype in cultured endothelial cells and stimulates neovascularization in vivo. *Am. J. Pathol.* 2000;157(5):1703-11.
174. Star GP, Giovinazzo M, Langleben D. Bone morphogenic protein-9 stimulates endothelin-1 release from human pulmonary microvascular endothelial cells: a potential mechanism for elevated ET-1 levels in pulmonary arterial hypertension. *Microvasc. Res.* 2010;80(3):349-54.
175. Star GP, Giovinazzo M, Langleben D. ALK2 and BMPR2 knockdown and endothelin-1 production by pulmonary microvascular endothelial cells. *Microvasc. Res.* 2013;85:46-53.
176. Adams DJ, Quail MA, Cox T, van der Weyden L, Gorick BD, Su Q, et al. A genome-wide, end-sequenced 129Sv BAC library resource for targeting vector construction. *Genomics.* 2005;86(6):753-8.
177. Luo F, Wang X, Luo X, Li B, Zhu D, Sun H, et al. Invasive Hemodynamic Assessment for the Right Ventricular System and Hypoxia-Induced Pulmonary Arterial Hypertension in Mice. JoVE. 2019(152).
178. Wang S, Iring A, Strilic B, Albarran Juarez J, Kaur H, Troidl K, et al. P2Y(2) and Gq/G(1)(1) control blood

pressure by mediating endothelial mechanotransduction. *J Clin Invest.* 2015;125(8):3077-86.

179. Lee KJ, Czech L, Waypa GB, Farrow KN. Isolation of pulmonary artery smooth muscle cells from neonatal mice. *JoVE.* 2013(80):e50889.
180. Kuenne C, Guenther S, Looso M, Zhang T, Krueger M, Zhou Y, et al. RNA-Seq analysis of isolated satellite cells in Prmt5 deficient mice. *Genom. Data.* 2015;5:122-5.
181. Gao R, Liang X, Cheedipudi S, Cordero J, Jiang X, Zhang Q, et al. Pioneering function of Isl1 in the epigenetic control of cardiomyocyte cell fate. *Cell. Res.* 2019;29(6):486-501.
182. Bolger AM, Lohse M, Usadel B. Trimmomatic: a flexible trimmer for Illumina sequence data. *Bioinformatics.* 2014;30(15):2114-20.
183. Dobin A, Davis CA, Schlesinger F, Drenkow J, Zaleski C, Jha S, et al. STAR: ultrafast universal RNA-seq aligner. *Bioinformatics.* 2013;29(1):15-21.
184. Zhang Y, Liu T, Meyer CA, Eeckhoute J, Johnson DS, Bernstein BE, et al. Model-based analysis of ChIP-Seq (MACS). *Genome. Biol*. 2008;9(9):R137.
185. Anders S, Huber W. Differential expression analysis for sequence count data. *Genome. Biol.* 2010;11(10):R106.
186. Xie C, Mao X, Huang J, Ding Y, Wu J, Dong S, et al. KOBAS 2.0: a web server for annotation and identification of enriched pathways and diseases. *Nucleic. Acids. Res.* 2011;39(Web Server issue):W316-22.
187. Hahne F, Ivanek R. Visualizing Genomic Data Using Gviz and Bioconductor. *Methods. Mol. Biol.* 2016;1418:335-51.
188. Durinck S, Spellman PT, Birney E, Huber W. Mapping identifiers for the integration of genomic datasets with the R/Bioconductor package biomaRt. *Nat. Protoc.* 2009;4(8):1184-91.
189. Subramanian A, Tamayo P, Mootha VK, Mukherjee S, Ebert BL, Gillette MA, et al. Gene set enrichment analysis: a knowledge-based approach for interpreting genome-wide expression profiles. *PNAS.* 2005;102(43):15545-50.
190. Tillet E, Ouarne M, Desroches-Castan A, Mallet C, Subileau M, Didier R, et al. A heterodimer formed by bone morphogenetic protein 9 (BMP9) and BMP10 provides most BMP biological activity in plasma. *J. Biol. Chem.* 2018;293(28):10963-10974.
191. Shi J, Yang Y, Cheng A, Xu G, He F. Metabolism of vascular smooth muscle cells in vascular diseases. *Am J Physiol Heart C.* 2020;319(3):H613-H631.
192. Pak O, Aldashev A, Welsh D, Peacock A. The effects of hypoxia on the cells of the pulmonary vasculature. *Eur. Respir. J.* 2007;30(2):364-72.
193. Schmid E, Hilberath JN, Blumenstock G, Shekar PS, Kling S, Shernan SK, et al. Tricuspid annular plane systolic excursion (TAPSE) predicts poor outcome in patients undergoing acute pulmonary embolectomy. *Heart, lung and vessels* 2015;7(2):151-158.
194. Xie F, Lv D, Chen L. ELABELA: a novel hormone in cardiac development acting as a new endogenous ligand for the APJ receptor. *Acta. Biochim. Biophys. Sin.* 2014;46(7):620-2.
195. Halpern W, Osol G, Coy GS. Mechanical behavior of pressurized in vitro prearteriolar vessels determined with a video system. *Ann. Biomed.Eng.* 1984;12(5):463-79.
196. Kautz L, Meynard D, Monnier A, Darnaud V, Bouvet R, Wang RH, et al. Iron regulates phosphorylation of Smad1/5/8 and gene expression of Bmp6, Smad7, Id1, and Atoh8 in the mouse liver. *Blood.* 2008;112(4):1503-9.
197. Fang F, Wasserman SM, Torres-Vazquez J, Weinstein B, Cao F, Li Z, et al. The role of Hath6, a newly identified shear-stress-responsive transcription factor, in endothelial cell differentiation and function. *J.*

Cell Sci. 2014;127(Pt 7):1428-40.

198. Liao XH, Xiang Y, Li H, Zheng L, Xu Y, Xi Yu C, et al. VEGF-A Stimulates STAT3 Activity via Nitrosylation of Myocardin to Regulate the Expression of Vascular Smooth Muscle Cell Differentiation Markers. *Sci. Rep.* 2017;7(1):2660.
199. Li L, Blumenthal DK, Terry CM, He Y, Carlson ML, Cheung AK. PDGF-induced proliferation in human arterial and venous smooth muscle cells: molecular basis for differential effects of PDGF isoforms. *J. Cell. Biochem.* 2011;112(1):289-98.
200. Kubin T, Poling J, Kostin S, Gajawada P, Hein S, Rees W, et al. Oncostatin M is a major mediator of cardiomyocyte dedifferentiation and remodeling. *Cell stem cell.* 2011;9(5):420-32.
201. Poling J, Gajawada P, Richter M, Lorchner H, Polyakova V, Kostin S, et al. Therapeutic targeting of the oncostatin M receptor-beta prevents inflammatory heart failure. *Basic. Res. Cardiol*. 2014;109(1):396.
202. Li L, Miano JM, Cserjesi P, Olson EN. SM22 alpha, a marker of adult smooth muscle, is expressed in multiple myogenic lineages during embryogenesis. *Circ. Res*. 1996;78(2):188-95.
203. Bleul CC, Boehm T. BMP signaling is required for normal thymus development. *J. Immun.* 2005;175(8):5213-21.
204. Hager-Theodorides AL, Outram SV, Shah DK, Sacedon R, Shrimpton RE, Vicente A, et al. Bone morphogenetic protein 2/4 signaling regulates early thymocyte differentiation. *J. Immun.* 2002;169(10):5496-504.
205. Kersten C, Dosen G, Myklebust JH, Sivertsen EA, Hystad ME, Smeland EB, et al. BMP-6 inhibits human bone marrow B lymphopoiesis--upregulation of Id1 and Id3. *Exp. Hematol.* 2006;34(1):72-81.
206. Sivertsen EA, Huse K, Hystad ME, Kersten C, Smeland EB, Myklebust JH. Inhibitory effects and target genes of bone morphogenetic protein 6 in Jurkat TAg cells. *Eur. J. Immunol.* 2007;37(10):2937-48.
207. Liu F, Wang X, Hu G, Wang Y, Zhou J. The transcription factor TEAD1 represses smooth muscle-specific gene expression by abolishing myocardin function. *J. Biol. Chem.* 2014;289(6):3308-16.
208. Creemers EE, Sutherland LB, McAnally J, Richardson JA, Olson EN. Myocardin is a direct transcriptional target of Mef2, Tead and Foxo proteins during cardiovascular development. *Development.* 2006;133(21):4245-56.
209. Xie C, Guo Y, Zhu T, Zhang J, Ma PX, Chen YE. Yap1 protein regulates vascular smooth muscle cell phenotypic switch by interaction with myocardin. *J. Biol. Chem.* 2012;287(18):14598-605.
210. Wang X, Hu G, Gao X, Wang Y, Zhang W, Harmon EY, et al. The induction of yes-associated protein expression after arterial injury is crucial for smooth muscle phenotypic modulation and neointima formation. *Arterioscler. Thromb. Vasc. Biol.* 2012;32(11):2662-9.
211. Cotton JL, Li Q, Ma L, Park JS, Wang J, Ou J, et al. YAP/TAZ and Hedgehog Coordinate Growth and Patterning in Gastrointestinal Mesenchyme. *Dev. cell.* 2017;43(1):35-47 e4.
212. Zhang Y, Shen H, Withers HG, Yang N, Denson KE, Mussell AL, et al. VGLL4 Selectively Represses YAP-Dependent Gene Induction and Tumorigenic Phenotypes in Breast Cancer. *Sci. Rep.* 2017;7(1):6190.
213. Lin Z, Guo H, Cao Y, Zohrabian S, Zhou P, Ma Q, et al. Acetylation of VGLL4 Regulates Hippo-YAP Signaling and Postnatal Cardiac Growth. *Dev. cell.* 2016;39(4):466-479.
214. Gan Q, Yoshida T, Li J, Owens GK. Smooth muscle cells and myofibroblasts use distinct transcriptional mechanisms for smooth muscle alpha-actin expression. *Circ. Res.* 2007;101(9):883-92.
215. ten Dijke P, Hill CS. New insights into TGF-beta-Smad signalling. *Trends. Biochem. Sci.* 2004;29(5):265-73.
216. Bidart M, Ricard N, Levet S, Samson M, Mallet C, David L, et al. BMP9 is produced by hepatocytes and circulates mainly in an active mature form complexed to its prodomain. *Cell. Mol. Life. Sci.* 2012;69(2):313-24.

217. West J, Fagan K, Steudel W, Fouty B, Lane K, Harral J, et al. Pulmonary hypertension in transgenic mice expressing a dominant-negative BMPRII gene in smooth muscle. *Circ. Res.* 2004;94(8):1109-14.
218. Wettschureck N, Strilic B, Offermanns S. Passing the Vascular Barrier: Endothelial Signaling Processes Controlling Extravasation. *Physiol. Rev.* 2019;99(3):1467-1525.
219. Brash L, Barnes GD, Brewis MJ, Church AC, Gibbs SJ, Howard L, et al. Short-Term Hemodynamic Effects of Apelin in Patients With Pulmonary Arterial Hypertension. *J Am Coll Cardiol Basic Trans Science.* 2018;3(2):176-186.
220. Deng C, Chen H, Yang N, Feng Y, Hsueh AJ. Apela Regulates Fluid Homeostasis by Binding to the APJ Receptor to Activate Gi Signaling. *J. Biol. Chem*. 2015;290(30):18261-8.
221. Xie C, Ritchie RP, Huang H, Zhang J, Chen YE. Smooth muscle cell differentiation in vitro: models and underlying molecular mechanisms. *Arterioscler. Thromb. Vasc. Biol.* 2011;31(7):1485-94.
222. Liu Q, Liu K, Cui G, Huang X, Yao S, Guo W, et al. Lung regeneration by multipotent stem cells residing at the bronchioalveolar-duct junction. *Nat. Genet.* 2019;51(4):728-738.
223. Zhou H, Liu J, Zhou C, Gao N, Rao Z, Li H, et al. In vivo simultaneous transcriptional activation of multiple genes in the brain using CRISPR-dCas9-activator transgenic mice. *Nat. Neurosci.* 2018;21(3):440-446.
224. Pan D. The hippo signaling pathway in development and cancer. Developmental cell 2010;19(4):491-505.
225. Zhao B, Li L, Lei Q, Guan KL. The Hippo-YAP pathway in organ size control and tumorigenesis: an updated version. *Genes. Dev.* 2010;24(9):862-74.
226. Varelas X. The Hippo pathway effectors TAZ and YAP in development, homeostasis and disease. *Development*. 2014;141(8):1614-26.
227. Pipes GC, Creemers EE, Olson EN. The myocardin family of transcriptional coactivators: versatile regulators of cell growth, migration, and myogenesis. *Genes. Dev.* 2006;20(12):1545-56.
228. Swartz EA, Johnson AD, Owens GK. Two MCAT elements of the SM alpha-actin promoter function differentially in SM vs. non-SM cells. *Am. J. Physiol. Cell Physiol.* 1998;275(2):C608-18.
229. Rindt H, Gulick J, Knotts S, Neumann J, Robbins J. In vivo analysis of the murine beta-myosin heavy chain gene promoter. *J. Biol. Chem.* 1993;268(7):5332-8.
230. Fujii M, Nakanishi H, Toyoda T, Tanaka I, Kondo Y, Osada H, et al. Convergent signaling in the regulation of connective tissue growth factor in malignant mesothelioma: TGFbeta signaling and defects in the Hippo signaling cascade. *Cell. cycle.* 2012;11(18):3373-9.
231. Yu PB, Beppu H, Kawai N, Li E, Bloch KD. Bone morphogenetic protein (BMP) type II receptor deletion reveals BMP ligand-specific gain of signaling in pulmonary artery smooth muscle cells. *J. Biol. Chem.* 2005;280(26):24443-50.
232. Dituri F, Cossu C, Mancarella S, Giannelli G. The Interactivity between TGFbeta and BMP Signaling in Organogenesis, Fibrosis, and Cancer. *Cells* 2019;8(10).
233. O'Reilly S, Ciechomska M, Cant R, Hugle T, van Laar JM. Interleukin-6, its role in fibrosing conditions. *Cytokine Growth Factor Rev.* 2012;23(3):99-107.
234. Lee SB, Kalluri R. Mechanistic connection between inflammation and fibrosis. *Kidney Int*. *Suppl*. 2010(119):S22-6.
235. Mack M. Inflammation and fibrosis. *Matrix Biol*. 2018;68-69:106-121.
236. Meng XM, Nikolic-Paterson DJ, Lan HY. TGF-beta: the master regulator of fibrosis. *Nat. Rev. Nephrol.* 2016;12(6):325-38.
237. Gabriel VA. Transforming Growth Factor-beta and Angiotensin in Fibrosis and Burn Injuries. *J Burn Care Res.* 2009;30(3):471-481.
238. Kinoshita K, Iimuro Y, Otogawa K, Saika S, Inagaki Y, Nakajima Y, et al. Adenovirus-mediated expression

of BMP-7 suppresses the development of liver fibrosis in rats. *Gut.* 2007;56(5):706-14.

239. Pegorier S, Campbell GA, Kay AB, Lloyd CM. Bone morphogenetic protein (BMP)-4 and BMP-7 regulate differentially transforming growth factor (TGF)-beta1 in normal human lung fibroblasts (NHLF). *Respir. Res.* 2010;11:85.
240. Liang D, Wang Y, Zhu Z, Yang G, An G, Li X, et al. BMP-7 attenuated silica-induced pulmonary fibrosis through modulation of the balance between TGF-beta/Smad and BMP-7/Smad signaling pathway. *Chem. Biol. Interact*. 2016;243:72-81.
241. Wang S, Hirschberg R. BMP7 antagonizes TGF-beta -dependent fibrogenesis in mesangial cells. *Am J Physiol. Renal. Physiol.* 2003;284(5):F1006-13.
242. Morine KJ, Qiao X, York S, Natov PS, Paruchuri V, Zhang Y, et al. Bone Morphogenetic Protein 9 Reduces Cardiac Fibrosis and Improves Cardiac Function in Heart Failure. *Circulation.* 2018;138(5):513-526.
243. De Langhe E, Cailotto F, De Vooght V, Aznar-Lopez C, Vanoirbeek JA, Luyten FP, et al. Enhanced endogenous bone morphogenetic protein signaling protects against bleomycin induced pulmonary fibrosis. *Respir. Res.* 2015;16:38.
244. Wang S, Sun A, Li L, Zhao G, Jia J, Wang K, et al. Up-regulation of BMP-2 antagonizes TGF-beta1/ROCK-enhanced cardiac fibrotic signalling through activation of Smurf1/Smad6 complex. *J. Cell. Mol. Med.* 2012;16(10):2301-10.
245. O'Reilly S, Ciechomska M, Cant R, van Laar JM. Interleukin-6 (IL-6) trans signaling drives a STAT3-dependent pathway that leads to hyperactive transforming growth factor-beta (TGF-beta) signaling promoting SMAD3 activation and fibrosis via Gremlin protein. *J. Biol. Chem.* 2014;289(14):9952-60.
246. Bi J, Ge S. Potential roles of BMP9 in liver fibrosis. *Int. J. Mol. Sci.* 2014;15(11):20656-67.
247. Herrera B, Addante A, Sanchez A. BMP Signalling at the Crossroad of Liver Fibrosis and Regeneration. *Int. J. Mol. Sci.* 2017;19(1).
248. Kanamori Y, Sugiyama M, Hashimoto O, Murakami M, Matsui T, Funaba M. Regulation of hepcidin expression by inflammation-induced activin B. *Sci. Rep.* 2016;6:38702.
249. Hruska KA, Mathew S, Saab G. Bone morphogenetic proteins in vascular calcification. *Circ.Res.* 2005;97(2):105-14.
250. Sucosky P, Balachandran K, Elhammali A, Jo H, Yoganathan AP. Altered Shear Stress Stimulates Upregulation of Endothelial VCAM-1 and ICAM-1 in a BMP-4-and TGF-beta 1-Dependent Pathway. *Arterioscl. Throm. Vas*. 2009;29(2):254-260.
251. Libby P. Inflammation in atherosclerosis. *Arterioscler. Thromb. Vasc. Biol.* 2012;32(9):2045-51.
252. Yao Y, Bennett BJ, Wang X, Rosenfeld ME, Giachelli C, Lusis AJ, et al. Inhibition of bone morphogenetic proteins protects against atherosclerosis and vascular calcification. *Circ. Res.* 2010;107(4):485-94.
253. Pi X, Lockyer P, Dyer LA, Schisler JC, Russell B, Carey S, et al. Bmper inhibits endothelial expression of inflammatory adhesion molecules and protects against atherosclerosis. *Arterioscl. Throm. Vas*. 2012;32(9):2214-22.
254. Morine KJ, Qiao X, Paruchuri V, Aronovitz MJ, Mackey EE, Buiten L, et al. Reduced activin receptor-like kinase 1 activity promotes cardiac fibrosis in heart failure. *Cardiovasc. Pathol.* 2017;31:26-33.
255. Frangogiannis NG. The mechanistic basis of infarct healing. *Antioxid. Redox. Signal.* 2006;8(11-12):1907-39.
256. Moore-Morris T, Cattaneo P, Puceat M, Evans SM. Origins of cardiac fibroblasts. *J. Mol. Cell. Cardiol.* 2016;91:1-5.
257. Ebelt H, Hillebrand I, Arlt S, Zhang Y, Kostin S, Neuhaus H, et al. Treatment with bone morphogenetic protein 2 limits infarct size after myocardial infarction in mice. *Shock.* 2013;39(4):353-60.

258. Wu X, Sagave J, Rutkovskiy A, Haugen F, Baysa A, Nygard S, et al. Expression of bone morphogenetic protein 4 and its receptors in the remodeling heart. *Life Sci*. 2014;97(2):145-54.
259. Qu X, Liu Y, Cao D, Chen J, Liu Z, Ji H, et al. BMP10 preserves cardiac function through its dual activation of SMAD-mediated and STAT3-mediated pathways. *J. Biol. Chem*. 2019;294(52):19877-19888.
260. Werfel S, Jungmann A, Lehmann L, Ksienzyk J, Bekeredjian R, Kaya Z, et al. Rapid and highly efficient inducible cardiac gene knockout in adult mice using AAV-mediated expression of Cre recombinase. *Cardiovasc. Res.* 2014;104(1):15-23.
261. Lin Z, von Gise A, Zhou P, Gu F, Ma Q, Jiang J, et al. Cardiac-specific YAP activation improves cardiac function and survival in an experimental murine MI model. *Circ. Res.* 2014;115(3):354-63.
262. Madeddu P. Therapeutic angiogenesis and vasculogenesis for tissue regeneration. *Exp. Physiol.* 2005;90(3):315-26.
263. van Oostrom MC, van Oostrom O, Quax PH, Verhaar MC, Hoefer IE. Insights into mechanisms behind arteriogenesis: what does the future hold? *J. Leukoc. Biol.* 2008;84(6):1379-91.
264. Ren G, Michael LH, Entman ML, Frangogiannis NG. Morphological characteristics of the microvasculature in healing myocardial infarcts. *J. Histochem. Cytochem.* 2002;50(1):71-9.
265. Cochain C, Channon KM, Silvestre JS. Angiogenesis in the infarcted myocardium. *Antioxid*. *Redox. Signal.* 2013;18(9):1100-13.
266. Haubner BJ, Adamowicz-Brice M, Khadayate S, Tiefenthaler V, Metzler B, Aitman T, et al. Complete cardiac regeneration in a mouse model of myocardial infarction. *Aging.* 2012;4(12):966-77.
267. Haubner BJ, Schuetz T, Penninger JM. A reproducible protocol for neonatal ischemic injury and cardiac regeneration in neonatal mice. *Basic. Res. Cardiol.* 2016;111(6):64.
268. Porrello ER, Mahmoud AI, Simpson E, Hill JA, Richardson JA, Olson EN, et al. Transient regenerative potential of the neonatal mouse heart. *Science.* 2011;331(6020):1078-80.
269. Hoeijmakers JH. DNA damage, aging, and cancer. *N*. *Engl. J. Med.* 2009;361(15):1475-85.
270. Maynard S, Schurman SH, Harboe C, de Souza-Pinto NC, Bohr VA. Base excision repair of oxidative DNA damage and association with cancer and aging. *Carcinogenesis*. 2009;30(1):2-10.
271. Moos PJ, Edes K, Fitzpatrick FA. Inactivation of wild-type p53 tumor suppressor by electrophilic prostaglandins. *PNAS.* 2000;97(16):9215-20.